Rotating Bose-Einstein Condensates

Diploma Thesis of

Sebastian Kling

submitted to
the Fachbereich Physik at
the **Freie Universität Berlin**

Supervisor: Prof. Dr. Hagen Kleinert

September 2005

Contents

Chapter 1

Basics of Bose-Einstein Condensation

We give a short introduction to the theory of Bose-Einstein condensation and its experimental realization. In particular, we report on recent experiments which have been performed in Paris at the École Normale Supérieure (ENS) in the group of Jean Dalibard in 2003 [1,2]. They have succeeded in setting a ^{87}Rb condensate into fast rotation and observed the nucleation of vortices. This fascinating experiment sets the ground for our considerations in this thesis. Finally, we give an overview of what we want to do in this work.

1.1 History

The phenomenon known as Bose-Einstein condensation (BEC) was predicted by A. Einstein 1924 [3,4] as he reviewed and translated a work of S.N. Bose [5] about the statistics of photons. Therein, Bose derived Planck's famous black-body radiation formula on the basis of the thermodynamic properties of quantized massless harmonic oscillators of some frequencies generating a free electromagnetic field, i.e. the radiation field. This corresponds to the possibility of regarding any radiation field as a linear superposition of plane waves of various frequencies. For the electromagnetic field these massless oscillators are termed photons. Therefrom, Einstein generalized the Bose statistics to arbitrary massive particles finding out that a system of particles satisfying both the Bose statistics and the conservation of the number of particles should undergo a before unknown phase transition at some critical temperature. Below this critical temperature a macroscopic fraction of all particles "condense" into one single state of the system, the quantum mechanical ground state. As these condensed particles do not contribute to the entropy of the system anymore, Einstein interpreted this phenomenon as a phase transition. Although Einstein's prediction was for an ideal Bose gas, that is a non-interacting gas satisfying the Bose statistics, F. London [6,7] suggested in 1938 to explain the observation of superfluidity in liquid ^{4}He, which is a strongly interacting gas, as a manifestation of a Bose-Einstein condensation. Remarkably, this is still the basis for our present understanding of superfluidity and superconductivity. In 1995, the existence of BEC was proven experimentally in helium from measurements of momentum distributions [8] and in semiconductors [9], where para-excitons were found to condense.
Also in 1995, pure BEC was observed in systems very different from ^{4}He, namely dilute alkali gases [10,11]. Such gases were confined in a magnetic trap and cooled down to extremely low temperatures of the order of fractions of microkelvins. The first evidence for the condensation emerged from time-of-flight measurements. The atoms were left to expand by switching off the confining trap and then imaged with optical methods. A sharp peak in the velocity distribution

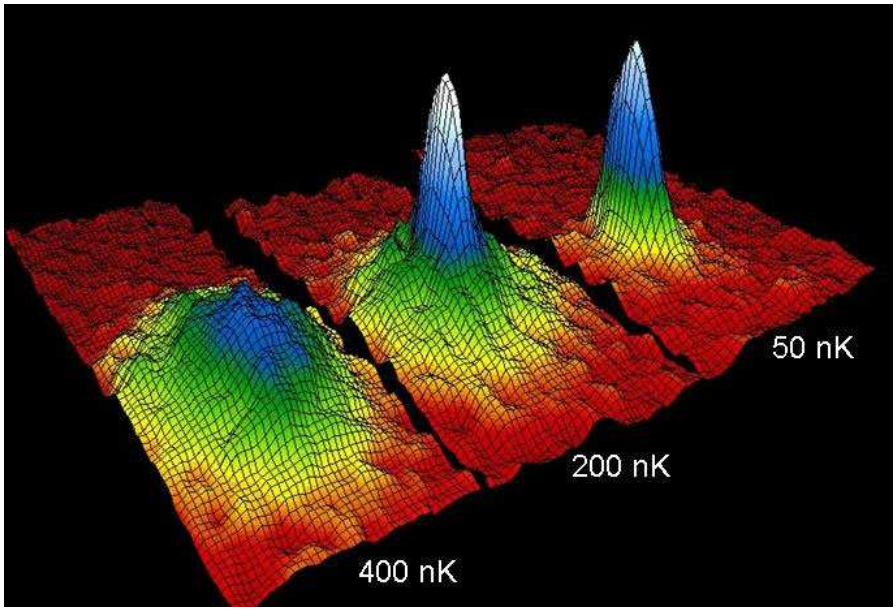

FIG. 1.1: Velocity distribution taken from JILA BEC Homepage [12]. The respective temperature is established by fitting two Gauss functions to the data, one for the thermal background and one for the condensate.

was observed below a certain critical temperature, providing a clear signature for BEC, as shown in Figure 1.1. Over the last years these systems have been the subject of a research explosion, which has taken place both experimentally and theoretically. Many different fields of physics like atomic collision, quantum optics, condensed matter or even astrophysics contributed ideas and problems to these specific systems displaying the attractiveness of BEC for researchers. Perhaps the most fascinating aspect of BEC is the possibility of describing about thousands to millions of atoms with a single wave function. As a consequence of this, quantum effects of a single atom which are essentially invisible may be spectacularly amplified up to a macroscopic level. An example is the phenomenon of superfluidity and not minor spectacular is the interference of two BEC's exhibiting the wave character of particles, see Figure 1.2. This property makes quantum mechanics nearly touchable and will certainly keep this field interesting for years.

1.2 What is BEC?

Bose-Einstein condensation is based on the indistinguishability and wave nature of particles, which are both basic concepts of quantum mechanics. Defining the phenomenon of Bose-Einstein condensation in one sentence, one could say, it is the occupation of the quantum mechanical ground state by a large number of particles. The words "large number" imply that the particles are assumed to be bosons, satisfying the Bose-Einstein statistics allowing arbitrary many particles to occupy one single quantum state. Fermions satisfy the Fermi-Dirac statistics and obey the Pauli exclusion principle, which does not allow the occupation of any single quantum state by more than one particle. To specify what is large enough, one has to look at the approximations used to describe the system.
If many particles are in the same quantum state, these particles display state coherence. Coherence occurs when the particles are strongly correlated with each other. The state coherence may be understood applying the de Broglie duality to an ensemble of atoms in thermal equilibrium at a temperature T. In a simplified picture, atoms in a gas may be regarded as wave packets

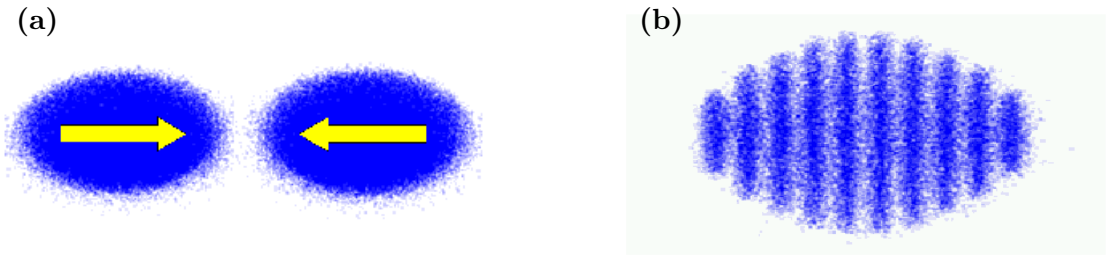

FIG. 1.2: Interference pattern of two BEC's displaying the wave nature of matter, taken from [13]. Wave-like behavior can be observed, for instance: (a) when two condensate clouds come together, (b) regular patterns of high and low density appear, where these 'matter waves' interfere constructively or destructively. This was experimentally proven in 1997 [14] and recently for an array of independent condensates in 2004 [15].

with an extension of the order of the thermal de Broglie wavelength which is

$$\lambda_T = \sqrt{\frac{2\pi\hbar^2}{Mk_BT}} \tag{1.1}$$

for an atom of mass M with a thermal energy k_BT. The thermal wavelength λ_T can be regarded as the position uncertainty associated with the thermal momentum distribution, which increases by lowering the temperature. Atoms become correlated with each other when their related waves "overlap", that is when λ_T gets comparable to the inter-atomic separation d: $\lambda_T \gtrsim d$. Then, the indistinguishability of particles becomes important, see Figure 1.3. At this temperature, bosons undergo a phase transition and form a Bose-Einstein condensate. More precisely, if we put free bosons in a volume V, the average atomic density $n = N/V$ for N atoms is related to the mean interatomic distance d through the equality $nd^3 = 1$. Inserting the correlation condition $\lambda_T \gtrsim d$ gives $n\lambda_T^3 \gtrsim 1$, which yields a relation between the temperature and the density:

$$T \lesssim \frac{2\pi\hbar^2}{Mk_B} n^{2/3} \,. \tag{1.2}$$

It tells us qualitatively that the state coherence or Bose-Einstein condensation may occur if the temperature is sufficiently low or the density of particles is sufficiently high.
Einstein considered an ideal, i.e. a non-interacting homogeneous, gas on the basis of the Bose-Einstein distribution

$$n(\mathbf{p}) = \frac{1}{\exp\left(\dfrac{\epsilon_{\mathbf{p}} - \mu}{k_BT}\right) - 1} \,, \tag{1.3}$$

describing the density of particles in the grand-canonical ensemble with a single-particle energy $\epsilon_{\mathbf{p}} = \mathbf{p}^2/2M$ for a momentum $\mathbf{p}$ and with a chemical potential μ. The total number of particles

$$N = \sum_{\mathbf{p}} n(\mathbf{p}) \tag{1.4}$$

defines the chemical potential for a given temperature. Assuming the thermodynamic limit, i.e. $N \to \infty$, $V \to \infty$ with $N/V = \text{const.}$, allows the replacement of the summation over $\mathbf{p}$ by an integral. The condensation into the state with $\mathbf{p} = \mathbf{0}$ begins, when the chemical potential approaches the ground-state energy $\epsilon_{\mathbf{0}}$, which defines the condensation temperature by (1.4) to

$$T_c = \frac{2\pi\hbar^2}{Mk_B} \left[\frac{n}{\zeta(3/2)}\right]^{2/3} \,, \tag{1.5}$$

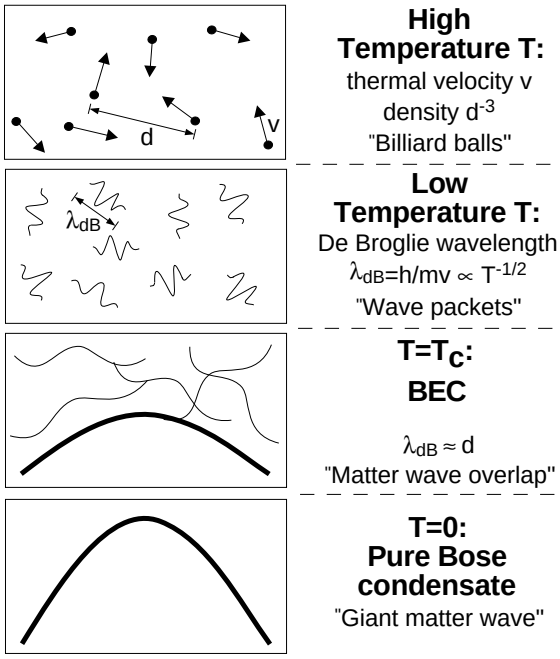

FIG. 1.3: Criterion for Bose-Einstein condensation, taken from Ref. [16]. At high temperatures atoms of a weakly interacting gas can be treated as hard balls. In the language of quantum mechanics the balls are wave packets with an extension $\lambda_{\rm dB} = \sqrt{\pi}\lambda_T$. BEC occurs at the temperature when λ_T becomes comparable to the mean distance between atoms. As the temperature approaches zero, the thermal cloud disappears leaving a pure Bose condensate.

where $\zeta(3/2) \approx 2.612$, so that T_c is about twice smaller than the right-hand side of inequality (1.2). The fraction of condensed particles, that is obtained by separating the number of particles occupying the ground state $n(\mathbf{0})$ from the sum in (1.4), is given by

$$n_0 = \frac{n(\mathbf{0})}{N} = 1 - \left(\frac{T}{T_c}\right)^{3/2}, \tag{1.6}$$

which is unity if T is zero. In an ideal gas, the Bose-Einstein condensed particles all occupy the same ground-state wave function, which is the product of $n(\mathbf{0})$ identical single-particle ground-state wave functions. This product of single-particle wave function is also called the condensate wave function or the macroscopic wave function. The condensate wave function of the single-particles is obtained from solving a non-linear Schrödinger equation, the so-called Gross-Pitaevskii equation.

Actually, the ideal gas does not exist since particles usually interact, at least "weakly". A system is called weakly interacting, if the characteristic interaction radius $r_{\rm int}$ is much shorter than the mean interparticle separation d: $r_{\rm int} \ll d$. As above, this can be written as $nr_{\rm int}^3 \ll 1$, therefore a weakly interacting system is called dilute. Considering a dilute gas, displaying Bose-Einstein condensation, one finds that the condensate fraction is smaller than unity at zero temperature. This phenomenon is termed depletion, one says that the interaction of particles depletes the condensate.

1.3 The System

The only necessary property for Bose-Einstein condensation is that the atoms are bosonic, which is not too restrictive: all stable elements have at least one bosonic isotope. The choice of an

	Temperature	Densities (cm^{-3})	Phase-Space density
Oven (heating)	500 K	10^{14}	10^{-13}
Laser cooling	50μK	10^{11}	10^{-6}
Evaporative cooling	500 nK	10^{14}	1
BEC	$\sim 0 - 500$ nK		10^{7}

Table 1.1: Multi-stage cooling to BEC, taken from Ref. [16]. Through a combination of optical and evaporative cooling, the temperature of a gas is reduced by a factor of 10^9, while the density at the BEC transition is similar to the initial density in the atomic oven (all numbers are approximate). In each step shown, the ground state population increases by about 10^6.

atom for a Bose condensation experiment is mainly determined by the trapping and cooling techniques. Magnetic trapping requires atoms with a strong magnetic moment and therefore unpaired electrons. Laser cooling is most efficient for atoms with strong transitions in the spectrum of the applied laser, hence in the visible or infrared region. So far, Bose-Einstein condensates have been realized with all alkali gases except francium. Very recently, in Stuttgart one has succeeded to realize Bose-Einstein condensation with chromium [17]. In contrast to alkali gases, chromium has in addition to the atomic interaction a non-vanishing dipole moment which influences the condensate.
For the densities realized in experiments, dilute alkali gases typically condense a la Bose-Einstein at temperatures around a few tens of nK up to some μK. To achieve the right conditions, the atoms must be cooled, trapped and compressed. In addition, the atoms must be thermally isolated from all material walls. This is done by trapping the atoms inside ultra high vacuum chambers with magnetic fields or with laser light. Such traps can store atoms for seconds and even minutes, which is enough time to condense and probe them.
It is clear that at these temperatures an atomic gas cannot be the stable thermodynamic state of N atoms, which would certainly corresponds to a solid. The formation of a solid requires as a first step the recombination of two atoms to form a diatomic molecule, and while this process is obviously exothermic, with formation energies around $0.4 - 1.2$ eV, it is very slow in the absence of a third atom to carry away the surplus energy, angular momentum, etc. Thus the dominant recombination processes are usually "three-body" ones. The rates per atom is typically $10^{-29} - 10^{-30}$ cm^6sec^{-1} [18] giving the sample the lifetime mentioned above.

1.3.1 Cooling the Sample

The elaborated cooling techniques involved in creating a Bose condensate are of minor importance for us, since the gas is assumed to be equilibrated at the realized temperature. Therefore, we just give a little sketch on the cooling steps and refer for the more technical details to [16,19] and the references therein.
Pre-cooling is a prerequisite for trapping because usually the atom traps are just a few mK deep. This is done by laser cooling in several steps leading to temperatures down to about $50\,\mu$K. Among other effects, Zeeman slowing [20] and Doppler molasses [21,22] are involved.
The pre-cooled atoms are transfered into a trap and further cooled by evaporative cooling. The evaporated atoms carry away more than the average energy, which means that the temperature of the remaining atoms decreases. Evaporative cooling is a phenomenon familiar to everyone, it is how coffee is cooled by blowing over the cup.

This is enough to achieve temperatures quite below the condensation temperature so that an almost pure condensate is obtainable. Table 1.1 shows how the temperature of the atoms decreases by a factor of a billion in these cooling processes.

1.3.2 Trapping Techniques

Atom traps fulfill two crucial roles in Bose-Einstein condensation: they keep the atoms tightly compressed during the cooling processes and confine the condensate for experimental studies. The requirements for the trap during the cooling are more stringent than they are for holding the condensate. For cooling, the trap needs a sufficiently high depth and a large volume to hold the pre-cooled cloud. Initially, this has been accomplished by combining magnetic trapping and evaporative cooling and we will concentrate on such configurations. After cooling, trap requirements are different, because the condensate is trapped more easily than hotter atoms. Consequently, the traps can be weaker and richer in properties, such as having a high anisotropy so that the condensate becomes quasi two or one dimensional. Traps with an additional anharmonicity have been created [1] to set the condensate into such a fast rotation that effectively the trapping potential became a Mexican-hat. Even a lattice structure of the trapping potential has been established with some lasers creating a standing wave [27]. The lattice provides a bunch of features to analyze such as tunneling processes or effects of random potentials.
However, the major role of the magnetic trap in Bose-Einstein condensation experiment is to confine the atoms and compress them to achieve high collision rates that makes evaporative cooling efficient. Magnetic traps favor atoms with a strong magnetic moment, such as alkali atoms, which have magnetic moments m in the order of a Bohr magneton due to their unpaired electron. The interaction of a magnetic dipole with an external magnetic field is given by $-\boldsymbol{\mu}_m\mathbf{B}$. The hyperfine levels in a magnetic field are $E(m_F) = g\mu_B m_F B$, where g is the nuclear g factor and m_F the quantum number of the projection of the total atomic spin $\mathbf{F} = \mathbf{J} + \mathbf{I}$ on the axis of the magnetic field $\mathbf{B}$.
If the system remains in one single m_F quantum state, the angle θ between the magnetic field $\mathbf{B}$ and the magnetic moment $\boldsymbol{\mu}_m$ is constant, giving an interaction energy $\boldsymbol{\mu}_m\mathbf{B} = \mu_m B\cos\theta$. This is in close analogy to the classical picture of fields and moments.
An atom trap requires a local minimum of the magnetic energy $E(m_F)$. States with $gm_F > 0$ minimize the magnetic energy in a local magnetic field minimum and are therefore called weak-field seeking states. States with $gm_F < 0$ requires a local maximum of the magnetic field to minimize $E(m_F)$, so they are termed high-field seeking states. Due to Maxwell's equations only a local magnetic field minimum is possible in free space so that only weak-field-seeking states can be trapped. The trap is only stable if the magnetic moments of atoms follow the direction of the magnetic field adiabatically. This means that the change of the direction of the magnetic field must be slower than the precession of the magnetic moment

$$\frac{\mathrm{d}\theta}{\mathrm{d}t} < \frac{\mu_m|\mathbf{B}|}{\hbar} = \omega_{\mathrm{Larmor}}\,. \tag{1.7}$$

The upper bound for $\mathrm{d}\theta/\mathrm{d}t$ in a magnetic trap is the trapping frequency. Because of this adiabatic condition there is no need to specify a direction of the magnetic field and we can concentrate on the magnitude of the field. So far, most magnetic traps used in Bose-Einstein condensation experiments are rotation-symmetric and are well approximated by

$$|\mathbf{B}(\mathbf{x})| = B_0 + \frac{1}{2}B_\perp r^2 + \frac{1}{2}B_z z^2\,, \tag{1.8}$$

where $\{r, z, \phi\}$ are cylindrical coordinates. Hence, the trapping potential can be re-written as

$$V_{\mathrm{trap}}(\mathbf{x}) = \mathrm{const} + \frac{M}{2}\omega_\perp^2 r^2 + \frac{M}{2}\omega_z^2 z^2\,, \tag{1.9}$$

where we have introduced the atom mass M and trap frequencies in an obvious way.

1.4 Paris Experiment

A fascinating experiment has been performed at the École Normale Supérieure (ENS) in Paris [1,2]. The group of Jean Dalibard succeeded in setting a Bose-Einstein condensate of ^{87}Rb atoms into fast rotation. In this regime a dramatic change occurs in the appearance of the quantum gas. Due to centrifugal forces the rotation changes the shape of the trapping potential from parabolic to Mexican hat shape. Crucial for the achievement of such fast rotation speeds was a superimposed quartic potential to the magnetic trap. The Bose gas is confined in a magnetic trap to which a focused, off-resonant Gaussian laser beam is superimposed.
The additional laser propagates along the z-direction and creates a quartic potential via

$$U(r) = U_0 \exp\left(-\frac{2r^2}{\mathrm{w}^2}\right) \approx U_0 - \frac{2U_0}{\mathrm{w}^2} r^2 + \frac{2U_0}{\mathrm{w}^4} r^4 \,, \tag{1.10}$$

where $r^2 = x^2 + y^2$. The laser's waist is $\mathrm{w} = 25\,\mu$m and the constant $U_0 = k_B \times 90$ nK represents a shift of the energy scale. Approximation (1.10) is valid for $r \lesssim \mathrm{w}/2$. The magnetic trap V_m is well approximated by a harmonic potential

$$V_m(\mathbf{x}) = \frac{M}{2}\omega_\perp^{(0)2} r^2 + \frac{M}{2}\omega_z^2 z^2 \,, \tag{1.11}$$

where M is the atom mass and $\omega_\perp^{(0)}$, ω_z are trapping frequencies. Hence, the combined magnetic-laser trap can be written as

$$V_{\mathrm{ens}}(\mathbf{x}) = \frac{M}{2}\omega_\perp^2 r^2 + \frac{M}{2}\omega_z^2 z^2 + \frac{k}{4} r^4 \,, \tag{1.12}$$

which contains the following notations

$$\omega_\perp^2 = \omega_\perp^{(0)2} - \frac{4U_0}{M\mathrm{w}^2} \,, \qquad k = \frac{8U_0}{\mathrm{w}^4} \,. \tag{1.13}$$

The gas in this trap is cooled down to about 15 nK so that it is initially a quasi pure condensate. Then the condensate is set into rotation with another additional laser beam acting as a stirrer, which propagates along the z-direction and is the rotation axis. This stirring laser creates an anisotropic potential in the xy-plane which rotates with frequency Ω_{stir}. The rotation injects an angular momentum into the system and modifies the trap by centrifugal forces. In the corotating frame the trapping potential can be written as

$$V_{\mathrm{rot}}(\mathbf{x}, \Omega) = \frac{M}{2}(\omega_\perp^2 - \Omega^2) r^2 + \frac{M}{2}\omega_z^2 z^2 + \frac{k}{4} r^4 \,, \tag{1.14}$$

which is depicted in Figure 1.5 for different rotation speeds Ω. Hence, the first term of (1.14) changes sign if $\Omega > \omega_\perp$. For the critical rotation speed $\Omega = \omega_\perp$, the trap (1.14) is purely quartic in the radial component.
To exceed fast rotation speeds in the order of the trap frequency $\Omega \approx \omega_\perp$, two excitation phases are used. First the rotation frequency is chosen to be $\Omega_{\mathrm{stir}}^{(1)} \approx \omega_\perp/\sqrt{2}$, so that the stirring laser resonantly excites the transverse quadrupole mode of the condensate at rest. The duration of the first excitation is 300 ms and then the condensate relaxes in the trap for 400 ms.
At this rotation speed typically 15 vortices appear. In the second phase the stirrer creates a rotation frequency $\Omega_{\mathrm{stir}}^{(2)}$ close to or above $\omega_\perp$. It lasts for 600 ms, followed by 500 ms to equilibrate again. At this state about $3 \cdot 10^5$ atoms are in the trap. Due to the relaxation time the effective rotation frequency Ω might differ significantly from the excitation frequency Ω_{stir}. The effective rotation speed Ω is determined by analyzing the Thomas-Fermi distribution

$$n(\mathbf{x}) = \frac{M}{4\pi\hbar^2 a}[\mu - V_{\mathrm{rot}}(\mathbf{x}, \Omega)] \,, \tag{1.15}$$

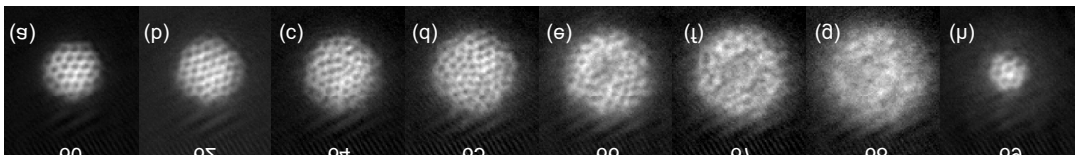

FIG. 1.4: Pictures of the rotating gas taken along the rotation axis, taken from Ref. [1]. The numbers below the pictures times 2π corresponds to the stirring frequency $\Omega^{(2)}_{\rm stirr}$ during the second phase of excitation. The real vertical size of each image is 306 μm.

where a is the s-wave scattering length and μ the chemical potential.
The act of probing is destructively by switching off the trap, letting the cloud expand during $t = 18$ ms and performing absorption imaging. For the quantitative analysis it is assumed that the expansion of the condensate out of the anharmonic trap is well approximated by the expansion of a condensate out of a harmonic trap where the initial distribution is scaled by a factor $(1 + \omega_\perp^2 t^2)^{1/2}$ [26]. Figure 1.4 shows pictures of the rotating condensate. With this procedure, effective rotation speeds have been realized from zero up to $\Omega \approx 1.04 \times \omega_\perp$.
At rotation speeds $\Omega \lesssim \omega_\perp$ a regular lattice of vortices is visible, which breaks for higher frequencies while the number of vortices seems to decrease. This is astonishing, since one usually assumes that the lattice structure is stable for all rotation frequencies and with higher rotation speeds the number of vortices just increases. To give some possible explanations, we note that the disordering of the lattice of vortices and the formation of a central hole for high rotation speeds might be interpreted as a melting process taking place with the developing of a double well. However, the determination of the effective rotation speed Ω, as described in the experiment [1], has shown that the visibility of vortices gets worse for increasing rotation speed. On the other hand, the central hole also might be interpreted as a giant vortex [23–25]. We summarize the experimental data of the experiment in the Table 1.2 To this end we introduce the harmonic oscillator length a_z as a length scale and an energy ϵ_z for the energy scale with respect to the z-component of the system, because the effective trapping frequency in the xy-plane changes with Ω while in z direction the trapping frequency is fixed. The scaling is given by

$$\epsilon_z = \hbar\omega_z \approx 7.291 \cdot 10^{-33}\,\mathrm{J}\,, \qquad a_z = \sqrt{\frac{\hbar}{M\omega_z}} \approx 3.245\,\mu\mathrm{m}\,, \tag{1.16}$$

with which we re-write (1.14) as

$$V_{\rm rot}(\mathbf{x}, \Omega) = \frac{\epsilon_z}{2}\left[\lambda^2\eta\frac{r^2}{a_z^2} + \frac{z^2}{a_z^2} + \frac{\kappa}{2}\frac{r^4}{a_z^4}\right], \tag{1.17}$$

where we have introduced the dimensionless parameters

$$\lambda = \omega_\perp/\omega_z \approx 6\,, \qquad \eta = 1 - \frac{\Omega^2}{\omega_\perp^2}\,, \qquad \kappa = \frac{k a_z^4}{\epsilon_z} \approx 0.4 \tag{1.18}$$

for the anisotropy, the rotation, and the anharmonicity, respectively.
In the beginning, when the condensate is at rest $\Omega = 0$, we have $\eta = 1$ and the anharmonicity κ is small compared to the anisotropy $\lambda^2\eta$. Then, the condensate is cigar shaped. The anisotropy of the xy-plane to the z-direction has been around $\lambda \approx 6$ with a residual anisotropy in the xy-plane <1%. For rotation speeds close to the critical rotation $\Omega \sim \omega_\perp$, the condensate was nearly spherical, and it remained stable for $\Omega \lesssim 1.05\,\omega$. Near the upper limit, the condensate exhibited a definite local minimum in the central density, confirming the Mexican hat shape of the trapping potential. .
With decreasing η the anharmonicity will not be small all the time compared to the anisotropy.

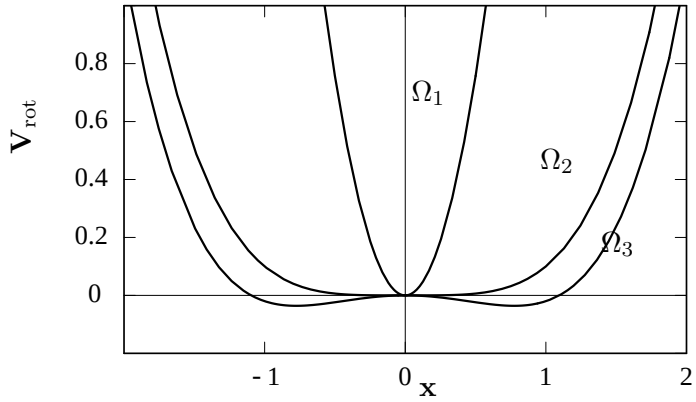

FIG. 1.5: Paris trap (1.17) in one direction of the xy-plane for the rotation speeds $\Omega_1 = 0$, $\Omega_2 = \omega_\perp$ and $\Omega_3 = 1.04 \times \omega_\perp$. The latter is the highest experimentally realized rotation speed.

It will become more and more important. Physical quantities show a strong dependence on the rotation speed Ω. Therefore, we choose it as a control parameter for the quantities which we analyze in this theses in order to illustrate the effect of rotation.

1.5 Thesis Plan

After this report on the fascinating experiment by Dalibard [1], we are prepared to give an overview of what we want to investigate in this theses. On the basis of the Paris experiment, we consider a rotating Bose gas in an anharmonic.
In Chapter 2 we discuss the thermodynamic properties of an ideal bosonic gas rotating in the anharmonic trap (1.17) as a grand-canonical ensemble. Since the gas is rotating, the rotation speed Ω enters explicitly in the Hamiltonian of the system and ends up in all quantities of interest as a variable control parameter. We analyze the critical temperature, at which the condensation process occurs, and the temperature dependence of the heat capacity, which is an indicator for the stability of the system. The parameters of the Paris experiment allow us to derive these quantities within the semiclassical approximation. In two special limits, namely as the rotation speed Ω tends to towards the critical value $\omega_\perp$, and a infinite fast rotation speed $\Omega \to \infty$, the results reduce to simple analytic expressions.
Furthermore, we investigate corrections to the critical temperature which are due to the finite size of the system and due to the interaction between the bosons. The interaction is assumed to be a two-body δ-interaction and is treated perturbatively. This is justified by the diluteness of the gas. Of course, both corrections depend on the rotation speed Ω.
Chapter 3 deals with the dynamics of the condensate at zero temperature. The coherent wave function Ψ of the condensed particles then obeys a non-linear Schrödinger equation, which has been found by Gross [29] and Pitaevskii [30]. The non-linearity accounts for the δ-interaction of the particles and is cubic in Ψ. We transform this equation into the corotating frame by a coordinate transformation which leads to an additional centrifugal force in the Hamiltonian. Analyzing in detail the transformed Gross-Pitaevskii equation, we discuss collective oscillations of the condensate, first in the hydrodynamic limit and second by a variational approach. To describe the oscillations in the hydrodynamic limit , i.e. the collective modes, we use the Thomas-Fermi approximation, which neglects the kinetic energy of the particles . The variational approach does not make use of this approximation but reproduces the results of the hydrodynamic collec-

mass of rubidium ^{87}Rb	$M = 1.445 \cdot 10^{-25}$ kg	
number of condensed particles	$N = 3 \cdot 10^5$	
s-wave scattering length	$a = 5.2$ nm	a=$1.6 \cdot 10^{-3}\, a_z$
trap frequency (z direction)	$\omega_z = 2\pi \cdot 11.0$ Hz	
trap frequency (xy plane)	$\omega_\perp = 2\pi \cdot 65.6$ Hz	$\omega_\perp = 5.96\, \omega_z$
anharmonicity (xy plane)	$k = 2.6(3) \cdot 10^{11}$ Jm^{-4}	$k = 0.39\, \epsilon_z / a_z^4$
rotation speed variation	$\Omega = 0 \ldots 68$	$\Omega = 0 \ldots 1.04\, \omega_\perp$
energy shift from laser	$U_0 = 90\ k_B$nK	$U_0 = 17\, \epsilon_z$
laser's waist	w $= 25\ \mu$m	w $= 7.7\, a_z$

Table 1.2: List of data. The values are taken from the experiment of Bretin [1].

tive modes in the limit of a strong δ-interaction, which means that the kinetic energy is small compared to the interaction energy.
Finally, in Chapter 4, we draw conclusions and discuss some perspectives for future investigations.

Chapter 2

Thermodynamic Properties of Bose Gases in Traps

To simplify calculations, we shall assume an infinite number of particles to be present (thermodynamic limit), although the experimental situation is different. This means, we determine the quantities of interest within the grand-canonical ensemble. In experiments the number of particles N within a trap is large but finite, it is about some hundred thousands. Therefore, the thermodynamic limit $N \to \infty$ is never reached. However, the results found in this way agree astonishingly well with the experiments. We determine the critical temperature at which the condensation of the Bose gas into its ground state begins within the semiclassical approximation as well as he heat capacity of the gas, which characterizes the order of the phase transition according to the Ehrenfest definition. We elaborate the known discussion for an ideal Bose gas in a harmonic trap, so that we can establish the same for a Bose gas in an anharmonic rotating trap. The finite-size effect is considered for the harmonically trapped Bose gas and we compare the semiclassical approximation in the low temperature limit with an exact calculation. Finally, we discuss the perturbative influence of a weak two particle δ-interaction in dilute gases.

2.1 Grand-Canonical Ensemble

In the grand-canonical ensemble, one describes an open system which exchanges both particles and energy with the environment. It is characterized by the grand-canonical partition function which is determined by the microstates ν of the system. The states are characterized through the population $n_{\mathbf{n}}$ of the one-particle states $\mathbf{n}$:

$$\nu = (n_{\mathbf{n}})\,. \tag{2.1}$$

Since the particles of an ideal gas are not interacting, the energy E_ν and the number of particles N_ν of the microstate ν are given by the sum of the one-particle energies $E_{\mathbf{n}}$ and the occupation numbers $n_{\mathbf{n}}$:

$$E_\nu = \sum_{\mathbf{n}} n_{\mathbf{n}} E_{\mathbf{n}}\,, \qquad N_\nu = \sum_{\mathbf{n}} n_{\mathbf{n}}\,. \tag{2.2}$$

Thus, the grand-canonical partition function reads

$$\mathcal{Z}_G = \sum_{\nu} e^{-\beta(E_\nu - \mu N_\nu)} = \prod_{\mathbf{n}} \sum_{n_{\mathbf{n}}} e^{-\beta n_{\mathbf{n}}(E_{\mathbf{n}} - \mu)}\,, \tag{2.3}$$

where $\beta = 1/k_B T$ is an inverse temperature. For the grand-canonical partition function (2.3) being finite we have to obey $E_{\mathbf{n}} \geq E_{\mathbf{0}} > \mu$. The energy in the exponential of (2.3) depends on

the energy of the microstate E_ν and the energy of the exchanged particles μN_ν. The quantum of energy μ corresponds to the exchange of one particle which is taken from ($\mu > 0$) or given to ($\mu < 0$) the environment. This distinguishes the grand-canonical from the canonical ensemble, where no particles can be exchanged. Hence, there is no chemical potential in the latter ensemble .

The grand-canonical free energy is related to the grand-canonical partition function $\mathcal{Z}_G$ (2.3) according to

$$\mathcal{F}_G = -\frac{1}{\beta} \ln \mathcal{Z}_G \,. \tag{2.4}$$

The grand-canonical free energy $\mathcal{F}_G$ obeys the thermodynamic relation

$$\mathcal{F}_G = U - TS - \mu N \ . \tag{2.5}$$

Here U denotes the internal energy, T the temperature, S the entropy, μ the chemical potential, and N the number of particles. For thermodynamic processes the total differential of the grand-canonical free energy $\mathcal{F}_G = \mathcal{F}_G\,(T, V, \mu)$ is given by

$$\mathrm{d}\mathcal{F}_G = -S\mathrm{d}T - p\mathrm{d}V - N\mathrm{d}\mu \,. \tag{2.6}$$

If the grand-canonical free energy is known, it determines the entropy S, the pressure p, and the number of particles N according to

$$S(T,V,\mu) = -\left.\frac{\partial \mathcal{F}_G(T,V,\mu)}{\partial T}\right|_{V,\mu} , \tag{2.7}$$

$$p(T,V,\mu) = -\left.\frac{\partial \mathcal{F}_G(T,V,\mu)}{\partial V}\right|_{T,\mu} , \tag{2.8}$$

$$N(T,V,\mu) = -\left.\frac{\partial \mathcal{F}_G(T,V,\mu)}{\partial \mu}\right|_{T,V} . \tag{2.9}$$

Furthermore the internal energy U allows to calculate the heat capacity at constant volume V

$$C_V = \left.\frac{\partial U}{\partial T}\right|_{N,V} . \tag{2.10}$$

It is related to the grand-canonical free energy according to

$$C_V = \left.\frac{\partial \mathcal{F}_G}{\partial T}\right|_{N,V} + S + T \left.\frac{\partial S}{\partial T}\right|_{N,V} + N \left.\frac{\partial \mu}{\partial T}\right|_{N,V} . \tag{2.11}$$

Inserting the grand-canonical partition function (2.3) into the free energy (2.4) we obtain

$$\mathcal{F}_G = -\frac{1}{\beta} \sum_{\mathbf{n}} \ln \left[\sum_{n_\mathbf{n}} e^{-\beta n_\mathbf{n} (E_\mathbf{n} - \mu)} \right] . \tag{2.12}$$

Since the occupation number for bosons may be any natural number $n_\mathbf{n} = 0, 1, 2, \ldots$ the geometric series in (2.12) can be evaluated and yields

$$\mathcal{F}_G = \frac{1}{\beta} \sum_{\mathbf{n}} \ln \left[1 - e^{-\beta (E_\mathbf{n} - \mu)} \right] . \tag{2.13}$$

If we consider the limit $\mu \uparrow E_\mathbf{0}$, the first term diverges, while all other terms of the sum are finite. To further investigate this term, we separate it from the sum:

$$\mathcal{F}_G = \frac{1}{\beta} \ln \left[1 - e^{-\beta (E_\mathbf{0} - \mu)} \right] + \frac{1}{\beta} \sum_{\mathbf{n} \neq \mathbf{0}} \ln \left[1 - e^{-\beta (E_\mathbf{n} - \mu)} \right] . \tag{2.14}$$

Let us consider the number of particles (2.9), which reads:

$$N = \frac{1}{e^{\beta(E_{\mathbf{0}}-\mu)}-1} + \sum_{\mathbf{n}\neq\mathbf{0}} \frac{1}{e^{\beta(E_{\mathbf{n}}-\mu)}-1}\,. \tag{2.15}$$

The first term in Eq. (2.15) also diverges if $\mu \uparrow E_{\mathbf{0}}$, while the second is finite. This means that the ground state is more and more populated when the chemical potential tends to the ground-state energy. Hence, we state that the ground state is occupied by a number of particles

$$N_{\mathbf{0}} = \frac{1}{e^{\beta(E_{\mathbf{0}}-\mu)}-1}\,, \tag{2.16}$$

which needs not necessarily to be finite as we work in the grand-canonical ensemble. Then, the sum in (2.15) yields the number of particles N_e occupying the excited states $\mathbf{n} \neq \mathbf{0}$. Thus, the total number of particles decomposes to

$$N = N_{\mathbf{0}} + N_e\,. \tag{2.17}$$

Quantities derived in the grand-canonical ensemble always have to be associated with the thermodynamic limit to provide results independently from the number of particles. The limit is taken by assuming a process where the number of particles N tends to infinity without changing the characteristics of the ensemble. In the thermodynamic limit, Eq. (2.17) implies that the fraction of ground state particles

$$\frac{N_{\mathbf{0}}}{N} = 1 - \frac{N_e}{N} \tag{2.18}$$

vanishes for $\mu < E_{\mathbf{0}}$ and is a finite quantity for $\mu = E_{\mathbf{0}}$. This means that the number of particles occupying the ground state is finite, if $\mu < E_{\mathbf{0}}$, or of the order of N, if $\mu = E_{\mathbf{0}}$. If $N_{\mathbf{0}}$ is of the order of N, it is termed to be macroscopically large and the phenomenon of having a macroscopically amount of particles in the ground state is called Bose-Einstein condensation.
Analogously to the number of Particles (2.17) we write for the grand-canonical free energy (2.14)

$$\mathcal{F}_G = \mathcal{F}_{\mathbf{0}} + \mathcal{F}_e\,, \tag{2.19}$$

where we have introduced the notation

$$\mathcal{F}_{\mathbf{0}} = \frac{1}{\beta}\ln\left[1 - e^{-\beta(E_{\mathbf{0}}-\mu)}\right], \qquad \mathcal{F}_e = \frac{1}{\beta}\sum_{\mathbf{n}\neq\mathbf{0}} \ln\left[1 - e^{-\beta(E_{\mathbf{n}}-\mu)}\right]. \tag{2.20}$$

Similarly, we consider the entropy to decompose to $S = S_{\mathbf{0}} + S_e$ and derive with (2.7) and (2.19) the ground state entropy $S_{\mathbf{0}}$ according to

$$S_{\mathbf{0}} = -k_B \ln\left[1 - e^{-\beta(E_{\mathbf{0}}-\mu)}\right] + \frac{E_{\mathbf{0}} - \mu}{T[\,e^{\beta(E_{\mathbf{0}}-\mu)} - 1]}\,. \tag{2.21}$$

Inserting (2.16) and (2.19) into (2.21) leads to

$$\mathcal{F}_{\mathbf{0}} = -TS_{\mathbf{0}} + N_{\mathbf{0}}(E_{\mathbf{0}} - \mu)\,. \tag{2.22}$$

At $T = 0$, all particles of the system are supposed to occupy the ground state and the entropy vanishes according to the third law of thermodynamics. Therefore, it is reasonable to say that the ground-state entropy $S_{\mathbf{0}}$ does not contribute to the total entropy of the system. Hence, the grand-canonical free energy (2.14) reads with (2.22)

$$\mathcal{F}_G = N_{\mathbf{0}}\,(E_{\mathbf{0}} - \mu) + \frac{1}{\beta}\sum_{\mathbf{n}\neq\mathbf{0}} \ln\left[1 - e^{-\beta(E_{\mathbf{n}}-\mu)}\right]. \tag{2.23}$$

Within the thermodynamic limit, we have neglected in fact the contribution of the ground state to the free energy (2.19), since either $N_{\mathbf{0}} = 0$ or $\mu = E_{\mathbf{0}}$.

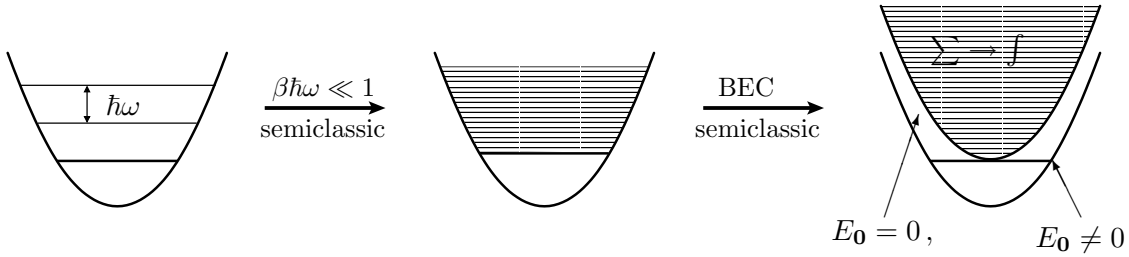

FIG. 2.1: Schematic view of the semiclassical approximation a la Bose-Einstein. For a better visibility, the ground state is not correctly mirrored, since it is $\hbar\omega/2$. From the left to the right we note that the level spacing is small in the trap. The usual semiclassical or Thomas-Fermi approximation is to take the limit $\hbar \to 0$ and to integrate over the phase-space. However, the integral treats the ground-state energy as a zero. The Bose-Einstein semiclassical approximation consists in separating the ground state from the integral, which in fact is not zero.

2.2 Semiclassical Approximation

Our goal now is to evaluate the grand-canonical free energy (2.14) within some approximations. The semiclassical approximation, roughly speaking, corresponds to the conversion of a sum into an integral. The name "semiclassical" arises from the analogy to classical mechanics. In classical mechanics the energy levels of a bounded system are continuous, so that the grand partition function (2.3) is a sum of infinitesimal small steps. Such a sum can be converted into a Riemann-Stieltjes integral that is defined on a closed interval $[a, b]$ for real-valued bounded functions $f(x)$ and $\alpha(x)$ by the Riemann sum

$$\int_a^b f(x)\,\mathrm{d}\alpha(x) := \sum_{i=0}^{N-1} f(\xi_i)\,[\alpha(x_{i+1}) - \alpha(x_i)] \tag{2.24}$$

for a partition by points $a = x_0 < x_1 < ... < x_N = b$ and with $\xi_i \in [x_i, x_{i+1}]$ and $f(x) \in C^1[x_0, x_N]$, if the sum tends to a fixed number I as $\max(x_{i+1} - x_i) \to 0$.
The new feature in quantum mechanics is that in a bounded system the energy levels are discrete and can be labeled with quantum numbers. For instance, a point particle trapped in a harmonic one-dimensional potential $V(x) = M\omega^2 x^2/2$, has the well-known energy eigenvalues $E_n = \hbar\omega(n + 1/2)$, see Figure 2.1. Beside this discrete and equidistant levels, there is another important difference between classical and quantum mechanics. The ground state $E_{\mathbf{0}}$ lies classically at the minimum of the trapping potential, which means that the particle is at rest. But in quantum mechanics this is not possible, because of the Heisenberg uncertainty principle. In fact the ground state is shifted a little.
If the level spacing is a small quantity, i.e for the harmonic trap this implies $\beta\hbar\omega \ll 1$, it is reasonable to apply the semiclassical approximation and integrate according to (2.24)

$$\mathcal{F}_{\mathrm{sc}} = N_{\mathbf{0}}(\mu_c - \mu) + \frac{1}{\beta}\int \frac{\mathrm{d}^3x\,\mathrm{d}^3p}{(2\pi\hbar)^3}\,\ln\left\{1 - e^{-\beta[H(\mathbf{p},\mathbf{x})-\mu]}\right\}, \tag{2.25}$$

where we have replaced the the ground-state energy $E_{\mathbf{0}}$ by the semiclassical critical chemical potential μ_c at which the condensation develops. By this, we take into account that the ground state does not contribute to the grand-canonical free energy. We have also identified the energy eigenvalues with the Hamiltonian of the system which reads in the standard notation

$$H(\mathbf{p}, \mathbf{x}) = \frac{\mathbf{p}^2}{2M} + V(\mathbf{x})\,, \tag{2.26}$$

where $\mathbf{p}$ denotes the momentum and V an external potential. However, the inverse temperature is involved in the smallness condition so that the semiclassical approximation gets worse with decreasing temperature and fails in the limit $T \downarrow 0$.
In general, regarding (2.12), all one needs to calculate the grand-canonical free energy is to know the energy eigenvalues of the one-particle Hamiltonian H. But within the semiclassical approximation one only needs to verify that the level spacing is small compared to the thermal energy.

2.3 Finite-Size Correction

One would like to know whether the semiclassical approximation is appropriate or not. Surely, one can test it afterwards by comparing the results with numerical ones or with experimental data. But obviously, one can expect this approximation to be suitable, if the condition of the average level spacing is fulfilled.
For having a more mathematical argument, we remark that in general sums can be transformed into more manageable sums or integrals [31–33]. One method is called partial summation, that is transforming the sum into a Riemann-Stieltjes integral and then integrate by parts. In this way one derives [34] the Euler-MacLaurin summation formula [35]

$$\begin{aligned}\sum_{a\le k\le b} f(k) &= \int_a^b \mathrm{d}t\, f(t) + \frac{1}{2}\left[f(a)+f(b)\right] + \sum_{m=1}^{n} \frac{B_{2m}}{(2m)!}\left[f^{(2m-1)}(b) - f^{(2m-1)}(a)\right] \\ &\quad + \int_a^b \mathrm{d}t\, P_{2n+1}(t) f^{(2n+1)}(t)\,. \end{aligned} \tag{2.27}$$

Here $n \ge 0$ is a fixed integer, $f(x) \in C^{2n+1}[a,b]$, B_m denotes the mth Bernoulli number and P_m is the mth periodic Bernoulli function defined by $P_m(x) = B_m(x - [x])$. Here $B_m(x)$ is the mth Bernoulli polynomial following from

$$\frac{ze^{xz}}{e^z - 1} = \sum_{m=0}^{\infty} B_m(x)\frac{z^m}{m!} \qquad (|z| < 2\pi), \tag{2.28}$$

so that $B_m = B_m(0)$, $B_1(x) = x - 1/2$, $B_2(x) = x^2 - x + 1/6$, and so on. The bracket [...] in the Bernoulli polynomials denotes the floor function.
We provide a prove of the Euler-MacLaurin formula (2.27) in the Appendix A. Comparing with the semiclassical approach, we see that the first term of (2.27) is identical with the semiclassic, so that the reminder terms can be regarded as corrections.

2.4 Bose Gas in Harmonic Trap

We consider a harmonic trap of the form

$$V(\mathbf{x}) = \frac{M}{2}\left(\omega_x^2 x^2 + \omega_y^2 y^2 + \omega_z^2 z^2\right)\,. \tag{2.29}$$

Most magnetic traps used in experiments are well approximated by such a harmonic potential. The trap frequencies $f_i = \omega_i/2\pi$ with $i = 1, 2, 3$ typically are of the order of 100 Hz. The spacing of the energy levels $h\bar{f}$, with the arithmetic mean $\bar{f} = (f_1 + f_2 + f_3)/3$, is small compared to the typical temperature $T = 100$ nK at which the condensation begins:

$$\frac{h\bar{f}}{k_B T} \approx 0.048 \ll 1\,. \tag{2.30}$$

Therefore, the semiclassical approximation is applicable and we calculate thermodynamic quantities from the grand-canonical free energy (2.25). With the Taylor series of the logarithm for

$$\ln(1-z) = -\sum_{j=1}^{\infty} \frac{z^j}{j} \tag{2.31}$$

and the Hamiltonian (2.26) and (2.29), we find for the grand-canonical free energy

$$\mathcal{F}_G = N_{\mathbf{0}}(\mu_c - \mu) - \sum_{j=1}^{\infty} \frac{1}{\beta j} \int \frac{\mathrm{d}^3x\, \mathrm{d}^3p}{(2\pi\hbar)^3} \exp\left\{-\beta j \left[\frac{\mathbf{p}^2}{2M} + \frac{M}{2}\left(\omega_x^2 x^2 + \omega_y^2 y^2 + \omega_z^2 z^2\right) - \mu\right]\right\}. \tag{2.32}$$

Thus, performing the Gaussian integrals leads to

$$\mathcal{F}_G = N_{\mathbf{0}}(\mu_c - \mu) - \frac{1}{\beta(\beta\hbar\tilde{\omega})^3} \sum_{j=1}^{\infty} \frac{e^{j\beta\mu}}{j^4}, \tag{2.33}$$

where $\tilde{\omega} = (\omega_x\omega_y\omega_z)^{1/3}$ is the geometric average of the trap frequencies. We can shorten the notation by generalizing the Riemann zeta-function

$$\zeta(\nu) := \sum_{j=1}^{\infty} \frac{1}{j^\nu} \tag{2.34}$$

to the polylogarithmic function

$$\zeta_\nu(z) := \sum_{j=1}^{\infty} \frac{z^j}{j^\nu}. \tag{2.35}$$

Then, the grand-canonical free energy takes the form

$$\mathcal{F}_G = N_{\mathbf{0}}(\mu_c - \mu) - \frac{\zeta_4(e^{\beta\mu})}{\beta(\beta\hbar\tilde{\omega})^3}. \tag{2.36}$$

2.4.1 Critical Temperature and Heat Capacity

In the semiclassical approximation of the grand-canonical free energy (2.36) the number of particles in the ground state is zero unless $\mu = \mu_c$. So the population of the ground state starts at a critical point, which defines a critical temperature. Therefore, we determine the number of particles N according to the thermodynamic relation (2.9)

$$N = N_{\mathbf{0}} + \frac{\zeta_3(e^{\beta\mu})}{(\beta\hbar\tilde{\omega})^3}, \tag{2.37}$$

and assume a temperature $T \geq T_c$, so that $N_{\mathbf{0}} = 0$. If we consider the limit $\mu \uparrow \mu_c = 0$, Eq. (2.37) defines the critical temperature T_c as

$$T_c = \frac{\hbar\tilde{\omega}}{k_B}\left(\frac{N}{\zeta(3)}\right)^{1/3} \approx 0.72\left(\frac{\tilde{\omega}}{100\,\mathrm{Hz}}\right) N^{1/3}\,\mathrm{nK}. \tag{2.38}$$

The proportionality to $N^{1/3}$ is remarkable, because it is problematic in the limit of $N \to \infty$. In order to observe Bose-Einstein condensation, we have to define a proper thermodynamic limit:

$$N \to \infty, \qquad \tilde{\omega} \to 0, \qquad N\tilde{\omega}^3 < \infty. \tag{2.39}$$

With this definition the transition temperature (2.38) is well defined in the thermodynamic limit. In the limit $\tilde{\omega} \to 0$ we expect to recover the results of the free gas. Considering the harmonic oscillator length $a_{\tilde{\omega}} = \sqrt{\hbar/M\tilde{\omega}}$ as the scale for the elongation of the condensate we obtain

$$\frac{N}{V} = \frac{N}{a_{\tilde{\omega}}^3} \propto N\tilde{\omega}^{3/2} \,. \tag{2.40}$$

This is, of course, a consequence of the fact that the Bose gas in a harmonic trap condenses in the phase-space, not in real space, whereas the free particles are said to condense in the momentum space. Inserting (2.38) into (2.37) one gets the T dependence of the condensate fraction for $T < T_c$:

$$\frac{N_{\mathbf{0}}}{N} = 1 - \left(\frac{T}{T_c}\right)^3 \,. \tag{2.41}$$

Relation (2.37) can also define a critical number of particles N_c at a given temperature T:

$$N_c = \zeta(3)\left(\frac{k_B}{\hbar\tilde{\omega}}\right)^3 T^3 \approx 2.7\left(\frac{100\,\mathrm{Hz}}{\tilde{\omega}}\right)^3 T^3/(\mathrm{nK})^3 \,. \tag{2.42}$$

It is interesting to express the critical temperature (2.38) in terms of the particle density at the origin $\mathbf{x} = \mathbf{0}$, which is at the critical point $\mu = 0$ due to (2.9) and (2.32)

$$N(\mathbf{0}) = \zeta(3/2)\left(\frac{k_B T_c}{2\pi\hbar\tilde{\omega}}\right)^{3/2} \,. \tag{2.43}$$

From this we obtain with $n_{\mathrm{o}}(\mathbf{0}) = N(\mathbf{0})/a_{\tilde{\omega}}^3$

$$k_B T_c = \frac{2\pi\hbar^2\tilde{\omega}}{\tilde{\omega}M}\left[\frac{n_{\mathrm{o}}(\mathbf{0})}{\zeta(3/2)}\right]^{2/3} = \frac{2\pi\hbar^2}{M}\left[\frac{n_{\mathrm{o}}(\mathbf{0})}{\zeta(3/2)}\right]^{2/3} \,. \tag{2.44}$$

Comparing this with the critical temperature of the free Bose gas (1.5), we see that they coincide. Therefore, the condensation begins at the origin of the trap, when the critical density of the free gas is reached.

In order to determine the temperature dependence of the heat capacity (2.11) we have to discuss the two regimes $T < T_c$ and $T > T_c$ separately. We begin the discussion with the latter regime. The grand-canonical free energy (2.36) reduces to

$$\mathcal{F}_G = -\frac{\zeta_4(e^{\beta\mu})}{\beta(\beta\hbar\tilde{\omega})^3} \,, \tag{2.45}$$

so the particle number (2.7) reads

$$N = \frac{\zeta_3(e^{\beta\mu})}{(\beta\hbar\tilde{\omega})^3} \tag{2.46}$$

and the entropy (2.9) is given by

$$S = k_B\left[\frac{\zeta_4(e^{\beta\mu})}{(\beta\hbar\tilde{\omega})^3} - \beta\mu\frac{\zeta_3(e^{\beta\mu})}{(\beta\hbar\tilde{\omega})^3}\right] \,. \tag{2.47}$$

For the internal energy (2.5) we get

$$U = -3\mathcal{F}_G \,. \tag{2.48}$$

Therefore, we can determine the heat capacity from (2.10) to be

$$\frac{C_V}{k_B} = 12\frac{\zeta_4(e^{\beta\mu})}{(\beta\hbar\tilde{\omega})^3} + \frac{3}{(\beta\hbar\tilde{\omega})^3}\left.\frac{\partial(\beta\mu)}{\partial T}\right|_{N,V}\left[\frac{\partial\zeta_4(e^{\beta\mu})}{\partial(\beta\mu)}\right] \,. \tag{2.49}$$

The inner derivative is obtained via deriving (2.46) with respect to T for constant N and V, which means constant $\tilde{\omega}$. This yields

$$0 = 3\frac{k_B}{\beta^2(\hbar\tilde{\omega})^3}\zeta_3(e^{\beta\mu}) + \frac{\zeta_2(e^{\beta\mu})}{(\beta\hbar\tilde{\omega})^3}\left.\frac{\partial(\beta\mu)}{\partial T}\right|_{N,V}, \tag{2.50}$$

so that we find

$$\left.\frac{\partial(\beta\mu)}{\partial T}\right|_{N,V} = -3k_B\beta\frac{\zeta_3(e^{\beta\mu})}{\zeta_2(e^{\beta\mu})}. \tag{2.51}$$

Inserting this into (2.49) and using (2.46) leads to

$$\frac{C_V}{k_BN} = 12\frac{\zeta_4(e^{\beta\mu})}{\zeta_3(e^{\beta\mu})} - 9\frac{\zeta_3(e^{\beta\mu})}{\zeta_2(e^{\beta\mu})}. \tag{2.52}$$

In the high temperature limit $T \to \infty$ the ζ-functions are approximated by $\zeta_\nu(e^{\beta\mu}) \approx e^{\beta\mu} \ll 1$, so that the heat capacity (2.52) obeys the Dulong-Petit law for the three-dimensional harmonic oscillator

$$\lim_{T\to\infty}\frac{C_V}{k_BN} = 3. \tag{2.53}$$

At the critical point $\mu_c = 0$ we get

$$\lim_{T\downarrow T_c}\frac{C_V}{k_BN} = 12\frac{\zeta(4)}{\zeta(3)} - 9\frac{\zeta(3)}{\zeta(2)} \approx 4.228. \tag{2.54}$$

Secondly, we have to discuss the case $T < T_c$. From the grand-canonical free energy (2.36) we know that the condensed particles do not contribute to the free energy, since $\mu = \mu_c$ for $T < T_c$. Therefore, the internal energy U (2.48) still holds and simplifies by inserting $\mu_c = 0$ and the number of particles (2.37) with $N_{\mathbf{0}} = 0$ to

$$U = 3k_BT_cN\frac{\zeta(4)}{\zeta(3)}\left(\frac{T}{T_c}\right)^4, \tag{2.55}$$

so that the heat capacity becomes

$$\frac{C_V}{k_BN} = 12\frac{\zeta(4)}{\zeta(3)}\left(\frac{T}{T_c}\right)^3. \tag{2.56}$$

At the critical point $T = T_c$ we now have

$$\lim_{T\uparrow T_c}\frac{C_V}{k_BN} = 12\frac{\zeta(4)}{\zeta(3)} \approx 10.805. \tag{2.57}$$

Hence, the heat capacity is discontinuous and we denote the jump at the critical temperature by

$$\mathrm{Dis} = \lim_{T\uparrow T_c}\frac{C_V}{k_BN} - \lim_{T\downarrow T_c}\frac{C_V}{k_BN} \approx 6.577. \tag{2.58}$$

The discontinuity at the critical point characterizes the phase transition to be of second order according to the Ehrenfest definition. Furthermore, we observe that the heat capacity (2.56) obeys the third law of thermodynamics, which demands a vanishing heat capacity at zero temperature.

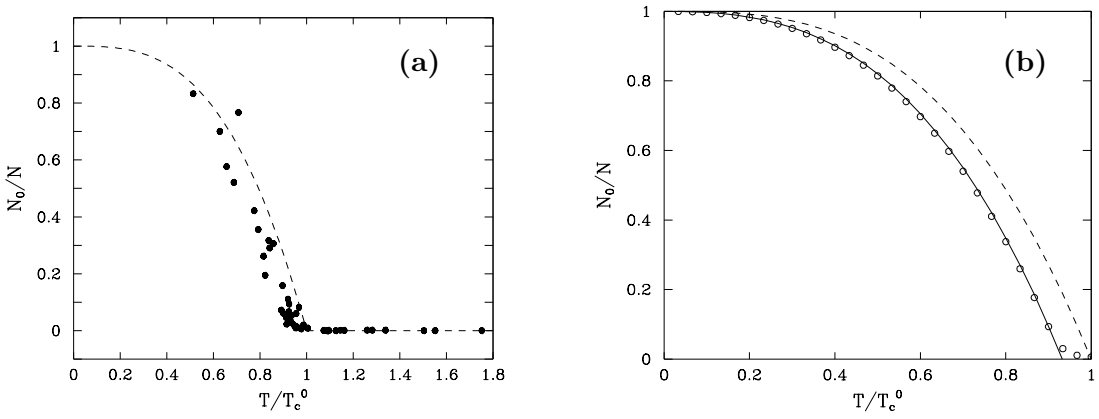

FIG. 2.2: Condensate fraction versus reduced temperature. Both pictures are taken from [55].(a) Circles are the experimental results of Ensher et al. [37], while the dashed line is Eq. (2.41). (b) The circles corresponds to the exact quantum calculation for $N = 1000$ atoms in a trap with spherical symmetry and the solid line to the finite-size corrected Eq. (2.64). The dashed line refers to the thermodynamic limit (2.41).

2.4.2 Finite-Size Correction

The number of atoms N that can be put into the traps is not truly macroscopic. In most experiments they range between about 10^5 and 10^7 atoms. Consequently, the thermodynamic limit $N \to \infty$, in which the micro-canonical, canonical and grand-canonical ensembles are supposed to provide the same results, is never reached exactly and their equivalence is not ensured. Therefore, we have to consider finite-size corrections.
It is also possible to carry out an exact calculation of the condensate fraction for N noninteracting particles, see Figure 2.2 part (b). The numerical calculation, done by Ketterle and van Druten [36], shows, that finite-size effects are significant only for rather small values of N, less than about 10^4. The condensate fraction $N_{\mathbf{0}}/N$, obtained in this way, is smaller than the prediction of (2.41) and the transition at the critical temperature is rounded off.
Analytically, the finite-size effect can be obtained by taking the first two terms of the Euler-MacLaurin formula (2.27) into account [31–33]. The grand-canonical free energy (2.23) then reads with (2.29), (A.11), and (2.35)

$$\mathcal{F}_G = N_{\mathbf{0}}(\mu_c - \mu) - \frac{1}{\beta(\beta\hbar\tilde{\omega})^3}\left[\zeta_4(e^{\beta\mu}) + \frac{3}{2}\hbar\bar{\omega}\beta\,\zeta_3(e^{\beta\mu})\right], \tag{2.59}$$

where $\bar{\omega} = (\omega_x + \omega_y + \omega_z)/3$ is the arithmetic and $\tilde{\omega} = (\omega_x\omega_y\omega_z)^{1/3}$ is the geometric mean of the trap frequencies. Furthermore, we have used the level spacing $\beta E_{\mathbf{n}} = \hbar\omega_i\beta = x_i$ and interpreted x_i as a continuous variable. From the free energy (2.59) we find for the number of particles (2.9)

$$N = N_{\mathbf{0}} + \frac{1}{(\hbar\beta\tilde{\omega})^3}\left[\zeta_3(e^{\beta\mu}) + \frac{3}{2}\,\hbar\beta\overline{\omega}\,\zeta_2(e^{\beta\mu})\right]. \tag{2.60}$$

We obtain at the critical point $N_{\mathbf{0}} = 0$ and $\mu = \mu_c = 0$ for the critical temperature T_c:

$$N = \left(\frac{k_B T_c}{\hbar\tilde{\omega}}\right)^3\left[\zeta(3) + \frac{3\zeta(2)\hbar\overline{\omega}}{2k_B T_c}\right]. \tag{2.61}$$

For $T_c = T_c^{(0)}[1 + \Delta T_c/T_c^{(0)}]$, where $T_c^{(0)}$ denotes the semiclassical critical temperature (2.38) of the previous Section, Eq. (2.61) yields in first order of $\beta\hbar\bar{\omega}$

$$T_c = \frac{\hbar\tilde{\omega}}{k_B}\left[\frac{N}{\zeta(3)}\right]^{1/3}\left[1 - \frac{\zeta(2)\overline{\omega}}{2\zeta^{2/3}(3)\tilde{\omega}N^{1/3}}\right]. \tag{2.62}$$

The correction term

$$\frac{\Delta T_c}{T_c^{(0)}} = -\frac{\zeta(2)\overline{\omega}}{2\zeta^{2/3}(3)\tilde{\omega}N^{1/3}} \approx -0.7275\,\frac{\overline{\omega}}{\tilde{\omega}N^{1/3}}\,. \tag{2.63}$$

lowers the critical temperature with respect to the thermodynamic limit. It decreases with $N^{-1/3}$ for large N. Therefore, it is called the (first order) finite-size correction. For an isotropic trap, where $\bar{\omega} = \tilde{\omega}$, and for about $N = 3\cdot 10^5$ particles it is of the order of 1.6 %, but for $N = 10$ it is about 34 %. Hence, the semiclassical approximation is exact in the thermodynamic limit. The condensate fraction obtained from (2.60) reads

$$\frac{N_{\mathbf{0}}}{N} = 1 - \left(\frac{T}{T_c^{(0)}}\right)^3 - \frac{3\bar{\omega}\zeta(2)}{2\tilde{\omega}[\zeta(3)]^{2/3}}\left(\frac{T}{T_c^{(0)}}\right)^2 N^{-1/3}\,. \tag{2.64}$$

The finite-size effect is shown in Figure 2.2 and is compared with experimental results Ref. [37]. The trap, used in the experiment [37], has the frequencies $f_1 = f_2$ and $f_3 = \sqrt{8}f_1 = 373$ Hz, so that the geometric and arithmetic mean is given by

$$\tilde{f} = \frac{f_3}{2} = 186.5\,\mathrm{Hz} \qquad \text{and} \qquad \bar{f} = \frac{2+\sqrt{2}}{6} f_3 \approx 212.25\,\mathrm{Hz}. \tag{2.65}$$

For $N = 40\,000$ atoms of ^{87}Rb this leads to a critical temperature

$$T_c^{(0)} = 287\,\mathrm{nK}\,. \tag{2.66}$$

The measurement of the critical temperature is estimated to be $T_c^{(\mathrm{exp})} = 0.94(5)\,T_c^{(0)}$. A part of this deviation is due to the finite-size effect (2.63):

$$\frac{\Delta T_c}{T_c^{(0)}} \approx 2.4\,\%\,. \tag{2.67}$$

The remaining discrepancy of about 3.1 % is due to the neglected two-particle interaction. In Figure 2.2 it is shown (a) an evaluation of (2.41) and it is compared to experimental results of [37]. The rather rough semiclassical approximation fits astonishingly well to experimental data. But an important discrepancy is also visible, i.e. the calculated critical temperature is to high compared with the experimental one. In part (b) of Figure 2.2 the semiclassical approximation is compared to an exact quantum calculation [36] and the finite-size corrected semiclassical approximation.

We are prepared now to examine the finite-size effect for the heat capacity. In the high temperature regime $T > T_c$, the internal energy (2.48) obtained from (2.59) reads

$$U = \frac{1}{\beta(\beta\hbar\tilde{\omega})^3}\left[3\zeta_4(e^{\beta\mu}) + \frac{9}{2}\hbar\bar{\omega}\beta\,\zeta_3(e^{\beta\mu})\right]\,. \tag{2.68}$$

Inserting (2.60) with $N_{\mathbf{0}} = 0$ into (2.68) yields in first order of $\hbar\bar{\omega}\beta$

$$U = \left\{\frac{3\zeta_4(e^{\beta\mu})}{\zeta_3(e^{\beta\mu})} + \frac{9}{2}\,\hbar\beta\overline{\omega}\,\left[1 - \frac{\zeta_4(e^{\beta\mu})\zeta_2(e^{\beta\mu})}{\zeta_3^2(e^{\beta\mu})}\right]\right\} k_B T N\,. \tag{2.69}$$

Therefore, the heat capacity (2.10) is given by

$$\begin{aligned}\frac{C_V}{k_B N} &= \frac{3\zeta_4(e^{\beta\mu})}{\zeta_3(e^{\beta\mu})} + Te^{-\beta\mu}\,\left.\frac{\partial e^{\beta\mu}}{\partial T}\right|_{N,V}\left[3\left(1 - \frac{\zeta_4(e^{\beta\mu})\zeta_2(e^{\beta\mu})}{\zeta_3^2(e^{\beta\mu})}\right)\right. \\ &\left. -\frac{9}{2}\,\hbar\beta\overline{\omega}\,\left(\frac{\zeta_2(e^{\beta\mu})}{\zeta_3(e^{\beta\mu})} + \frac{\zeta_4(e^{\beta\mu})\zeta_1(e^{\beta\mu})}{\zeta_3^2(e^{\beta\mu})} - 2\,\frac{\zeta_4(e^{\beta\mu})\zeta_2^2(e^{\beta\mu})}{\zeta_3^3(e^{\beta\mu})}\right)\right]\,.\end{aligned} \tag{2.70}$$

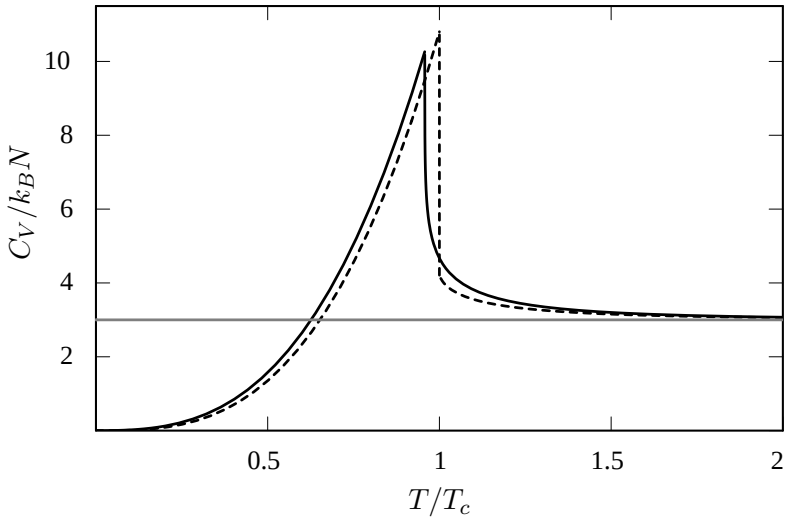

FIG. 2.3: Heat capacity in harmonic trap. The horizontal solid gray line corresponds to the Dulong-Petit law (2.53). The dashed curve is the semiclassical heat capacity (2.52) and (2.56) for an ideal gas in the harmonic trap of the Paris experiment (1.17) with $\kappa = 0$. The dashed curve is the first order finite-size corrected heat capacity (2.72) and (2.75) for the same trap.

The inner derivative is obtained from (2.60) by a derivation with respect to T for constant N, V, and $N_{\mathbf{0}} = 0$ implying

$$-\frac{T}{3}e^{-\beta\mu}\left.\frac{\partial e^{\beta\mu}}{\partial T}\right|_{N,V} = \frac{\zeta_3\left(e^{\beta\mu}\right)}{\zeta_2\left(e^{\beta\mu}\right)} + \frac{3}{2}\hbar\beta\overline{\omega}\left[1 - \frac{\zeta_3\left(e^{\beta\mu}\right)\zeta_1\left(e^{\beta\mu}\right)}{\zeta_2^2\left(e^{\beta\mu}\right)}\right]. \tag{2.71}$$

Inserting (2.71) into (2.70) results in

$$\frac{C_V}{k_BN} = 12\,\frac{\zeta_4\left(e^{\beta\mu}\right)}{\zeta_3\left(e^{\beta\mu}\right)} - 9\,\frac{\zeta_3\left(e^{\beta\mu}\right)}{\zeta_2\left(e^{\beta\mu}\right)} - \frac{27}{2}\,\hbar\beta\overline{\omega}\left[\frac{\zeta_4\left(e^{\beta\mu}\right)\zeta_2\left(e^{\beta\mu}\right)}{\zeta_3^2\left(e^{\beta\mu}\right)} - \frac{\zeta_3\left(e^{\beta\mu}\right)\zeta_1\left(e^{\beta\mu}\right)}{\zeta_3^2\left(e^{\beta\mu}\right)}\right]. \tag{2.72}$$

In the high temperature limit this reproduces the Dulong-Petit law (2.53). The first two terms in (2.72) correspond to the zeroth order semiclassical approximation (2.52), the remaining term is the finite-size correction to it. At the critical point, the finite-size contribution in (2.72) causes a divergency, because of the function $\zeta(1)$ so that

$$\lim_{T\downarrow T_c}\frac{C_V}{k_BN} = \infty\,. \tag{2.73}$$

For the low temperature regime $T < T_c$, we have to take the chemical potential at its critical value $\mu_c = 0$. Since the condensed particles do not contribute to the grand-canonical free energy, the internal energy (2.69) is still valid and reads due to the critical temperature (2.62) and the critical chemical potential $\mu_c = 0$:

$$U = k_BT_cN\left\{\frac{3\zeta(4)}{\zeta(3)}\left(\frac{T}{T_c}\right)^4 + \frac{9\overline{\omega}\zeta^{1/3}(3)}{2\tilde{\omega}N^{1/3}}\left[\left(\frac{T}{T_c}\right)^3 - \frac{\zeta(2)\zeta(4)}{\zeta^2(3)}\left(\frac{T}{T_c}\right)^4\right]\right\}. \tag{2.74}$$

From this we obtain the heat capacity (2.10)

$$\frac{C_V}{k_BN} = \frac{12\zeta(4)}{\zeta(3)}\left(\frac{T}{T_c}\right)^3 + \frac{27\overline{\omega}\zeta^{1/3}(3)}{2\tilde{\omega}N^{1/3}}\left[\left(\frac{T}{T_c}\right)^2 - \frac{4\zeta(2)\zeta(4)}{3\zeta^2(3)}\left(\frac{T}{T_c}\right)^3\right]. \tag{2.75}$$

In the low temperature limit $T \downarrow 0$, the heat capacity (2.75) tends to zero as it should according to the third law of thermodynamics. At the critical point $T \uparrow T_c$ it tends to the finite value

$$\lim_{T\uparrow T_c} \frac{C_V}{k_B N} = \frac{12\zeta(4)}{\zeta(3)} + \frac{27\overline{\omega}\zeta^{1/3}(3)}{2\tilde{\omega}N^{1/3}} \left[1 - \frac{4\zeta(2)\zeta(4)}{3\zeta^2(3)}\right] \approx 10.8047 - 8.67828\frac{\overline{\omega}}{\tilde{\omega}N^{1/3}}\,, \tag{2.76}$$

thus the finite-size effects lead to a small decrease. For the trap frequencies (2.65) of Ensher's experiment [37] this yields

$$\lim_{T\uparrow T_c} \frac{C_V}{k_B N} \approx 10.5159\,. \tag{2.77}$$

We show an evaluation of the heat capacity (2.52) and (2.56) and the finite-size correction (2.72) and (2.75) to it in Figure 2.3 for the values of the Paris experiment, see Table 1.2. For $N = 3\times10^5$ particles the effect is rather small, so that we can expect the semiclassical approximation to be applicable also in the anharmonic trap.

2.4.3 Low Temperature Limit of the Semiclassical Approximation

In order to investigate the accuracy of the semiclassical approximation, we determine the low temperature behavior of a Bose gas in an isotropic harmonic trap. The trapping potential is given by

$$V(\mathbf{x}) = \frac{M\omega_0^2}{2}\left(x^2 + y^2 + z^2\right)\,, \tag{2.78}$$

so that the energy eigenvalues of the Hamiltonian (2.26) read

$$E_{\mathbf{n}} = \hbar\omega_0\left(n_x + n_y + n_z + 3/2\right)\,. \tag{2.79}$$

The numbers n_x, n_y, n_z are the quantum numbers and run from zero to infinity. For the reduced chemical potential $\mu_r = \mu - 3\hbar\omega_0/2$, the grand-canonical free energy (2.13) simplifies to

$$\beta\mathcal{F}_G = \ln\left[1 - e^{\beta\mu_r}\right] + \sum_{\mathbf{n}\neq\mathbf{0}}^{\infty} \ln\left[1 - e^{-\beta[\hbar\omega_0(n_1+n_2+n_3)-\mu_r]}\right]. \tag{2.80}$$

The reduced chemical potential is defined implicitly over the number of particles for which we obtain with (2.9)

$$N = \frac{1}{e^{-\beta\mu_r} - 1} + \sum_{\mathbf{n}\neq\mathbf{0}}^{\infty} \left[e^{\beta[\hbar\omega_0(n_1+n_2+n_3)-\mu_r]} - 1\right]^{-1} \tag{2.81}$$

To obtain Bose-Einstein condensation the occupation number of the ground state has to become macroscopically large, which implies that the chemical potential mets with $\mu_r \uparrow 0^-$. At zero temperature $T = 0$, all particles are supposed to occupy the ground state so that the chemical potential has to be of the form

$$\mu_r = \frac{1}{\beta}\ln\left(\frac{N}{N+1}\right) + \delta\mu_r \tag{2.82}$$

to preserve the number of particles. The correction term in (2.82) has to tend faster in the low temperature limit to zero than $1/\beta$, that is $\beta\delta\mu_r \to 0$ for $T \to 0$. Inserting (2.82) into (2.81) we obtain

$$N = \frac{N}{(N+1)e^{-\beta\delta\mu_r} - N} + \sum_{\mathbf{n}\neq\mathbf{0}}^{\infty} \left[\frac{N+1}{N} e^{\beta[\hbar\omega_0(n_1+n_2+n_3)-\delta\mu_r]} - 1\right]^{-1} \tag{2.83}$$

In the low temperature limit the leading contribution reads

$$0 = N(N+1)(1 - e^{-\beta\delta\mu_r}) + \frac{N}{N+1}e^{-\beta\hbar\omega_0}\,, \tag{2.84}$$

where we have expanded the first term on the right hand side with respect to the small value $1 - e^{-\beta\delta\mu_r}$. The solution of (2.84) yields an exponentially small correction term

$$\delta\mu_r \sim e^{-\beta\hbar\omega_0} \tag{2.85}$$

to the chemical potential (2.82). In order to calculate the heat capacity, we have to determine the internal energy given by

$$U = \frac{\partial\beta\mathcal{F}_G}{\partial\beta} + \left(\mu_r + \frac{3}{2}\hbar\omega_0\right) N\,. \tag{2.86}$$

For low temperatures, the internal energy (2.86) yields with (2.80)

$$U \approx \frac{-\mu_r}{1 - e^{\beta\mu_r}} + \left(\mu_r + \frac{3}{2}\hbar\omega_0\right) N \tag{2.87}$$

up to exponentially vanishing terms. By inserting (2.82) into (2.87) we obtain by using (2.84) and (2.85) also exponentially vanishing correction terms to the ground state energy in the low temperature limit proportional to $e^{-\beta\hbar\omega_0}$. Therefore, with the internal energy also the heat capacity (2.10) is for low temperatures corrected by an exponentially small amount proportional to $e^{-\beta\hbar\omega_0}$. The same applies to the condensate fraction (2.18) with (2.83) due to the chemical potential (2.85). However, the semiclassical approximation predicted for both quantities a power law approach to zero, namely with the power T^3. Hence, we note that the semiclassical approximation fails in describing the low temperature behavior correctly. This is due to the non fulfiled smallness condition of the level spacing $\beta\hbar\omega_0 \ll 1$ for low temperatures which ensures the validity of the semiclassical approximation, see discussion below Eq. (2.24).

2.5 Bose Gas in a Rotating Anharmonic Trap

We consider a rotating anharmonic trap of the form (1.17) with a quadratic and quartic potential which has been employed in the Paris experiment [1]. The Hamiltonian (2.26) of such a system is given by

$$H = \frac{\mathbf{p}^2}{2M} + \frac{\epsilon_z}{2}\left[\lambda^2\eta\frac{r^2}{a_z^2} + \frac{z^2}{a_z^2} + \frac{\kappa}{2}\frac{r^4}{a_z^4}\right]. \tag{2.88}$$

Here $r = \sqrt{x^2 + y^2}$ and z denote the space coordinates, whereas $\epsilon_z = \hbar\omega_z$ sets the energy scale and $a_z = \sqrt{\hbar/(M\omega_z)}$ the length scale. As in Chapter 1, we have introduced dimensionless parameters setting an anisotropy $\lambda = \omega_\perp/\omega_z$, an anharmonicity $\kappa = a_z^4 k/\epsilon_z > 0$, and a deformation of the harmonic potential $\eta = 1 - \Omega^2/\omega_\perp^2$ which depends on the rotation speed Ω and can change its sign.
Inserting (2.88) into the semiclassical approximation for the grand-canonical free energy (2.25) and integrating the momentum and the z-dependency yields

$$\begin{aligned}\mathcal{F}_G &= N_{\mathbf{0}}(\mu_c - \mu) \\ &\quad - \sum_{j=1}^{\infty}\left(\frac{M}{2\pi\hbar^2\beta}\right)^{3/2}\frac{a_z^3(2\pi)^{3/2}}{j^3\beta\sqrt{\beta\epsilon_z}}\int_0^\infty \mathrm{d}u\,\exp\left[-j\beta\epsilon_z\kappa\left(u^2 + \frac{\lambda^2\eta}{\kappa}u - \frac{\mu_z}{\kappa}\right)\right].\end{aligned} \tag{2.89}$$

We have performed a change of variables $a_z\zeta = z$ and $2a_z^2 u = r^2$ as well as introduced the dimensionless temperature and the reduced chemical potential:

$$\beta\epsilon_z = \frac{1}{T_z}\,, \qquad \mu = \mu_z\epsilon_z\,. \tag{2.90}$$

For the Paris experiment, the real temperature is obtained by $T = 0.524 \times T_z$ nK. Performing the remaining integral in (2.89) leads to:

$$\int_0^\infty \mathrm{d}u \, \exp\left[-j\beta\epsilon_z\kappa\left(u^2 + \frac{\lambda^2\eta}{\kappa}u - \frac{\mu_z}{\kappa}\right)\right] =$$

$$\frac{\sqrt{\pi}}{2\sqrt{j\beta\epsilon_z\kappa}} \exp\left[j\beta\epsilon_z\left(\mu_z + \frac{\lambda^4\eta^2}{4\kappa}\right)\right] \mathrm{erfc}\left(\frac{\lambda^2\eta}{2\sqrt{\kappa}}\sqrt{j\beta\epsilon_z}\right) , \tag{2.91}$$

where $\mathrm{erfc}(z)$ is the complementary error function

$$\mathrm{erfc}(z) = \frac{2}{\sqrt{\pi}} \int_z^\infty \mathrm{d}t \, e^{-t^2} . \tag{2.92}$$

Then, the grand-canonical free energy (2.89) reads

$$\mathcal{F}_G = N_{\mathbf{0}}(\mu_c - \mu) - \epsilon_z \sum_{j=1}^{\infty} \frac{\sqrt{\pi}}{2\sqrt{\kappa}} \left(\frac{T_z}{j}\right)^{7/2} \exp\left[\left(\mu_z + \frac{\lambda^4\eta^2}{4\kappa}\right)\frac{j}{T_z}\right] \mathrm{erfc}\left(\frac{\lambda^2\eta}{2\sqrt{\kappa}}\sqrt{\frac{j}{T_z}}\right) . \tag{2.93}$$

In analogy to the treatment of the harmonic trap we define a new ζ-function, which will shorten the notation:

$$\zeta_\nu(z, x) := \sum_{j=1}^{\infty} \frac{z^j}{j^\nu} \mathrm{E}_\sigma(xj) , \tag{2.94}$$

where we used $\sigma = \mathrm{sign}(\eta)$ and defined

$$\mathrm{E}_\sigma(x) := \sqrt{\pi x} \exp(x) \mathrm{erfc}\left(\sigma\sqrt{x}\right) . \tag{2.95}$$

Thus, with $\sigma = +1$ and $\sigma = -1$ we denote the undercritical rotation $\omega_\perp > \Omega$ and the overcritical rotation $\Omega > \omega_\perp$ respectively. The function (2.95) is related to more general functions, for instance to the Mittag-Leffler function [38–40] and therefore also to hypergeometric functions [41,42]. Many properties of the ζ-functions (2.94) are reviewed in the Appendix B. With this the grand-canonical free energy (2.89) takes the compact form

$$\mathcal{F}_G = N_{\mathbf{0}}(\mu_c - \mu) - \epsilon_z \frac{\sigma T_z^4}{\lambda^2\eta} \zeta_4(z, \tilde{\beta}) , \tag{2.96}$$

with the notations

$$z = e^{\mu_z/T_z} , \qquad \tilde{\beta} = \frac{\lambda^4\eta^2}{4\kappa T_z} . \tag{2.97}$$

Here, z denotes the fugacity whereas $\tilde{\beta}$ is a dimensionless inverse temperature scaled by a factor accounting for the trap geometry. We note that both arguments of the ζ-function in (2.96) depend on the temperature. The harmonic limit $\kappa \to 0$ is related to the limit $\tilde{\beta} \to \infty$. The special case of a critical rotation $\Omega = \omega_\perp$, where $\eta = 0$, has to be treated carefully within this notation, since one formally divides by zero. But according to (2.93), which is equivalent to (2.96), we know that no singularity occurs at the critical rotation speed $\eta = 0$. Hence, the grand-canonical free energy (2.96) is a well-behaved function for any rotation speed.
However, for the critical rotation speed $\Omega = \omega_\perp$ the effective trapping potential in (2.88) is purely quartic in the xy-plane. Thus, this case can be investigated analytically.

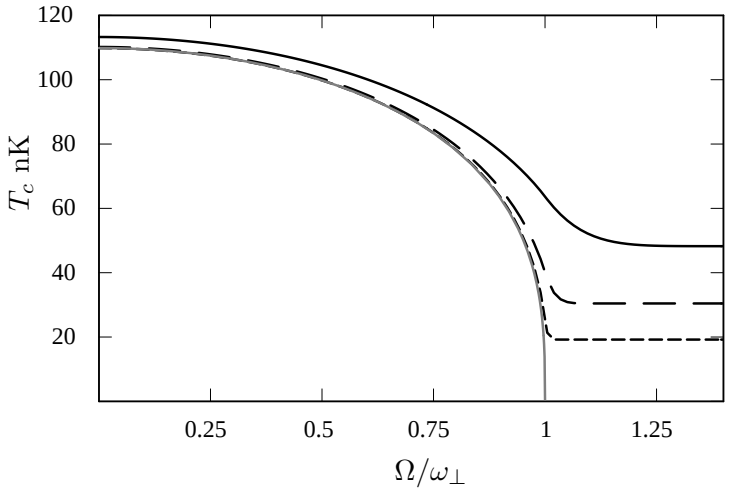

FIG. 2.4: Critical temperature versus rotation speed $\Omega/\omega_\perp$. The highest lying line (black solid) corresponds to the data of the Paris experiment [1], see Table 1.2, with $\kappa = 0.4$. For the deeper lying lines we varied the anharmonicity parameter κ: (a) $\kappa = 0.04$ (long dashes), (b) $\kappa = 0.004$ (short dashes), and (c) the harmonic limit $\kappa = 0$ (gray solid).

2.5.1 Critical Temperature

Now we determine the number of particles (2.9) which simply leads to

$$N = N_{\mathbf{0}} + \frac{\sigma T_z^3}{\lambda^2 \eta} \zeta_3(z, \tilde{\beta}) \,. \tag{2.98}$$

At the critical temperature $T_{z,c}$, where the condensation begins, the chemical potential is equal to the classical ground-state energy. This means, the critical chemical potential has the value of the minimum of the trapping potential (1.17), see Figure 1.5, so that for the classical ground state $\mathbf{p} = 0$ the condition $H - \mu > 0$ is fulfilled. Therefore, the critical chemical potential is given by

$$\mu_{z,c} = \begin{cases} 0 & \text{for} \quad \Omega \leq \omega_\perp \,, \\ -\dfrac{\lambda^4 \eta^2}{4\kappa} & \text{for} \quad \Omega > \omega_\perp \,. \end{cases} \tag{2.99}$$

Thus, Eq. (2.98) reduces with $N_{\mathbf{0}} = 0$, (2.94) and (2.95) to

$$N = \frac{\sqrt{\pi}}{2\sqrt{\kappa}} \sum_{j=1}^{\infty} \left(\frac{T_{z,c}}{j} \right)^{5/2} \exp\left[\frac{\lambda^4 \eta^2 j}{4\kappa T_{z,c}} \Theta(\eta) \right] \mathrm{erfc}\left[\frac{\lambda^2 \eta \sqrt{j}}{2\sqrt{\kappa T_{z,c}}} \right] , \tag{2.100}$$

where Θ is the unit step function, which is a discontinuous function also known as the Heaviside step function. Considering the thermodynamic limit, we find here that with $N \to \infty$ also κ must go to zero in such a way that $N\sqrt{\kappa}$ remains finite. In this limit $\kappa \to 0$ while $\eta > 0$, we should re-obtain the results of the harmonic trap. Indeed, we find with (B.10)

$$N \to \frac{\zeta(3)}{\lambda^2 \eta} T_{z,c}^3 \,, \tag{2.101}$$

which reproduces within the right dimensions (1.16) the previous result (2.38).
Figure 2.4 shows a plot of the critical temperature following from (2.100) for various anharmonicities κ. Remarkable is the saturation of the critical temperature in the limit of a infinite

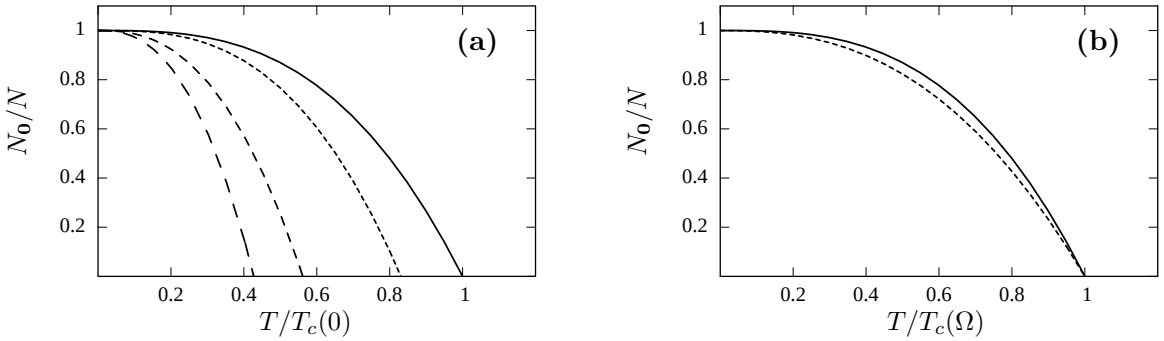

Figure 2.5: Condensate fraction versus reduced temperature. In part (a) the temperature is normed to the critical temperature for the non-rotating condensate $\Omega = 0$ in the anharmonic trap of the Paris experiment [1], see Table 1.2. The condensate fraction (2.106) is evaluated for various rotation speeds, the lines correspond to $\Omega = 0$ (solid), $\Omega = \omega_\perp/\sqrt{2}$ (short dashes), $\Omega = \omega_\perp$ (longer dashes), and $\Omega = \sqrt{3}\omega_\perp/\sqrt{2}$ (long dashes). In part (b) the temperature is normed to the corresponding fraction displaying the different temperature dependence. The solid line corresponds to the rotation speed $\Omega = 0$ and the dashed line corresponds to the critical $\Omega = \omega_\perp$.

rotation speed $\Omega \to \infty$. In the limit of infinite fast rotation $\Omega \to \infty$, the number of particles reduces to the following analytical expression

$$N = \sqrt{\frac{\pi}{\kappa}}\, T_{z,c}^{5/2} \zeta(5/2)\,, \tag{2.102}$$

which leads for the Paris trap to an critical temperature

$$\lim_{\Omega\to\infty} T_c = 48.24\,\mathrm{nK}\,. \tag{2.103}$$

Furthermore, for the critical rotation speed $\Omega = \omega_\perp$, Eq. (2.100) simplifies to

$$N = \sqrt{\frac{\pi}{4\kappa}}\, T_{z,c}^{5/2} \zeta(5/2)\,, \tag{2.104}$$

which leads for the anharmonicity $\kappa = 0.4$ of the Paris trap (1.18) to the critical temperature

$$\lim_{\Omega\to\omega_\perp} T_c = 63.66\,\mathrm{nK}\,. \tag{2.105}$$

We can also calculate the condensate fraction from (2.98):

$$\frac{N_\mathbf{0}}{N} = 1 - \frac{\sigma\, T_z^3}{\lambda^2 \eta N}\, \zeta_3(z_c, \tilde{\beta})\,, \tag{2.106}$$

where the critical fugacity is $z_c = \exp(\mu_z/T_z)$ with the critical chemical potential given by (2.99). The condensate fraction (2.106) can be approximated for low temperatures $T_z \ll T_{z,c}$ due to (B.10) by

$$\frac{N_\mathbf{0}}{N} = \begin{cases} 1 - \dfrac{\zeta(3)}{\lambda^2\eta N}\, T_z^3 + \dfrac{2\,\kappa\,\zeta(4)}{\lambda^6\eta^3 N}\, T_z^4 + \ldots & \text{for} \quad \Omega < \omega_\perp\,, \quad T_z \ll T_{z,c} \\ 1 - \dfrac{\sqrt{\pi}}{\sqrt{\kappa}}\, \zeta(5/2)\, T_z^{5/2} + \dfrac{\zeta_3(z_c)}{\lambda^2|\eta|N}\, T_z^3 + \ldots & \text{for} \quad \Omega \geq \omega_\perp\,, \quad T_z \ll T_{z,c} \end{cases}\,. \tag{2.107}$$

Due to (B.10) and (B.11), the condensate fraction (2.106) in the limit of infinite fast rotation $\Omega \to \infty$ and in the limit of the critical rotation $\Omega \to \omega_\perp$ respectively reduces to the analytic expression

$$\frac{N_\mathbf{0}}{N} = 1 - \frac{\sqrt{\pi}}{\sqrt{\kappa}} \zeta(5/2) T_z^{5/2}\,. \tag{2.108}$$

Comparing (2.102), (2.104) and (2.108), we note that the limits $T \downarrow 0$ and $\eta \to 0$ do not commute with each other. We show an evaluation of (2.106) in Figure 2.5. In part (a) of Figure 2.5 we show the dependence of the condensate fraction (2.106) on the rotation speed Ω. With increasing Ω the condensate fraction moves to lower temperatures which is due to the normalization of the temperature to the non-rotating critical temperature. In part (b) we show the change in the temperature dependence of the condensate fraction for undercritical rotation ($\Omega = 0$) and overcritical rotation ($\Omega = \omega_\perp$).

2.5.2 Heat Capacity

Now we determine the temperature dependence of the heat capacity. In the high temperature regime $T > T_c$ the grand-canonical free energy (2.96) becomes

$$\mathcal{F}_G = -\epsilon_z \frac{\sigma T_z^4}{\lambda^2 \eta} \zeta_4(z, \tilde{\beta}) \,. \tag{2.109}$$

In order to calculate the entropy (2.9), we need the derivative of the ζ-function (2.94) with respect to the temperature. Since both arguments z, $\tilde{\beta}$ (2.97) of the ζ-function depend on the temperature, we obtain

$$\frac{\partial \zeta_\nu(z, \tilde{\beta})}{\partial T_z} = \left(\frac{\partial}{\partial T_z} \frac{\mu_z}{T_z} \right) \zeta_{\nu-1}(z, \tilde{\beta}) - \frac{1}{2T_z} \zeta_\nu(z, \tilde{\beta}) + \frac{\lambda^4 \eta^2}{4\kappa T_z^2} \left[\sigma \zeta_{\nu-1}(z) - \zeta_{\nu-1}(z, \tilde{\beta}) \right] . \tag{2.110}$$

The entropy reads due to (2.7), (2.98) with $N_{\mathbf{0}} = 0$, and (2.110)

$$S = k_B \left[\frac{7}{2} \frac{\sigma T_z^3}{\lambda^2 \eta} \zeta_4(z, \tilde{\beta}) + \frac{\lambda^2 \eta T_z^2}{4\kappa} \zeta_3(z) - \frac{N}{T_z} \left(\mu_z + \frac{\lambda^4 \eta^2}{4\kappa} \right) \right] . \tag{2.111}$$

And the internal energy (2.11) reads due the number of particles (2.98) with $N_{\mathbf{0}} = 0$ and the entropy (2.111)

$$U = \epsilon_z N \left[\frac{5T_z}{2} \frac{\zeta_4(z, \tilde{\beta})}{\zeta_3(z, \tilde{\beta})} + \frac{\lambda^4 \eta^2}{4\kappa} \frac{\sigma \zeta_3(z) - \zeta_3(z, \tilde{\beta})}{\zeta_3(z, \tilde{\beta})} \right] . \tag{2.112}$$

Then, the heat capacity (2.10) above T_c reads due to the derivative of the ζ-function (2.110) and the internal energy (2.112)

$$\begin{aligned} \frac{C_>}{k_B N} &= \frac{5\zeta_4(z, \tilde{\beta})}{2\zeta_3(z, \tilde{\beta})} + \frac{5T_z}{2\zeta_3(z, \tilde{\beta})} \left\{ \mathcal{D}\zeta_3(z, \tilde{\beta}) - \frac{1}{2T_z} \zeta_4(z, \tilde{\beta}) + \frac{\lambda^4 \eta^2}{4\kappa T_z^2} \left[\sigma \zeta_3(z) - \zeta_3(z, \tilde{\beta}) \right] \right\} \\ &\quad - \frac{5T_z \zeta_4(z, \tilde{\beta})}{2\zeta_3^2(z, \tilde{\beta})} \left\{ \mathcal{D}\zeta_2(z, \tilde{\beta}) - \frac{1}{2T_z} \zeta_3(z, \tilde{\beta}) + \frac{\lambda^4 \eta^2}{4\kappa T_z^2} \left[\sigma \zeta_2(z) - \zeta_2(z, \tilde{\beta}) \right] \right\} + \frac{\lambda^4 \eta^2}{4\kappa} \frac{\sigma \mathcal{D}\zeta_2(z)}{\zeta_3(z, \tilde{\beta})} \\ &\quad - \frac{\lambda^4 \eta^2}{4\kappa} \frac{\sigma \zeta_3(z)}{\zeta_3^2(z, \tilde{\beta})} \left\{ \mathcal{D}\zeta_2(z, \tilde{\beta}) - \frac{1}{2T_z} \zeta_3(z, \tilde{\beta}) + \frac{\lambda^4 \eta^2}{4\kappa T_z^2} \left[\sigma \zeta_2(z) - \zeta_2(z, \tilde{\beta}) \right] \right\} , \end{aligned} \tag{2.113}$$

wherein occurs the inner derivative

$$\mathcal{D} \equiv \left. \frac{\partial}{\partial T_z} \frac{\mu_z}{T_z} \right|_{N,V} . \tag{2.114}$$

The derivative of the chemical potential with respect to the temperature at constant volume V and constant number of particles N is determined by taking the derivative of (2.98), yielding

$$\mathcal{D} = -\frac{5}{2T_z} \frac{\zeta_3(z, \tilde{\beta})}{\zeta_2(z, \tilde{\beta})} - \frac{\lambda^4 \eta^2}{4\kappa T_z^2} \frac{\sigma \zeta_2(z) - \zeta_2(z, \tilde{\beta})}{\zeta_2(z, \tilde{\beta})} \,. \tag{2.115}$$

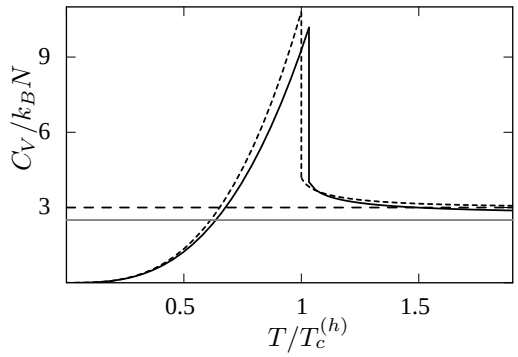

FIG. 2.6: Heat capacity versus temperature, reduced to the critical temperature $T_c^{(h)}$ of the harmonic trap (1.17) with $\kappa = 0$. The dashed line corresponds to the harmonic trap heat capacity (2.52), (2.56) for the Paris trap (1.17) with $\kappa = 0$, see Table 1.2. The black solid line is the heat capacity (2.116), (2.127) for the anharmonic Paris trap (1.17) with no rotation, $\Omega = 0$. The horizontal lines correspond to the Dulong-Petit law: harmonic trap (2.53) (dashed) and anharmonic trap (2.118) (gray).

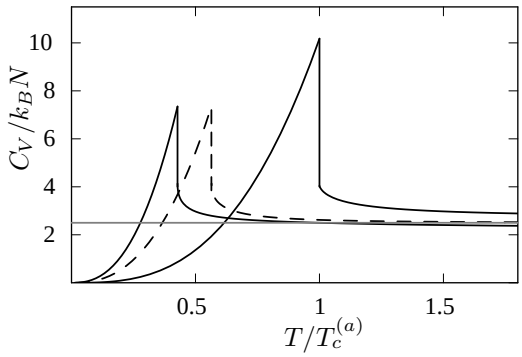

FIG. 2.7: Heat capacity (2.116) and (2.127) versus temperature, reduced to the critical temperature $T_c^{(a)}$ of the anharmonic trap (1.17) with $\kappa = 0.4$ for varying rotation speeds. The lines correspond to $\Omega = 0$ (solid), $\Omega = \omega_\perp$ (long dashes), and $\Omega = 2\omega_\perp$ (short dashes). The gray solid line corresponds to the Dulong-Petit law (2.118). We note that for $\Omega = 2\omega_b ot$ and $T > T_c$ the heat capacity crosses the Dulong-Petit limes.

Inserting (2.115) into (2.113) results in

$$\begin{aligned}\frac{C_>}{k_BN} &= \frac{35}{4}\frac{\zeta_4(z,\tilde\beta)}{\zeta_3(z,\tilde\beta)} - \frac{25}{4}\frac{\zeta_3(z,\tilde\beta)}{\zeta_2(z,\tilde\beta)} + \frac{\sigma\lambda^4\eta^2}{8\kappa T_z}\left[11\frac{\zeta_3(z)}{\zeta_3(z,\tilde\beta)} - 10\frac{\zeta_2(z)}{\zeta_2(z,\tilde\beta)}\right] \\ &\quad - \frac{\lambda^8\eta^4}{16\kappa^2 T_z^2}\left[\frac{\zeta_2(z)-\sigma\zeta_2(z,\tilde\beta)}{\zeta_3(z,\tilde\beta)}\frac{\zeta_2(z)}{\zeta_2(z,\tilde\beta)}\right]. \end{aligned} \tag{2.116}$$

At first we show that this formula reproduces the result of the harmonic trap. Therefore, we take the limit $\kappa \to 0$, which is equivalent to $\tilde\beta \to \infty$ while $\Omega > \omega_\perp$, and use (B.10) to find

$$\frac{C_>}{k_BN} = \frac{35}{4}\frac{\zeta_4(z)}{\zeta_3(z)} - \frac{25}{4}\frac{\zeta_3(z)}{\zeta_2(z)} + \left[\frac{11}{4}\frac{\zeta_4(z)}{\zeta_3(z)} - \frac{10}{4}\frac{\zeta_3(z)}{\zeta_2(z)} - \frac{1}{4}\frac{\zeta_3(z)}{\zeta_2(z)} + \frac{2}{4}\frac{\zeta_4(z)}{\zeta_3(z)}\right] \tag{2.117}$$

which leads indeed to the known result of the harmonic trap in (2.52). The next interesting case for the heat capacity (2.116) is the high temperature limit in which $\tilde\beta = \lambda^4\eta^2/(4\kappa T_z) \to 0$. Using (B.11) we find

$$\lim_{T\to\infty}\frac{C_>}{k_BN} = \frac{5}{2}, \tag{2.118}$$

which represents the Dulong-Petit law in our anharmonic trap and is 1/2 smaller than the corresponding one in the harmonic trap.

In Figure 2.6 we compare the harmonic heat capacity (2.52) with the anharmonic one (2.116) for the values of the Paris experiment. The latter is shifted a little to the right compared to the harmonic heat capacity and the jump at $T = T_c$ is lower. Furthermore, the Dulong-Petit law has changed and the convergence to it is slower than in the harmonic trap. In Figure 2.7 we investigate the dependence of the heat capacity of the Bose gas in the anharmonic trap of the Paris experiment on the rotation speed. The jump at the critical point seems to decrease for increasing rotation speed. Furthermore, we note that the heat capacity above T_c crosses the Dulong-Petit law for an overcritical rotation speed. In order to investigate the approach to this

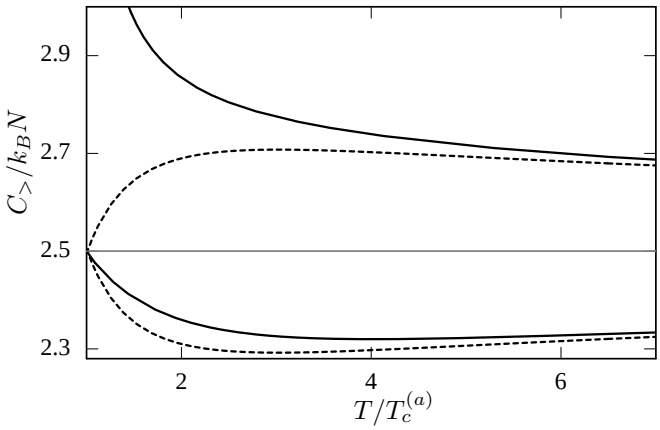

FIG. 2.8: Approach of the heat capacity to the Dulong-Petit law (2.118), the gray horizontal line. Shown is an evaluation of (2.116), the exact heat capacity (solid lines), and the approach to it (2.121) for the rotation speeds $\Omega = 0$ and $\Omega = \sqrt{2}\omega_\perp$ (dashed lines).

Dulong-Petit law, we use (B.11) and expand the ζ-function for large T_z as

$$\zeta_\nu\left(z, \frac{\lambda^4\eta^2}{4\kappa T_z}\right) \approx z\left(\sqrt{\frac{\pi\lambda^4\eta^2}{4\kappa T_z}} - 2\sigma\frac{\lambda^4\eta^2}{4\kappa T_z} + ...\right) + \frac{z^2}{2^\nu}\left(\sqrt{\frac{2\pi\lambda^4\eta^2}{4\kappa T_z}} - 4\sigma\frac{\lambda^4\eta^2}{4\kappa T_z} + ...\right) + ... \,. \quad (2.119)$$

From the number of particles (2.98) we get in first order by inserting (2.119) the fugacity

$$z \approx \frac{2\sqrt{\kappa}N}{\sqrt{\pi}\, T_z^{5/2}} \,. \quad (2.120)$$

Inserting (2.119) and (2.120) into (2.116) and performing a large T_z expansion yields

$$\frac{C_>}{k_BN} = \frac{5}{2} + \frac{\lambda^2\eta}{4\sqrt{\pi\kappa T_z}} + \frac{\lambda^6\eta^3\,(\pi-4)}{32\,(\pi\kappa T_z)^{3/2}} \,. \quad (2.121)$$

Hence, with the first η depending term in (2.121) the approach changes its behavior, from being larger ($\Omega < \omega_\perp$) than the limit to being smaller ($\Omega > \omega_\perp$). In Figure 2.8 we show the approach of the heat capacity of a Bose gas in the anharmonic trap to the Dulong-Petit law (2.118) together with the high temperature approximation (2.121). For temperatures about six times larger than the critical temperature, the approximation agrees very well with the exact semiclassical approximation.

We note that in both limits of the critical $\Omega \to \omega_\perp$ and the infinite fast $\Omega \to \infty$ rotation, the heat capacity (2.116) reduces with (B.10) and (B.11), respectively, to

$$\frac{C_>}{k_BN} = \frac{35}{4}\frac{\zeta_{7/2}(\tilde{z})}{\zeta_{5/2}(\tilde{z})} - \frac{25}{4}\frac{\zeta_{5/2}(\tilde{z})}{\zeta_{3/2}(\tilde{z})} \,, \quad (2.122)$$

where we have replaced $z = \tilde{z}\exp(-\tilde{\beta})$ in (B.10), which is due to the decomposition of the chemical potential according to $\mu = \tilde{\mu} + \mu_c$. The critical values for the fugacity and the scaled inverse temperature are denoted by

$$z_c = \begin{cases} 1 & \Omega \le \omega_\perp \\ \exp\left(-\dfrac{\lambda^4\eta^2}{4\kappa T_z}\right) & \Omega > \omega_\perp \end{cases} \,, \qquad \tilde{\beta}_c = \frac{\lambda^4\eta^2}{4\kappa T_{z,c}}. \quad (2.123)$$

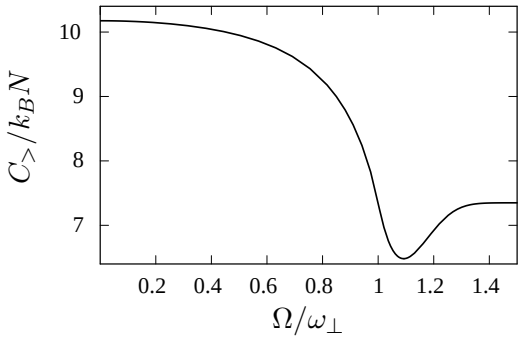

FIG. 2.9: Heat capacity just below the critical point versus rotation speed. For the values of the Paris experiment it is shown the evaluation of (2.130).

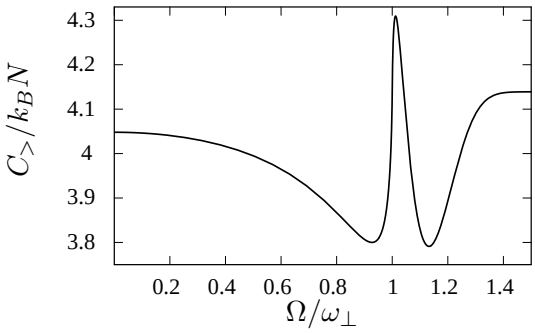

FIG. 2.10: Heat capacity just above the critical point versus rotation speed. For the values of the Paris experiment it is shown the evaluation of (2.125).

We note that in the overcritical rotation regime $\Omega > \omega_\perp$, the critical fugacity z_c still depends on the temperature. Therefore, we denote the critical fugacity at the critical temperature as

$$\bar{z}_c = \exp\left(-\tilde{\beta}_c\right). \tag{2.124}$$

Furthermore, we write for the heat capacity above T_c at the critical point

$$C_{>,c} \equiv \lim_{T_z \downarrow T_{z,c}} C_> = C_>(\bar{z}_c, \tilde{\beta}_c). \tag{2.125}$$

Hence, at the critical point $\tilde{z} = 1$ and in both limits $\Omega \to \omega_\perp$ and $\Omega \to \infty$ the heat capacity (2.122) has the value

$$\frac{C_>}{k_BN} = \frac{35}{4}\frac{\zeta(7/2)}{\zeta(5/2)} - \frac{25}{4}\frac{\zeta(5/2)}{\zeta(3/2)} \approx 4.14. \tag{2.126}$$

In the condensate regime $T_z < T_{z,c}$, we have to return to the internal energy U (2.112) to determine the heat capacity. With the critical values (2.123), (2.124), and the number of particles (2.98) with $N_{\mathbf{0}} = 0$ we obtain for the heat capacity (2.10)

$$\begin{aligned}\frac{C_<}{k_BN} &= \left(\frac{T_z}{T_{z,c}}\right)^3 \left\{\frac{35}{4}\frac{\zeta_4(z_c,\tilde{\beta})}{\zeta_3(\bar{z}_c,\tilde{\beta}_c)} + \frac{\lambda^4\eta^2}{4\kappa T_z}\left[\frac{11\sigma\zeta_3(z_c)}{2\zeta_3(\bar{z}_c,\tilde{\beta}_c)} - 5\Theta(\eta)\frac{\zeta_3(z_c,\tilde{\beta})}{\zeta_3(\bar{z}_c,\tilde{\beta}_c)}\right]\right. \\ &\left. + \frac{\lambda^8\eta^4}{16\kappa^2T_z^2}\left[\Theta(-\eta)\frac{\sigma\zeta_2(z_c)}{\zeta_3(\bar{z}_c,\tilde{\beta}_c)} - \Theta(\eta)\frac{\sigma\zeta_2(z_c) - \Theta(\eta)\zeta_2(z_c,\tilde{\beta})}{\zeta_3(\bar{z}_c,\tilde{\beta}_c)}\right]\right\}. \end{aligned} \tag{2.127}$$

In the low temperature limit $T \downarrow 0$, the heat capacity (2.127) tends to zero with the following power-law behavior

$$\frac{C_<}{k_BN} \approx \begin{cases} \dfrac{35}{4}\dfrac{\zeta(4)}{\zeta_3(\bar{z}_c,\tilde{\beta}_c)}\left(\dfrac{T_z}{T_{z,c}}\right)^3 & \text{for} \quad \Omega < \omega_\perp, \quad T_z \ll T_{z,c} \\ \dfrac{35}{2}\dfrac{\zeta(7/2)}{\zeta_3'(\bar{z}_c,\tilde{\beta}_c)}\left(\dfrac{T_z}{T_{z,c}}\right)^{5/2} & \text{for} \quad \Omega \geq \omega_\perp, \quad T_z \ll T_{z,c}, \end{cases} \tag{2.128}$$

where the prime on the ζ-function denotes $\sqrt{\pi x_c}\zeta_3'(\bar{z}_c,\tilde{\beta}_c) = \zeta_3(\bar{z}_c,\tilde{\beta}_c)$. We note that the low temperature behavior of the heat capacity (2.128) is the same as the corresponding one of the condensate fraction (2.107). In the harmonic limit $\kappa \to 0$, the heat capacity (2.127) reduces due to (B.9) to the previous result (2.56). In the limit of the critical rotation $\Omega \to \omega_\perp$ and in the

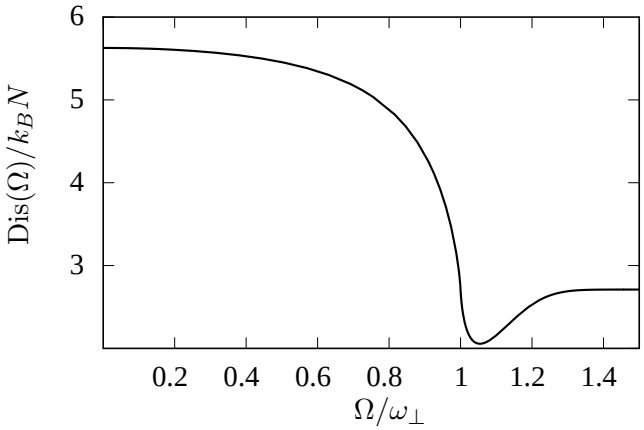

FIG. 2.11: Discontinuity (2.132) versus rotation speed. It is always positive but has a minimum at $\Omega/\omega_\perp \approx 1.125$ and tends for fast rotations to the constant (2.133).

limit of infinite fast rotation $\Omega \to \infty$, the heat capacity (2.127) reduces with (B.11) and (B.10) respectively to

$$\frac{C_<}{k_B N} = \frac{35}{4}\frac{\zeta(7/2)}{\zeta(5/2)}\left(\frac{T_z}{T_{z,c}}\right)^{5/2} . \tag{2.129}$$

At the critical point $T = T_c$ and $\mu = \mu_c$, we denote the heat capacity below T_c by

$$C_{<,c} \equiv \lim_{T_z \uparrow T_{z,c}} C_< = C_<(\bar{z}_c, \tilde{\beta}_c) , \tag{2.130}$$

which reduces in both limits $\Omega \to \omega_\perp$ and $\Omega \to \infty$ to the analytical expression

$$\frac{C_{<,c}}{k_B N} = \frac{35}{4}\frac{\zeta(7/2)}{\zeta(5/2)} \approx 7.35 . \tag{2.131}$$

For the values of the Paris experiment we show in Figure 2.9 and Figure 2.10 the dependence of the heat capacity (2.130) and (2.125) on the rotation speed. For increasing rotation speeds Ω, we have a remarkable strong dependence of the heat capacity around the critical rotation $\Omega = \omega_\perp$. Below the critical temperature T_c, the heat capacity (2.130) shows a similar developing as the critical temperature itself, see Figure 2.4, except for the appearance of a minimum slightly above the critical rotation speed $\Omega = \omega_\perp$. In the limit $\Omega \to \infty$ the heat capacity (2.130) approaches the constant (2.131). Above the critical temperature, the heat capacity (2.125) has a little peak around the critical rotation speed but tends also to constant value in the limit of an infinite fast rotation.
The jump at the critical point, which characterizes the discontinuity of the heat capacity is denoted by

$$\mathrm{Dis}(\Omega) = C_{<,c} - C_{>,c} . \tag{2.132}$$

It tends in the limit of the critical rotation $\Omega \to \omega_\perp$ and in the limit of a infinite fast rotation $\Omega \to \infty$ to the value

$$\frac{\mathrm{Dis}(\Omega)}{k_B N} = 3.21 , \tag{2.133}$$

which is smaller than that of the harmonic trap (2.58). In Figure 2.11 we show an evaluation of the discontinuity at the critical point. It is always positive, indicating that the Bose gas undergoes for all rotation speeds a second-order phase transition according to the Ehrenfest definition.

2.6 BEC on a Cylinder

The critical temperature (2.100) of a Bose gas in the anharmonic trap (1.17) as well as the heat capacity at the critical point tends to a constant value if $\Omega \to \infty$. This phenomenon might be explained by an intuitive consideration [43].
When the minimum of the trapping potential in the xy-plane is deep enough, it is approximately a ring with radius r_m. The valley around the circular minimum of the trapping potential has nearly the curvature of a harmonic oscillator. Hence, effectively in this case, the Bose gas has two oscillatory degrees of freedom, namely the z-direction and the radial direction, plus the freedom to 'walk' around the circle like a free particle in a one-dimensional box of the length

$$L = 2\pi r_m \,. \tag{2.134}$$

For $\eta < 0$, the radius r_m is given by the minimum of the trapping potential (1.17) in the xy-plane and reads

$$r_m = \sqrt{\frac{\lambda^2|\eta|}{\kappa}} \,. \tag{2.135}$$

The curvature γ_r of the trapping potential is given by the second derivative, which we have to evaluate at the radius (2.135) yielding

$$\gamma_r = 2\lambda^2|\eta|\epsilon_z \,. \tag{2.136}$$

Hence, we can approximate the trapping potential (1.14) for a fast rotation speed Ω by

$$V(\mathbf{x},\Omega) \approx V_{\mathrm{cyc}}(\mathbf{x},\Omega) = \frac{\epsilon_z}{2}\left[2\lambda^2|\eta|\frac{\delta r^2}{a_z^2} + \frac{z^2}{a_z^2} + \left(\frac{\xi}{a_z}\right)^s\right] , \tag{2.137}$$

where we have introduced ξ for the degree of freedom of the gas moving around the circle as free particles in a box and δr for the deviation from the radius of the circular minimum, i.e. $r = r_m + \delta r$. The number of the non-condensed particles (2.9) is then due to the semiclassical approximation (2.25) given by

$$N = \sum_{j=1}^{\infty} \int \frac{\mathrm{d}^3p}{(2\pi\hbar)^3)} \int_{-\infty}^{\infty} \mathrm{d}\delta r \, \mathrm{d}z \int_0^L \mathrm{d}\xi \, \exp\left\{-\beta j \left[\frac{\mathbf{p}^2}{2M} + V_{\mathrm{cyc}}(\mathbf{x},\Omega) - \tilde{\mu}_z\right]\right\} , \tag{2.138}$$

Performing the integrals results in

$$N = \sum_{j=1}^{\infty} \frac{z^j}{j^{3/2}\lambda_T^3} \sqrt{\frac{2a_z^2\pi T_z}{j}} \sqrt{\frac{a_z^2\pi T_z}{\lambda^2|\eta|j}} \, a_z 2\pi r_m \Gamma(1+1/s) \,. \tag{2.139}$$

Taking the limit $s \to \infty$, we obtain for the number of particles (2.139) with the scaling (1.16)

$$N = \sqrt{\frac{\pi}{\kappa}} \zeta_{5/2}(\tilde{z}) T_z^{5/2} \,, \tag{2.140}$$

where $\tilde{z} = \exp\left(-\tilde{\mu_z}/T_z\right)$ denotes the fugacity. At the critical point $\tilde{z}_c = 1$ the number of particles (2.140) leads to the critical temperature

$$T_{z,c} = \left(\frac{\kappa}{\pi}\right)^{1/5} \left[\frac{N}{\zeta(5/2)}\right]^{2/5} , \tag{2.141}$$

which coincides with the previous result (2.102). For the number of particles the intuition led to the right solution. Thus, all thermodynamic quantities calculated so far can be checked in the limit of an infinite fast rotation in the same way.

Nearly the same integrals as in (2.138) lead to the grand-canonical free energy, we just have to divide the integrand by βj, so that we find

$$\mathcal{F}_G = -\epsilon_z T_z^{7/2} \sqrt{\frac{\pi}{\kappa}} \zeta_{7/2}(\tilde{z}) \,. \tag{2.142}$$

We obtain the entropy from (2.7) with (2.142) according to

$$\frac{S}{k_B} = \frac{7}{2} T_z^{5/2} \sqrt{\frac{\pi}{\kappa}} \zeta_{7/2}(\tilde{z}) - \mu_z T_z^{3/2} \sqrt{\frac{\pi}{\kappa}} \zeta_{5/2}(\tilde{z}) \,. \tag{2.143}$$

From (2.5) we find for the internal energy

$$U = -\frac{5}{2} \mathcal{F}_G \,. \tag{2.144}$$

The value 5/2 can be interpreted now as the sum of the degree of freedoms, 1 for each oscillator dimension and 1/2 for one box dimension. Above the critical temperature $T > T_c$, the heat capacity (2.10) of an ideal Bose gas on a cylinder reads with (2.144)

$$\frac{C_>}{k_B N} = \frac{35}{4} \frac{\zeta_{7/2}(\tilde{z})}{\zeta_{5/2}(\tilde{z})} - \frac{25}{4} \frac{\zeta_{5/2}(\tilde{z})}{\zeta_{3/2}(\tilde{z})} \,, \tag{2.145}$$

which is indeed the same result as (2.122). For temperatures below $T < T_c$, we take the chemical potential at its critical value $\tilde{z}_c = 1$ and insert the number of particles (2.140) into (2.144):

$$U = \epsilon_z N \frac{5}{2} T_{z,c} \frac{\zeta(7/2)}{\zeta(5/2)} \left(\frac{T_z}{T_{z,c}} \right)^{7/2} . \tag{2.146}$$

Then, the heat capacity (2.10) below T_c reads

$$\frac{C_<}{k_B N} = \frac{35}{4} \frac{\zeta(7/2)}{\zeta(5/2)} \left(\frac{T_z}{T_{z,c}} \right)^{5/2} , \tag{2.147}$$

which again coincides with the previous result (2.129).
However, we should mention that considering the limit of very fast or even infinite fast rotation speeds Ω conflicts with the Paris experiment [1]. In particular, we can also use (2.135) to calculate the maximum rotation speed Ω_M for which the expansion (1.10) of the trapping potential of the Paris experiment is valid:

$$\Omega_M = 1.08 \, \omega_\perp \,. \tag{2.148}$$

Hence, considering an infinite fast rotation speed $\Omega \to \infty$ in such an anharmonic trap is not suitable for this experiment.

2.7 Effect of Interaction

Within the ideal gas model particle interactions are neglected. In the following, we investigate a two-particle interaction perturbatively within the path integral formalism [45]. This is justified due to the diluteness of the gas. For dilute gases the inter-atom interaction is well approximated by a two particle δ-interaction. The grand-canonical free energy $\mathcal{F}_G$ (2.13) from the ideal gas is regarded as the zeroth order approximation and we now deduce the first order correction to it.

2.7.1 Grand-Canonical Free Energy

For $T > T_c$, the grand-canonical partition function in the path integral formalism is given by

$$\mathcal{Z} = \int \mathcal{D}\psi^* \int \mathcal{D}\psi \, e^{-\mathcal{A}[\psi^*,\psi]/\hbar} , \tag{2.149}$$

where the functional integral is performed over all bosonic fields $\psi(\mathbf{x},\tau)$ and its complex conjugate $\psi^*(\mathbf{x},\tau)$, that is they are periodic in imaginary time $\tau \in [0,\hbar\beta]$. The Euclidean action decomposes according to

$$\mathcal{A}[\psi^*,\psi] = \mathcal{A}^{(0)}[\psi^*,\psi] + \mathcal{A}^{(\mathrm{int})}[\psi^*,\psi] . \tag{2.150}$$

Here the interaction-free contribution reads

$$\mathcal{A}^{(0)}[\psi^*,\psi] = \hbar \int_0^{\hbar\beta} \mathrm{d}\tau \int_0^{\hbar\beta} \mathrm{d}\tau' \int \mathrm{d}^3x \int \mathrm{d}^3x' \, \psi^*(\mathbf{x},\tau)\, G^{(0)\,-1}(\mathbf{x},\tau;\mathbf{x}',\tau')\, \psi(\mathbf{x}',\tau') , \tag{2.151}$$

with the integral kernel

$$G^{(0)\,-1}(\mathbf{x},\tau;\mathbf{x}',\tau') = \frac{1}{\hbar}\,\delta(\mathbf{x}-\mathbf{x}')\delta(\tau-\tau') \left\{ \hbar\frac{\partial}{\partial\tau} - \frac{\hbar^2}{2M}\,\mathbf{\Delta} + V(\mathbf{x}) - \mu \right\} , \tag{2.152}$$

where M denotes the particle mass, $V(\mathbf{x})$ the trap potential, and μ the chemical potential, as in the previous Sections. Due to the diluteness of the Bose gas, we can restrict ourselves to deal with a two-particle interaction and have

$$\mathcal{A}^{(\mathrm{int})}[\psi^*,\psi] = \frac{1}{2}\int_0^{\hbar\beta} \mathrm{d}\tau \int \mathrm{d}^3x \int \mathrm{d}^3x' \; V^{(\mathrm{int})}(\mathbf{x}-\mathbf{x}')\, \psi^*(\mathbf{x},\tau)\psi^*(\mathbf{x}',\tau)\psi(\mathbf{x},\tau)\psi(\mathbf{x}',\tau) , \tag{2.153}$$

where $V^{(\mathrm{int})}(\mathbf{x}-\mathbf{x}')$ denotes the interaction potential. By expanding the functional integral (2.149)–(2.153) in powers of $V^{(\mathrm{int})}(\mathbf{x}-\mathbf{x}')$, the expansion coefficients of the grand-canonical partition function consist of interaction-free expectation values. These are evaluated with the help of Wick's rule as a sum of Feynman integrals, which are pictured as diagrams constructed from lines and vertices. A straight line with an arrow represents the interaction-free correlation function

$$\mathbf{x},\tau \;\longleftarrow\; \mathbf{x}',\tau' \quad \equiv \quad G^{(0)}(\mathbf{x},\tau;\mathbf{x}',\tau') , \tag{2.154}$$

which follows from solving

$$\int_0^{\hbar\beta} \mathrm{d}\tau'' \int \mathrm{d}^3x'' \, G^{(0)\,-1}(\mathbf{x},\tau;\mathbf{x}'',\tau'')\, G^{(0)}(\mathbf{x}'',\tau'';\mathbf{x}',\tau') = \delta(\mathbf{x}-\mathbf{x}')\,\delta(\tau-\tau') \tag{2.155}$$

with periodic boundary conditions in imaginary time. Treating the trap potential $V(\mathbf{x})$ semiclassically we are led to the Fourier representation [45]

$$\begin{aligned} G^{(0)}(\mathbf{x},\tau;\mathbf{x}',\tau') \;&=\; \int \frac{\mathrm{d}^3p}{(2\pi\hbar)^3} \, \frac{e^{\frac{i}{\hbar}\mathbf{p}(\mathbf{x}-\mathbf{x}')}}{2\sinh\frac{\beta}{2}\left[\frac{\mathbf{p}^2}{2M} + V\left(\frac{\mathbf{x}+\mathbf{x}'}{2}\right) - \mu\right]} \\ &\times \left\{ \Theta(\tau-\tau')\, e^{-\frac{1}{\hbar}\left[\frac{\mathbf{p}^2}{2M}+V\left(\frac{\mathbf{x}+\mathbf{x}'}{2}\right)-\mu\right](\tau-\tau'-\frac{\hbar\beta}{2})} + \Theta(\tau'-\tau)\, e^{-\frac{1}{\hbar}\left[\frac{\mathbf{p}^2}{2M}+V\left(\frac{\mathbf{x}+\mathbf{x}'}{2}\right)-\mu\right](\tau-\tau'+\frac{\hbar\beta}{2})} \right\} . \end{aligned} \tag{2.156}$$

Furthermore, two vertices connected by a dashed line picture spatio-temporal integrals over the two-particle interaction potential

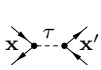

$$\equiv -\frac{1}{\hbar}\int_0^{\hbar\beta} \mathrm{d}\tau \int \mathrm{d}^3x \int \mathrm{d}^3x'\, V^{(\mathrm{int})}(\mathbf{x}-\mathbf{x}') \quad . \tag{2.157}$$

In the following we apply these Feynman rules and determine the grand-canonical partition function within first-order perturbation theory for the anharmonic trap (1.17) of the Paris experiment. The two-body δ-interaction is given by

$$V^{(\mathrm{int})}(\mathbf{x}-\mathbf{x}') = g\delta(\mathbf{x}-\mathbf{x}')\,, \tag{2.158}$$

where the two-particle coupling constant is given by

$$g = \frac{4\pi\hbar^2 a}{M}\,, \tag{2.159}$$

wherein the s-wave scattering length a occurs. The coupling constant may be derived within the pseudo-potential method which was established by Enrico Fermi [46]. For δ-interactions, we have to remove the dashed lines in the Feynman diagrams and glue the dots together, so that the diagram (2.157) reduces to

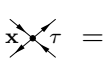

$$= -\frac{g}{\hbar}\int_0^{\hbar\beta} \mathrm{d}\tau \int \mathrm{d}^3x\,. \tag{2.160}$$

We start with the connected vacuum diagrams which contribute to the grand-canonical free energy

$$\mathcal{F}_G = -\frac{1}{\beta}\ln \mathcal{Z}\,. \tag{2.161}$$

Up to the first order in the two-particle δ-interaction it reads

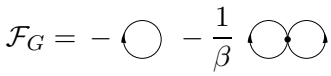

$$\mathcal{F}_G = \; - \quad - \frac{1}{\beta} \quad + \; \ldots\,. \tag{2.162}$$

By passing we note that all higher-order connected vacuum diagrams together with their proper weights follow from solving a graphical recursion relation [47]. The zeroth-order term in (2.162) stands for

$$\mathcal{F}_G^{(0)} \equiv \; - \quad = \frac{1}{\beta}\,\mathrm{Tr}\,\ln G^{(0)\,-1}\,, \tag{2.163}$$

where the tracelog of an operator G is defined by the sum over the logarithms of its eigenvalues g_i

$$\mathrm{Tr}\,\ln G = \sum_i \ln g_i\,. \tag{2.164}$$

A semiclassical treatment of the trapping potential $V(\mathbf{x})$ leads to

$$\mathcal{F}_G^{(0)} = -\frac{1}{\beta\lambda_T^3}\int \mathrm{d}^3x\, \zeta_{5/2}\left(e^{\beta[\mu-V(\mathbf{x})]}\right)\,. \tag{2.165}$$

Here, we have used the thermal de Broglie wave length (1.1) and the polylogarithmic function (2.35). For the parameters of the Paris trap, see Table 1.2, this leads to the previous result (2.96) with $N_{\mathbf{0}} = 0$:

$$\mathcal{F}_G^{(0)} = -\epsilon_z \frac{T_z^4}{\lambda^2|\eta|}\zeta_4(z,\tilde{\beta}) \tag{2.166}$$

The first-order diagram in (2.162) corresponds to

$$\mathcal{F}_G^{(1)} \equiv -\frac{1}{\beta}$$ $$= \frac{g}{\hbar\beta}\int_0^{\hbar\beta} \mathrm{d}\tau \int \mathrm{d}^3x\, G^{(0)}(\mathbf{x},\tau;\mathbf{x},\tau)G^{(0)}(\mathbf{x},\tau;\mathbf{x},\tau)\,. \tag{2.167}$$

It contains the interaction-free correlation function with equal imaginary times

$$G^{(0)}(\mathbf{x},\tau;\mathbf{x},\tau) = \lim_{\tau'\downarrow\tau} G^{(0)}(\mathbf{x},\tau;\mathbf{x},\tau') \tag{2.168}$$

which has, due to Eq. (2.156), the series representation

$$G^{(0)}(\mathbf{x},\tau;\mathbf{x},\tau) = \frac{1}{\lambda_T^3}\sum_{n=1}^{\infty}\frac{e^{n\beta\mu}}{n^{3/2}}\,\exp\left[-n\beta V(\mathbf{x})\right] \tag{2.169}$$

Inserting (2.169) into (2.167) we obtain

$$\mathcal{F}_G^{(1)} = \frac{g}{\lambda_T^6}\sum_{n=1}^{\infty}\sum_{n'=1}^{\infty}\frac{e^{(n+n')\beta\mu}}{(2\pi nn')^{3/2}}\int \mathrm{d}^3x\, e^{-(n+n')\beta V(\mathbf{x})}\,. \tag{2.170}$$

For the Paris trap (1.17), we obtain for the first order diagram (2.170)

$$\mathcal{F}_G^{(1)} = \frac{g}{\lambda_T^6}\sum_{n=1}^{\infty}\sum_{n'=1}^{\infty}\frac{e^{(n+n')\beta\mu}}{(nn')^{3/2}}\frac{\sqrt{2}\,\pi^2 T_z a_z^3}{\sqrt{\kappa}(n+n')}\exp\left(\frac{\lambda^4\eta^2(n+n')}{4\kappa T_z}\right)\mathrm{erfc}\left(\frac{\lambda^2\eta\sqrt{n+n'}}{2\sqrt{\kappa T_z}}\right)\,. \tag{2.171}$$

Inserting (1.1) and (2.159), we can re-write (2.171) as

$$\mathcal{F}_G^{(1)} = \epsilon_z\frac{\sqrt{2}\,a\,T_z^{9/2}}{\sqrt{\pi}\,a_z\,\lambda^2|\eta|}\,\zeta_{\frac{3}{2},\frac{3}{2},\frac{3}{2}}(z,\tilde{\beta})\,, \tag{2.172}$$

where we have introduced the new ζ-function

$$\zeta_{a,b,c}(z,\tilde{\beta}) = \sum_{n=1}^{\infty}\sum_{n'=1}^{\infty}\frac{z^{n+n'}}{n^a n'^b(n+n')^c}E_\sigma[(n+n')x]\,. \tag{2.173}$$

The exponential function E is given by the Eq. (B.4). Above the critical temperature $T > T_c$, the grand-canonical free energy up to the first order takes with (2.165) and (2.172) the form

$$\mathcal{F}_G = -\epsilon_z\left[\frac{T_z^4}{\lambda^2|\eta|}\zeta_4(z,\tilde{\beta}) - \frac{\sqrt{2}aT_z^{9/2}}{\sqrt{\pi}a_z\lambda^2|\eta|}\zeta_{\frac{3}{2},\frac{3}{2},\frac{3}{2}}(z,\tilde{\beta})\right]\,. \tag{2.174}$$

2.7.2 Self-Energy

Including interaction in the Hamiltonian adds an extra energy to the system and therefore influences its eigenvalues, in particular the ground state. As a consequence, we have to consider also the effect of the interaction to the critical point which consists in finding the critical chemical potential .

The phase transition from a Bose gas to a Bose-Einstein condensate occurs when the correlation function

$$G(\mathbf{x},\tau;\mathbf{x}',\tau') = \frac{1}{\mathcal{Z}}\int\mathcal{D}\psi^*\int\mathcal{D}\psi\,\psi(\mathbf{x},\tau)\psi^*(\mathbf{x}',\tau')\,e^{-\mathcal{A}[\psi^*,\psi]/\hbar} \tag{2.175}$$

diverges. Therefore, we determine its functional inverse $G^{-1}(\mathbf{x},\tau;\mathbf{x}',\tau')$ analogously to (2.155) from

$$\int_0^{\hbar\beta}\mathrm{d}\tau''\int\mathrm{d}^3x''\,G^{-1}(\mathbf{x},\tau;\mathbf{x}'',\tau'')\,G(\mathbf{x}'',\tau'';\mathbf{x}',\tau') = \delta(\mathbf{x}-\mathbf{x}')\,\delta(\tau-\tau') \tag{2.176}$$

and investigate when it vanishes. Due to the two-particle interaction, the integral kernel (2.152) is modified by the self-energy $\Sigma(\mathbf{x},\tau;\mathbf{x}',\tau')$ according to

$$G^{-1}(\mathbf{x},\tau;\mathbf{x}',\tau') = G^{(0)\,-1}(\mathbf{x},\tau;\mathbf{x}',\tau') - \Sigma(\mathbf{x},\tau;\mathbf{x}',\tau')\,. \tag{2.177}$$

A Fourier-Matsubara decomposition

$$G^{-1}(\mathbf{x},\tau;\mathbf{x}',\tau') = \frac{1}{\hbar\beta}\sum_{m=-\infty}^{\infty} e^{-i\omega_m(\tau-\tau')}\int\frac{\mathrm{d}^3p}{(2\pi\hbar)^3}\,e^{\frac{i}{\hbar}\mathbf{p}(\mathbf{x}-\mathbf{x}')}\,G^{-1}(\mathbf{p},\omega_m;\mathbf{x})\,, \tag{2.178}$$

with the Matsubara frequencies $\omega_m = 2\pi m/\hbar\beta$ leads with (2.152) and (2.177) to

$$G^{-1}(\mathbf{p},\omega_m;\mathbf{x}) = \frac{1}{\hbar}\left\{-i\hbar\omega_m + \frac{\mathbf{p}^2}{2M} + V(\mathbf{x}) - \mu\right\} - \Sigma(\mathbf{p},\omega_m;\mathbf{x})\,, \tag{2.179}$$

where the Fourier-Matsubara transformed of the self-energy follows from

$$\Sigma(\mathbf{p},\omega_m;\mathbf{x}) = \int_0^{\hbar\beta}\mathrm{d}\tau\int d^3x'\,e^{i\omega_m\tau-\frac{i}{\hbar}\mathbf{p}\mathbf{x}'}\,\Sigma(\mathbf{x},\tau;\mathbf{x}-\mathbf{x}',0)\,. \tag{2.180}$$

A zero of $G^{-1}(\mathbf{p},\omega_m;\mathbf{x})$ can only occur for vanishing momentum $\mathbf{p}=\mathbf{0}$ and for vanishing Matsubara frequency $\omega_m = 0$. This motivates to define the effective potential according to

$$V_{\mathrm{eff}}(\mathbf{x},\mu) = \hbar\,G^{-1}(\mathbf{0},0;\mathbf{x})\,, \tag{2.181}$$

which decomposes due to (2.179) according to

$$V_{\mathrm{eff}}(\mathbf{x},\mu) = V(\mathbf{x}) - \mu - \hbar\,\Sigma(\mathbf{0},0;\mathbf{x})\,. \tag{2.182}$$

The zero point of this effective potential defines the critical value of the chemical potential μ_c according to

$$\mu_c = \min_{\mathbf{x}}\left[V(\mathbf{x}) - \hbar\,\Sigma(\mathbf{0},0;\mathbf{x})\right]. \tag{2.183}$$

Thus, for a vanishing two-particle interaction, we obtain from (2.182) with $\Sigma = 0$ and (2.183) the critical chemical potential $\mu_c^{(0)}$ from the minimal value of the trap potential:

$$\mu_c^{(0)} = \min_{\mathbf{x}} V(\mathbf{x}) \equiv V_{\min}\,. \tag{2.184}$$

Now, we elaborate how this criterion changes to first-order in perturbation theory. Once the connected vacuum diagrams of the grand-canonical free energy are known, we can follow Refs. [48,49] so that amputating a line leads to the one-particle irreducible diagrams of the self-energy:

$\Sigma(\mathbf{x},\tau;\mathbf{x}',\tau') =$ 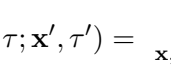 $+\ \ldots\ .$ (2.185)

Its analytical expression up to first order in the two-particle δ-interaction reads

$$\Sigma(\mathbf{x},\tau;\mathbf{x}',\tau') \;=\; \frac{-2g}{\hbar}\,\delta(\tau-\tau')\delta(\mathbf{x}-\mathbf{x}')G^{(0)}(\mathbf{x},\tau;\mathbf{x}',\tau)\,. \tag{2.186}$$

The associated Fourier-Matsubara transformed (2.180) is given by

$$\Sigma(\mathbf{p},\omega_m;\mathbf{x}) \;=\; \frac{-2g}{\hbar}\,G^{(0)}(\mathbf{x},\tau;\mathbf{x},\tau)\,. \tag{2.187}$$

Inserting (2.169) yields

$$\Sigma(\mathbf{p},\omega_m;\mathbf{x}) \quad = \quad \frac{-2g}{\hbar\lambda_T^3}\sum_{n=1}^{\infty}\frac{e^{n\beta\mu}}{n^{3/2}}e^{-n\beta V(\mathbf{x})}\,. \tag{2.188}$$

According to (2.183) the critical chemical potential is obtained up to the first order by

$$\mu_c = V_{\min} + \frac{2g}{\lambda_T^3}\sum_{n=1}^{\infty}\frac{e^{n\beta\mu_c}}{n^{3/2}}e^{-n\beta V_{\min}}\,. \tag{2.189}$$

Inserting the critical chemical potential (2.184) into (2.189) it can be approximated up to the first order in g by

$$\mu_c \approx \mu_c^{(0)} + \frac{2g}{\lambda_T^3}\zeta(3/2)\,. \tag{2.190}$$

We note, the shifting of the critical chemical potential is independent on the trapping potential, but depends on the temperature and the interaction strenght g.
For the trap (1.14) of the Paris experiment we have the scaling (1.16) and the interaction strength (2.159), thus we can write (2.190) dimensionless as

$$\mu_{z,c} \approx \mu_{z,c}^{(0)} + \frac{4a}{\sqrt{2\pi}a_z}\,T_z^{3/2}\zeta(3/2)\,, \tag{2.191}$$

with the semiclassical critical chemical potential (2.99).

2.7.3 Critical Temperature

From the free energy (2.174) we determine the critical temperature T_c below which the Bose gas forms a condensate. Due to (2.9), the number of particles is given by

$$N = \frac{T_z^3}{\lambda^2|\eta|}\zeta_3(z,\tilde{\beta}) - \sqrt{\frac{2}{\pi}}\frac{aT_z^{7/2}}{a_z\lambda^2|\eta|}\zeta_{\frac{3}{2},\frac{3}{2},\frac{1}{2}}(z,\tilde{\beta})\,. \tag{2.192}$$

At the critical point, we denote the fugacity and the inverse temperature as

$$\bar{z}_c = e^{\mu_{z,c}/T_{z,c}}\,, \qquad \tilde{\beta}_c = \frac{\lambda^4\eta^2}{4\kappa T_{z,c}}\,. \tag{2.193}$$

Inserting the critical values (2.193) with the critical chemical potential (2.191) into (2.192) and performing a Taylor expansion around $\mu_{z,c}^{(0)}$ up to the first order in a/a_z yields

$$N = \frac{T_{z,c}^3}{\lambda^2|\eta|}\zeta_3(z_c^{(0)},\tilde{\beta}_c) + \frac{a}{a_z}\sqrt{\frac{2}{\pi}}\frac{T_{z,c}^{7/2}}{\lambda^2|\eta|}\left[2\zeta(3/2)\zeta_2(z_c^{(0)},\tilde{\beta}_c) - \zeta_{\frac{3}{2},\frac{3}{2},\frac{1}{2}}(z_c^{(0)},\tilde{\beta}_c)\right]\,, \tag{2.194}$$

where $z_c^{(0)} = \exp\left(\mu_{z,c}^{(0)}/T_{z,c}\right)$ is the semiclassical critical chemical potential. For the interaction free gas, $a = 0$, the transition temperature $T_{z,c}^{(0)}$ is determined through (2.100). For a non-vanishing interaction, we expand $T_{z,c}$ around $T_{z,c}^{(0)}$

$$T_{z,c} = T_{z,c}^{(0)}\left(1 + \frac{\Delta T_{z,c}}{T_{z,c}^{(0)}}\right) \tag{2.195}$$

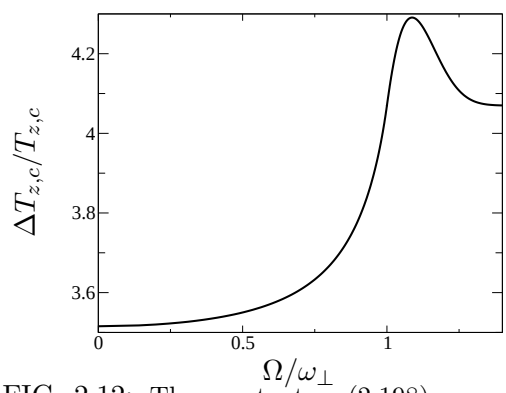

FIG. 2.12: The constant c_δ (2.198) versus rotation speed Ω. Increasing the rotation speed increases the c_δ. For very fast rotation it saturates.

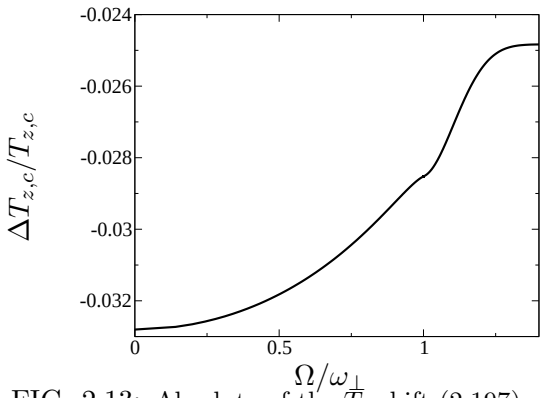

FIG. 2.13: Absolute of the T_c-shift (2.197) versus rotation speed Ω. The correction to the critical temperature ranges between 2.5 % and 3.3 %. Although the constant c_δ (2.198) increases with the rotation effectively the T_c-shift decreases.

and insert it into (2.194) to get in first order of a/a_z and $\Delta T_{z,c}$

$$\begin{aligned} N &= \frac{T_{z,c}^{(0)\,3}}{\lambda^2|\eta|}\left\{\zeta_3(z_c^{(0)},\tilde\beta_c^{(0)}) - \left[\frac{\mu_{z,c}^{(0)}}{T_{z,c}^{(0)}}\zeta_2(z_c^{(0)},\tilde\beta_c^{(0)}) - \frac{5}{2}\zeta_3(z_c^{(0)},\tilde\beta_c^{(0)})\right.\right. \\ &\left.\left. - \tilde\beta_c^{(0)}\left(\sigma\zeta_2(z_c^{(0)}) - \zeta_2(z_c^{(0)},\tilde\beta_c^{(0)})\right)\right]\frac{\Delta T_{z,c}}{T_{z,c}^{(0)}}\right\} + \frac{a}{a_z}\sqrt{\frac{2}{\pi}}\,\frac{T_{z,c}^{(0)\,7/2}}{\lambda^2|\eta|}\left[2\zeta(3/2)\zeta_2(z_c^{(0)},\tilde\beta_c^{(0)})\right. \\ &\left. -\zeta_{\frac{3}{2},\frac{3}{2},\frac{1}{2}}(z_c^{(0)},\tilde\beta_c^{(0)})\right]. \end{aligned} \tag{2.196}$$

Here, $\tilde\beta_c^{(0)} = \lambda^4\eta^2/(4\kappa T_{z,c}^{(0)})$ is the semiclassical inverse temperature. Using (2.98) with $N_{\mathbf{0}} = 0$ equation (2.196) leads to

$$\frac{\Delta T_{z,c}}{T_{z,c}^{(0)}} = -\frac{a}{\lambda_T^{(0)}}\cdot c_\delta(\Omega)\,, \tag{2.197}$$

where the thermal de Broglie wave length is $\lambda_T^{(0)} = a_z\sqrt{2\pi/T_{z,c}^{(0)}}$ and the coefficient

$$c_\delta(\Omega) = \frac{8\left(\zeta(3/2)\zeta_2(z_c^{(0)},\tilde\beta_c^{(0)}) - \zeta_{\frac{1}{2},\frac{3}{2},\frac{3}{2}}(z_c^{(0)},\tilde\beta_c^{(0)})\right)}{5\zeta_3(z_c^{(0)},\tilde\beta_c^{(0)}) - 2\left[\frac{\mu_{z,c}^{(0)}}{T_{z,c}^{(0)}}\zeta_2(z_c^{(0)},\tilde\beta_c^{(0)}) - \tilde\beta_c^{(0)}\left(\sigma\zeta_2(z_c^{(0)}) - \zeta_2(z_c^{(0)},\tilde\beta_c^{(0)})\right)\right]}\,. \tag{2.198}$$

Note that we have made use of the fact

$$\zeta_{a,b,c-1}(z,\tilde\beta) = \zeta_{a-1,b,c}\,(z,\tilde\beta) + \zeta_{a,b-1,c}\,(z,\tilde\beta)\,, \tag{2.199}$$

which follows immediately from (2.173).
Although the critical chemical potential (2.191) is not influenced by the anharmonicity κ, the coefficient of the shift to the temperature (2.198) does depend on it. But this is only due to the involved ζ-functions. In the harmonic trap limit, i.e. $\tilde\beta_c^{(0)} \to \infty$, equation (2.198) reduces to

$$c_\delta = \frac{4}{3}\cdot\left[\zeta(3/2)\zeta(2) - \zeta_{\frac{1}{2},\frac{3}{2},\frac{3}{2}}(1)\right] \approx 3.427\,, \tag{2.200}$$

where we have introduced in close analogy to (2.173)

$$\zeta_{a,b,c}\,(1) = \sum_{n=1}^{\infty}\sum_{n'=1}^{\infty}\frac{1}{n^a n'^b(n+n')^c}\,. \tag{2.201}$$

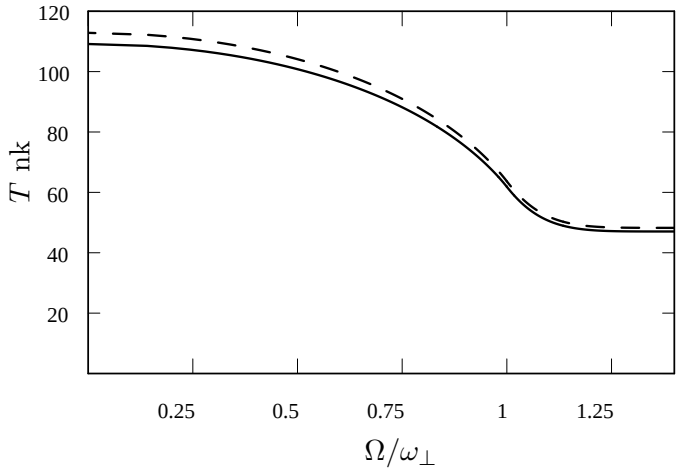

Figure 2.14: Shift of the critical temperature due to interaction versus rotation speed. The dashed line is the zeroth order semiclassical approximation, the solid line the first order corrected semiclassical critical temperature.

Eq. (2.200) was first derived by S. Giorgini et al. [50] for a non rotating harmonic trap and was experimentally confirmed by A. Aspect et al. [51] in 2004 with a Bose-Einstein condensate of ^{87}Rb.
For the non rotating ($\Omega = 0$) trap of the Paris experiment (1.17), the coefficient (2.198) has the value

$$c_\delta(0) \approx 3.52\,. \tag{2.202}$$

Hence, the anharmonicity κ increases the coefficient compared to that of the harmonic trap.
In Figure 2.12, we show the dependency of the coefficient (2.198) on the rotation speed Ω. There is a strong dependence and we ask if the interaction still can be treated perturbatively. In Figure 2.13 we see that the first order correction to the critical temperature (2.197) ranges between 2.5% and 3.3%, hence this is consistent with perturbational treatment of the interaction. Surprisingly, the shift of the critical temperature (2.197) decreases with increasing rotation speed. This effect s due to the critical temperature itself, since the coupling constant c_δ (2.198) in fact increases. Next, we should certainly concern two further limits, the limit $\Omega \to \omega_\perp$ and the limit $\Omega \to \infty$ for which in both cases we find

$$c_\delta = \frac{4\,\zeta(3/2)^2}{5\,\zeta(5/2)} \approx 4.07\,, \tag{2.203}$$

where we have used

$$\zeta_{\,a,b,0}\,(1) = \sum_{n=1}^{\infty}\sum_{n'=1}^{\infty} \frac{1}{n^a n'^b} = \zeta(a)\zeta(b)\,. \tag{2.204}$$

We note that the constant (2.198) in the limit $\Omega \to \infty$ is larger than that of a pure harmonic trap.
In Figure 2.14 we present the semiclassical critical temperature and the first order corrected one according to the δ-interaction for a Bose gas of ^{8}7Rb and the values of the Paris experiment, see Table 1.2. We note that in the fast rotation regime both temperatures are very close to each other.

Chapter 3

Dynamics of a Trapped Condensate

In the first Sections 3.1 and 3.2 of this Chapter we derive the hydrodynamic equations for the condensate wave function, which are similar to the equations of a perfect fluid. The reason for this similarity is that they are related with conservation laws for particle number and for total momentum. In Section 3.3 of this chapter we describe a rotating trap in the corotating frame by performing a coordinate transformation. By this we get an effective trapping potential, which depends on the rotation frequency Ω of the trap. In the Sections 3.4–3.7 we investigate the hydrodynamic collective oscillations for various traps and analyze their dependence on the rotation speed Ω. We compare the results of Section 3.4 with a variational consideration in Section 3.8. Finally, we determine in Section 3.9 the free expansion of the cloud after switching off the trap which is important for analyzing experimental data.

3.1 General Formalism

From the theoretical point of view a Bose-Einstein condensate at zero temperature is described by the Gross-Pitaevskii equation, which is a generalization of the Schrödinger equation:

$$\left\{ i\hbar\frac{\partial}{\partial t} + \frac{\hbar^2}{2M}\Delta - V(\mathbf{x},t) - g|\Psi|^2 \right\} \Psi = 0\,. \tag{3.1}$$

Here M denotes the atomic mass, $V(\mathbf{x},t)$ the trapping potential and g the interaction strength (2.159). The normalization condition for the condensate wave function $\Psi(\mathbf{x},t)$ is given by

$$\int \mathrm{d}^3x\, |\Psi|^2 = N_{\mathbf{0}}, \tag{3.2}$$

where $N_{\mathbf{0}}$ is the mean number of atoms occupying the ground state. The time-dependent Gross-Pitaevskii equation (3.1) may be derived from the principle of minimal action

$$\delta\mathcal{A}[\Psi^*,\Psi] = 0\,, \tag{3.3}$$

where the star denotes the complex conjugation and the Gross-Pitaevskii action is given by

$$\mathcal{A}[\Psi^*,\Psi] = \int_{t_1}^{t_2} \mathrm{d}t \int \mathrm{d}^3x\; \mathcal{L}\,, \tag{3.4}$$

with the Lagrangian density

$$\mathcal{L} = i\hbar\Psi^*\frac{\partial\Psi}{\partial t} - \frac{\hbar^2}{2M}\boldsymbol{\nabla}\Psi^*\boldsymbol{\nabla}\Psi - V(\mathbf{x},t)\Psi^*\Psi - \frac{g}{2}(\Psi^*\Psi)^2. \tag{3.5}$$

Indeed, the minimal action principle (3.4) yields the Euler-Lagrange equation

$$\frac{\partial \mathcal{L}}{\partial \Psi^*} - \boldsymbol{\nabla} \frac{\partial \mathcal{L}}{\partial \boldsymbol{\nabla} \Psi^*} - \frac{\partial}{\partial t} \frac{\partial \mathcal{L}}{\partial \dfrac{\partial \Psi^*}{\partial t}} = 0\,, \tag{3.6}$$

which leads with (3.5) to the time-dependent Gross-Pitaevskii equation (3.1).

3.2 Hydrodynamic Equations

One obtains the continuity equation of the condensate by multiplying the time-dependent Gross-Pitaevskii equation (3.1) with $\Psi^*(\mathbf{x}, t)$ and subtracting the complex conjugate of the resulting equation. So the continuity equation reads

$$\frac{\partial}{\partial t}|\Psi|^2 + \boldsymbol{\nabla} \cdot \left[\frac{\hbar}{2Mi} \left(\Psi^* \boldsymbol{\nabla} \Psi - \Psi \boldsymbol{\nabla} \Psi^* \right) \right] = 0\,, \tag{3.7}$$

which coincides with that of the Schrödinger equation. This is due to the fact that the non linear term in the Gross-Pitaevskii equation (3.1) is real. Introducing the particle density $n = |\Psi|^2$ Eq. (3.7) may be re-written as

$$\frac{\partial}{\partial t} n + \boldsymbol{\nabla} \cdot (n \boldsymbol{v}) = 0\,, \tag{3.8}$$

where the velocity of the condensate is defined by

$$\boldsymbol{v} = \frac{\hbar}{2iMn} \left(\Psi^* \boldsymbol{\nabla} \Psi - \Psi \boldsymbol{\nabla} \Psi^* \right)\,. \tag{3.9}$$

If we decompose the complex wave function Ψ in its amplitude η and phase φ according to

$$\Psi = \eta e^{i\varphi}\,, \tag{3.10}$$

we find simple expressions for the density n and the velocity of the condensate $\boldsymbol{v}$:

$$n = \eta^2\,, \qquad\qquad \boldsymbol{v} = \frac{\hbar}{M} \boldsymbol{\nabla} \varphi\,. \tag{3.11}$$

If φ is non-singular, it follows immediately that the condensate is irrotational, since $\boldsymbol{v}$ is a gradient field, i.e. $\boldsymbol{\nabla} \times \boldsymbol{v} = \mathbf{0}$. Therefore, the flow of the condensate is more restricted than that of a classical fluid.
The hydrodynamic aspect of the condensate is reflected by the equations of motion for η and φ. They may be found by inserting (3.10) into (3.1) and separating the real and the imaginary parts. We obtain from the real part

$$-\hbar \frac{\partial \varphi}{\partial t} = -\frac{\hbar^2}{2M} \left[\frac{\Delta \eta}{\eta} - (\boldsymbol{\nabla} \varphi)^2 \right] + V(\mathbf{x}, t) + g\eta^2 \tag{3.12}$$

and from the imaginary part we get

$$\frac{\hbar}{\eta} \frac{\partial \eta}{\partial t} = \frac{\hbar^2}{2M} \left[2 \boldsymbol{\nabla} \varphi \frac{\boldsymbol{\nabla} \eta}{\eta} + \Delta \varphi \right]\,. \tag{3.13}$$

The latter equation (3.13) is again the continuity equation (3.7). To see this we multiply (3.13) with $2\eta^2$ and arrive at

$$\frac{\partial \eta^2}{\partial t} + \boldsymbol{\nabla} \cdot \left(\eta^2 \frac{\hbar}{M} \boldsymbol{\nabla} \varphi \right) = 0\,. \tag{3.14}$$

With Eqs. (3.9) and (3.11) we make out the equivalence of (3.14) with (3.7).
From the real part (3.12) we derive the equation of motion for the velocity field (3.11). To this end we take the gradient of equation (3.12) and have with (3.11):

$$\frac{\partial \boldsymbol{v}}{\partial t} = -\boldsymbol{\nabla} \cdot \left[\frac{v^2}{2} - \frac{\hbar^2}{2M^2} \frac{\boldsymbol{\nabla}^2 \sqrt{n}}{\sqrt{n}} + \frac{V(\mathbf{x},t) + gn}{M} \right] . \tag{3.15}$$

We compare the equations (3.14) and (3.15) with the hydrodynamic equations for a perfect fluid, which are the continuity equation (3.7) and the Euler equation, see [52]

$$n \left[\frac{\partial \boldsymbol{v}}{\partial t} + (\boldsymbol{v} \cdot \boldsymbol{\nabla}) \boldsymbol{v} \right] = n\mathbf{f} - \boldsymbol{\nabla} p \,, \tag{3.16}$$

where $\mathbf{f}$ is the force and p the pressure.
Since

$$(\boldsymbol{v} \cdot \boldsymbol{\nabla}) \boldsymbol{v} = \frac{1}{2} \boldsymbol{\nabla} v^2 - \boldsymbol{v} \times (\boldsymbol{\nabla} \times \boldsymbol{v}) \,, \tag{3.17}$$

we can rewrite the Euler equation (3.16) as

$$\frac{\partial \boldsymbol{v}}{\partial t} - \boldsymbol{v} \times (\boldsymbol{\nabla} \times \boldsymbol{v}) = \mathbf{f} - \frac{1}{2} \boldsymbol{\nabla} \, v^2 - \frac{\boldsymbol{\nabla} p}{n} \,. \tag{3.18}$$

Thus the equations (3.15) and (3.18) are very similar, if we identify

$$\mathbf{f} = \frac{1}{M} \boldsymbol{\nabla} [V(\mathbf{x},t) + gn], \qquad p = -\frac{\hbar^2}{2M^2} \sqrt{n} \boldsymbol{\nabla}^2 \sqrt{n} \,. \tag{3.19}$$

But there are two important differences between (3.15) and (3.18). The first is that the Euler equation (3.18) contains the additional term $\boldsymbol{v} \times (\boldsymbol{\nabla} \times \boldsymbol{v})$. However, since the velocity field of the superfluid (3.11) corresponds to a potential flow, $\boldsymbol{\nabla} \times \boldsymbol{v} = \mathbf{0}$, the term $\boldsymbol{v} \times (\boldsymbol{\nabla} \times \boldsymbol{v})$ does not contribute to the Euler equation (3.18). Actually, the latter term corresponds to a friction force from which an ideal fluid is not infected. Nevertheless, this is only true if φ is not singular, which applies here but fails in the discussion of the motion of vortices.
Hence, the more crucial difference between (3.15) and (3.18) is the term we identified with the pressure p to which we refer to as the quantum pressure. It describes forces due to the spatial variations in the magnitude of the wave function for the condensed state. We remark that if the spatial scale of variations of the condensate wave function is l, the quantum pressure p is of order $\hbar^2 (2M^2 l^5)^{-1}$ while the pressure corresponding to the term $gM^{-1}\eta^2$ is of order $g(Ml^3)^{-1}$. Therefore, we can neglect the quantum pressure p if l is large enough.

3.3 Rotating Trap

Consider a three-dimensional vector space which is spanned by the unit vectors $\{\mathbf{u}_\alpha\}$ with $\alpha \in \{x, y, z\}$. We suppose that the trap is rotating about an axis with a frequency Ω and is constant in time elsewise so that in the corotating frame $(\mathbf{u}', t)$ we have $V(\mathbf{x}, t) = V(\mathbf{x}')$. Note that $\mathbf{x}'$ depends on t. Without loss of generality, we may also assume that the trapping potential $V(\mathbf{x}, t)$ rotates about the z-axis with the rotation vector $\boldsymbol{\Omega} = \Omega \mathbf{u}_z$.
Then, the transformation is given by the rotation matrix

$$R(t) = \begin{pmatrix} \cos \Omega t & -\sin \Omega t & 0 \\ \sin \Omega t & \cos \Omega t & 0 \\ 0 & 0 & 1 \end{pmatrix} . \tag{3.20}$$

The unit vectors transform like $\mathbf{u}'_\alpha(t) = R(t)\,\mathbf{u}_\alpha$. Thus, the time derivative of the unit vectors $\mathbf{u}'_\alpha(t)$ becomes

$$\frac{\mathrm{d}}{\mathrm{d}t}\mathbf{u}'_\alpha(t) = \dot{R}(t)\cdot\mathbf{u}_\alpha = \dot{R}(t)\cdot R^T(t)\cdot\mathbf{u}'_\alpha(t)\,. \tag{3.21}$$

To shorten notation, we write $\tilde{R}(t) = \dot{R}(t)\cdot R^T(t)$, which reads due to (3.20)

$$\tilde{R}(t) = \Omega\begin{pmatrix} 0 & -1 & 0\\ 1 & 0 & 0\\ 0 & 0 & 0\end{pmatrix}. \tag{3.22}$$

We note that $\tilde{R}(t)$ is an antisymmetric matrix. This is a general fact, since for any rotation matrix $R(t)\cdot R(t)^T = 1$ is valid from which follows by a derivation with respect to the time t that $\dot{R}(t)\cdot R^T(t) + [\dot{R}(t)\cdot R^T(t)]^T = 0$. Furthermore, the rotation matrix $\tilde{R}(t)$ is a total antisymmetric matrix, which can be expressed by the rotation vector $\mathbf{\Omega}$

$$\tilde{R}_{ij}(t) = -\epsilon_{ijk}\mathbf{\Omega}_k\,, \tag{3.23}$$

where we have used Einstein's sum convention. With ϵ_{ijk} we denote the total antisymmetric Levi-Cività tensor which is related to the vector-cross product via

$$\epsilon_{ijk}\,\tilde{R}_k\cdot\left(\mathbf{u}'_\alpha(t)\right)_j = \left(\mathbf{u}'_\alpha(t)\times\mathbf{\Omega}\right)_i\,. \tag{3.24}$$

Therefore, we can write for (3.21)

$$\frac{\mathrm{d}}{\mathrm{d}t}\mathbf{u}'_\alpha(t) = -\mathbf{u}'_\alpha(t)\times\mathbf{\Omega}\,. \tag{3.25}$$

An arbitrary vector $\mathbf{b}(t)$ can be expressed either in the frame $(\mathbf{u},t)$ or in $(\mathbf{u}',t)$:

$$b_i(t)\,\mathbf{u}_i = b'_i(t)\,\mathbf{u}'_i(t)\,. \tag{3.26}$$

But for the time derivative of such a vector $\mathbf{b}(t)$ holds with(3.25):

$$\frac{\mathrm{d}}{\mathrm{d}t}\mathbf{b}(t) \;=\; \frac{\mathrm{d}}{\mathrm{d}t}\,b_i(t)\,\mathbf{u}_i \;=\; \frac{\mathrm{d}\,b'_i(t)}{\mathrm{d}t}\,\mathbf{u}'_i(t) + \mathbf{\Omega}\times\mathbf{b}(t)\,. \tag{3.27}$$

We apply this transformation to the Lagrange density (3.5) with the assumption that the primed frame is the corotating one. Hence, the primed coordinates are constant in time. With $\Psi(\mathbf{x},t) = \Psi'(\mathbf{x}',t)$ the derivation with respect to the time t yields according to the chain rule

$$\frac{\partial}{\partial t}\Psi(\mathbf{x},t) = \frac{\partial}{\partial t}\Psi'(\mathbf{x}',t) + \left(\mathbf{\Omega}\times\mathbf{x}'\right)\boldsymbol{\nabla}'\Psi'(\mathbf{x}',t)\,, \tag{3.28}$$

where the first derivation on the right hand side of (3.28) is due to the second argument of the wave function. The transformation $R(t)$ is not depending on the spatial coordinates, therefore the gradient remains unchanged in the new frame

$$\boldsymbol{\nabla}\to\boldsymbol{\nabla}' = \boldsymbol{\nabla}\,. \tag{3.29}$$

Inserting (3.28) and (3.29) into the Lagrange density (3.5) yields

$$\mathcal{L} = \Psi'^\star i\hbar\left[\frac{\partial}{\partial t} + (\mathbf{\Omega}\times\mathbf{x}')\cdot\boldsymbol{\nabla}'\right]\Psi' - \frac{\hbar^2}{2M}\boldsymbol{\nabla}'\Psi'^\star\boldsymbol{\nabla}'\Psi' - V(\mathbf{x}')\Psi'^\star\Psi' - \frac{g}{2}(\Psi'^\star\Psi')^2. \tag{3.30}$$

We omit the primes and use

$$i\hbar(\mathbf{\Omega}\times\mathbf{x})\cdot\boldsymbol{\nabla} = -\mathbf{\Omega}\hat{\mathbf{L}}\,, \tag{3.31}$$

where $\hat{\mathbf{L}} = \hbar/i\ (\mathbf{x} \times \boldsymbol{\nabla})$ is the first quantized one-particle angular momentum operator which reduces here for $\boldsymbol{\Omega} = \Omega \mathbf{u}_z$ to $\hat{\mathbf{L}}\mathbf{u}_z = \hat{L}_z$. Inserting the angular momentum $\hat{L}_z$ into (3.30) and performing a partial integration on the kinetic term, with the assumption that the border of integration does not contribute, we arrive at

$$\mathcal{L} = \Psi^* \left[i\hbar \frac{\partial}{\partial t} - \Omega \hat{L}_z \right] \Psi + \frac{\hbar^2}{2M} \Psi^* \Delta \Psi - V(\mathbf{x}) \Psi^* \Psi - \frac{g}{2} (\Psi^* \Psi)^2 \,. \tag{3.32}$$

In order to eliminate the extra (linear) spatial derivative $\Omega \hat{L}_z$, we perform a phase shift to the wave function and choose a proper phase in the end. The transformation is given by

$$\Psi = \Psi' e^{i\varphi(\mathbf{x})} \,, \tag{3.33}$$

where $\varphi(\mathbf{x})$ is real. Then, the Lagrange density (3.32) becomes omitting the primes

$$\begin{aligned} \mathcal{L} \;\; = \;\; & \Psi^* \left[i\hbar \frac{\partial}{\partial t} - \Omega \hat{L}_z - i\Omega (\hat{L}_z \varphi) \right] \Psi - V(\mathbf{x}) \Psi^* \Psi - \frac{g}{2} (\Psi^* \Psi)^2 \\ & - \frac{\hbar^2}{2M} \Psi^* \left[\Delta \Psi + 2i (\boldsymbol{\nabla} \varphi)(\boldsymbol{\nabla} \Psi) + (\boldsymbol{\nabla} \varphi)^2 \Psi \right] \,. \end{aligned} \tag{3.34}$$

We specify the phase $\varphi(\mathbf{x})$ by assuming

$$i \frac{\hbar^2}{M} \Psi^* (\boldsymbol{\nabla} \varphi)(\boldsymbol{\nabla} \Psi) = -\Psi^* i\hbar \Omega \hat{L}_z \Psi = -\Psi^* i\hbar \left(\boldsymbol{\Omega} \times \mathbf{x} \right) \boldsymbol{\nabla} \Psi \,, \tag{3.35}$$

which implies

$$\boldsymbol{\nabla} \varphi(\mathbf{x}) = -\frac{M}{\hbar} \left(\boldsymbol{\Omega} \times \mathbf{x} \right) = \frac{M\Omega}{\hbar} \begin{pmatrix} y \\ -x \\ 0 \end{pmatrix} \,. \tag{3.36}$$

Hence, it is not a integrable function and we conclude that the phase $\varphi(\mathbf{x})$ has to be singular as

$$\boldsymbol{\nabla} \times \boldsymbol{\nabla} \varphi(\mathbf{x}) = \frac{M\Omega}{\hbar} 2\mathbf{u}_z \neq \mathbf{0} \,. \tag{3.37}$$

Thus, the phase $\varphi(\mathbf{x})$ can not be derivated twice continuously. Inserting (3.35) and (3.36) into (3.34) we arrive at

$$\mathcal{L} = \Psi^* i\hbar \frac{\partial \Psi}{\partial t} - \frac{\hbar^2}{2M} \boldsymbol{\nabla} \Psi^* \boldsymbol{\nabla} \Psi - V(\mathbf{x}, \boldsymbol{\Omega}) \Psi^* \Psi - \frac{g}{2} (\Psi^* \Psi)^2 \,, \tag{3.38}$$

where we denote the rotating trap according to

$$V(\mathbf{x}, \boldsymbol{\Omega}) = V(\mathbf{x}) - \frac{M\Omega^2}{2} (x^2 + y^2) \,. \tag{3.39}$$

Thus, in the corotating frame the rotating trap obtains an additional repulsive harmonic potential in the xy-plane of the corotating frame.

3.4 Collective Modes in Traps

We consider the equilibrium of the condensate described by the Gross-Pitaevskii equation (3.1). The equilibrium wave function is constant in time wherefore we separate the condensate function according to

$$\Psi(\mathbf{x}, t) = \Psi(\mathbf{x}) e^{-i\mu t/\hbar} \,, \tag{3.40}$$

with a constant chemical potential μ. The chemical potential plays the same role as the energy eigenvalue does in the ordinary linear Schrödinger theory. With the separation (3.40) the stationary Gross-Pitaevskii equation reads in the corotating frame

$$\left\{\mu + \frac{\hbar^2}{2M}\Delta - V(\mathbf{x}) - g|\Psi(\mathbf{x})|^2\right\}\Psi(\mathbf{x}) = 0\,. \tag{3.41}$$

In the Thomas-Fermi approximation, which consists in neglecting the kinetic energy, the stationary Gross-Pitaevskii equation (3.41) simplifies to

$$\left[V(\mathbf{x}) + g|\Psi(\mathbf{x})|^2\right]\Psi(\mathbf{x}) = \mu\Psi(\mathbf{x})\,. \tag{3.42}$$

We note that the Thomas-Fermi approximation is closely related to the semiclassical approximation, since it is related with the classical limit $\hbar \to 0$. The Thomas-Fermi approximation (3.42) of the Gross-Pitaevskii equation (3.41) yields an algebraic equation for the density

$$n_{\mathrm{TF}} \equiv |\Psi(\mathbf{x})|^2 = \frac{\mu - V(\mathbf{x})}{g}\,. \tag{3.43}$$

In the Thomas-Fermi approximation, the chemical potential μ is due to the normalization condition (3.2) obtained from (3.43) by a spatial integration over the positive integrand.
We extend the Thomas-Fermi approximation to the Euler Equation (3.15) by taking the limit $\hbar \to 0$ which results in neglecting the kinetic energy and the spatial variations of the density according to the quantum pressure p (3.19)

$$M\frac{\partial \boldsymbol{v}}{\partial t} = -\boldsymbol{\nabla}\cdot\left[\frac{v^2}{2} + V(\mathbf{x}) + gn\right]\,, \tag{3.44}$$

where the velocity field is given through (3.9). We note that the Thomas-Fermi approximated density (3.43) and a vanishing velocity field are the equilibrium solutions of the Euler equation (3.44)

$$n_{\mathrm{eq}} = \frac{\mu - V(\mathbf{x})}{g}\,, \qquad \boldsymbol{v}_{\mathrm{eq}} = \mathbf{0}\,, \tag{3.45}$$

We are interested in periodic solutions of the Gross-Pitaevskii equation (3.1) which oscillate around the equilibrium state of the condensate, the hydrodynamic collective modes. Therefore, we decompose the density n into the equilibrium density n_{eq} and a small deviation from it δn and analogously the velocity field $\boldsymbol{v}$. We write explicitly

$$n = n_{\mathrm{eq}} + \delta n\,, \qquad \boldsymbol{v} = \boldsymbol{v}_{\mathrm{eq}} + \delta\boldsymbol{v}\,. \tag{3.46}$$

We linearize the continuity equation (3.8) and the Euler equation (3.44) with respect to the departures from the equilibrium δn and $\delta\boldsymbol{v}$. For the continuity equation (3.8) insertion of (3.46) together with (3.45) yields

$$\frac{\partial\,\delta n}{\partial t} = -\boldsymbol{\nabla}\left[\frac{\mu - V(\mathbf{x})}{g}\,\delta\boldsymbol{v}\right]\,. \tag{3.47}$$

Inserting (3.46) with (3.45) into the Thomas-Fermi approximated Euler equation (3.44) leads to

$$M\frac{\partial\,\delta\boldsymbol{v}}{\partial t} = -g\boldsymbol{\nabla}\delta n\,. \tag{3.48}$$

Combining the two coupled partial differential equations (3.47) and (3.48) by taking the time derivative of (3.47) we obtain the equation of motion for the deviation from the equilibrium density (3.45)

$$M\frac{\partial^2\delta n}{\partial t^2} = [\,\mu - V(\mathbf{x})\,]\,\boldsymbol{\nabla}^2\,\delta n - \boldsymbol{\nabla}V(\mathbf{x})\cdot\boldsymbol{\nabla}\delta n\,, \tag{3.49}$$

where we have used the fact that μ is constant under stationary conditions so that $\boldsymbol{\nabla}\mu = 0$. We consider oscillations around this equilibrium density with a time dependence $\delta n = \delta n(\mathbf{x})\, e^{i\omega t}$. Then, the equation of motion (3.49) takes the form

$$M\omega^2 \delta n(\mathbf{x}) = -\left[\,\mu - V(\mathbf{x})\,\right] \boldsymbol{\nabla}^2\, \delta n(\mathbf{x}) + \boldsymbol{\nabla} V(\mathbf{x}) \cdot \boldsymbol{\nabla} \delta n(\mathbf{x})\,. \tag{3.50}$$

For any trap $V(\mathbf{x})$, Eq. (3.50) represents a partial differential equation for the deviation δn of the equilibrium density (3.43) in the Thomas-Fermi approximation. In the following subsections we discuss some solutions of (3.50) for harmonic and anharmonic trapping potentials.

3.5 Harmonic Trap with Spherical Symmetry

We consider a harmonic, isotropic trap with the trapping potential

$$V(\mathbf{x}) = \frac{M\omega_0^2}{2}(x^2 + y^2 + z^2)\,. \tag{3.51}$$

The geometry of the trap suggests to work in spherical coordinates, where the gradient and the Laplacian reads

$$\boldsymbol{\nabla} = \mathbf{u}_r \frac{\partial}{\partial r} + \mathbf{u}_\theta \frac{1}{r}\frac{\partial}{\partial \theta} + \mathbf{u}_\phi \frac{1}{r\sin\theta}\frac{\partial}{\partial \phi}\,, \tag{3.52}$$

$$\boldsymbol{\nabla}^2 = \frac{1}{r^2}\,\frac{\partial}{\partial r}\left(r^2 \frac{\partial}{\partial r}\right) + \frac{1}{r^2 \sin\theta}\,\frac{\partial}{\partial \theta}\left(\sin\theta \frac{\partial}{\partial \theta}\right) + \frac{1}{r^2\sin^2\theta}\,\frac{\partial^2}{\partial \phi^2}\,, \tag{3.53}$$

where we have transformed the Cartesian coordinates $\{x, y, z\}$ into spherical $\{r, \theta, \phi\}$ ones. The equilibrium density (3.45) is due to the Thomas-Fermi approximation in the harmonic trap (3.51) given by

$$n_{\mathrm{eq}} = \frac{2\mu - M\omega_0^2 r^2}{2g} \tag{3.54}$$

and is a positive quantity. Since μ is a constant in stationary conditions, Eq. (3.54) sets a maximal radius R at which the equilibrium density (3.54) vanish:

$$R^2 = \frac{2\mu}{M\omega_0^2}\,. \tag{3.55}$$

This maximal radius R is called the Thomas-Fermi radius and describes under stationary conditions the elongation of the condensate. Here, the condensate cloud is a ball of the radius R. Inserting (3.55 into the equation of motion (3.50) we obtain

$$\hat{G}_s\, \delta n(\mathbf{x}) = \gamma^2\, \delta n(\mathbf{x})\,, \tag{3.56}$$

with the differential operator

$$\hat{G}_s = r\frac{\partial}{\partial r} - \frac{1}{2}(R^2 - r^2)\boldsymbol{\nabla}^2\,, \tag{3.57}$$

whereas $\gamma = \omega/\omega_0$ denotes the square root of the eigenvalue of $\hat{G}_s$. Because of the spherical symmetry, the angular and the radial part of the solution can be separated according to

$$\delta n(\mathbf{x}) = A(r) Y_{lm}(\theta, \phi)\,, \tag{3.58}$$

where $Y_{lm}(\theta, \phi)$ are the spherical harmonics. With this ansatz (3.58), we obtain from (3.56) with (3.57) an ordinary differential equation for $A(r)$:

$$\gamma^2 A(r) = rA'(r) - \frac{1}{2}\left(R^2 - r^2\right)\left\{\frac{\partial^2}{\partial r^2} + \frac{2}{r}\frac{\partial}{\partial r} - \frac{l(l+1)}{r^2}\right\} A(r)\,, \tag{3.59}$$

where a prime denotes a derivation with respect to r. We remark that the first term in (3.57) preserves the power of r but the second does not. In order to find the general solution it is convenient to separate out the radial dependence due to the centrifugal barrier $l(l+1)/r^2$ by defining the new radial function $B(r) = A(r)/r^l$. The resulting ordinary differential equation for $B(r)$ reads

$$\gamma^2 B(r) = lB(r) + rB'(r) - \frac{1}{2}\left(R^2 - r^2\right)\left[B''(r) + \frac{2(l+1)B'(r)}{r}\right]. \tag{3.60}$$

We introduce a new dimensionless variable $u = r^2/R^2$ so that (3.60) simplifies to

$$u(1-u)B''(u) + \left(\frac{2l+3}{2} - \frac{2l+5}{2}u\right)B'(u) + \frac{\gamma^2 - l}{2}B(u) = 0\,, \tag{3.61}$$

where a prime now denotes a derivation with respect to u. This differential equation (3.61) is of the form

$$\left\{u(1-u)\frac{\partial^2}{\partial u^2} + [c - (a+b+1)u]\,\frac{\partial}{\partial u} - ab\right\}F(a,b;c;u) = 0 \tag{3.62}$$

which is known as the hypergeometric differential equation. One of the two solutions of the hypergeometric differential equation (3.62) is the hypergeometric series

$$F(a,b;c;u) = \sum_{\nu=0}^{\infty}\frac{(a)_\nu (b)_\nu}{(c)_\nu}\frac{u^\nu}{\nu!} = 1 + \frac{ab}{c}u + \frac{a(a+1)b(b+1)}{c(c+1)}\frac{u^2}{2} + \dots\,, \tag{3.63}$$

where $(a)_\nu$ denotes the Pochhammer symbol

$$(a)_\nu = a(a+1)\dots(a+\nu-1) = \frac{\Gamma(a+\nu)}{\Gamma(a)}\,. \tag{3.64}$$

We list some properties of the hypergeometric function in Appendix C. The second solution (C.2) of (3.62) must be neglected to avoid possible divergencies at the origin of the trap. This is necessary for the conservation of the number of particles and the smallness condition $\delta n/n \ll 1$. The function (3.63) is behaved in the limit $r \to \infty$ and $u \to \infty$ respectively, if it reduces to a finite sum. Therefore, either a or b must be a negative integer $-n_r$. Because of the symmetry $F(a,b;c;u) = F(b,a;c;u)$ we can choose freely and set $a = -n_r$. Comparing the coefficients of (3.61) and (3.62), one sees that $c = l + 3/2$ and $b = n_r + l + 3/2$. , while for the eigenvalue $\gamma = \omega/\omega_0$ one finds

$$\omega = \omega_0\sqrt{l + 3n_r + 2n_r l + 2n_r^2}\,. \tag{3.65}$$

The normal modes of the cloud are sums of terms of the form

$$\delta n(\mathbf{x}) = \delta n(n_r, l, m) = Cr^l F\left(-n_r, n_r + l + \frac{3}{2}; l + \frac{3}{2}; \frac{r^2}{R^2}\right)Y_{lm}(\theta,\phi)\,. \tag{3.66}$$

For $n_r = 0$ and with increasing l, the modes (3.66) become more localized near the surface of the cloud, since $\delta n \propto r^l$ with the restriction $\delta n/n_{\rm eq} \ll 1$. Therefore, they are referred to as surface waves. The $l = 0$ mode is trivial. It represents a change of the density which is constant everywhere. The resulting change of the chemical potential is likewise the same everywhere inside the cloud. Therefore, there is no restoring force and the frequency of the mode is zero. The three $l = 1$ modes correspond to a translation of the cloud with no change in the internal structure.

For the mode $l = 1$, $m = 0$, the density variation is proportional to $r\cos\theta = z$. In equilibrium, the density profile (3.54) is with (3.55) $n_{\rm eq}(r) \propto (1 - r^2/R^2)$. If the center of the cloud is moved in the z direction a distance ζ, the change in the density is given by $\delta n = -\zeta\partial n_{\rm eq}/\partial z \propto z$. They behave like particles in an external harmonic potential. The motion of the center of mass

l	m	$\delta n(0,l,m)$	γ
2	0	$r^2\sqrt{\frac{5}{16\pi}}\,(3\cos^2\theta-1)$	$\sqrt{2}$
2	±1	$r^2\sqrt{\frac{5}{24\pi}}3\sin\theta\cos\theta\,e^{\pm i\phi}$	$\sqrt{2}$
2	±2	$r^2\sqrt{\frac{5}{96\pi}}3\sin^2\theta\,e^{\pm i2\phi}$	$\sqrt{2}$
l	$\pm l$	$r^l\sin^l\theta\,e^{\pm il\phi}$	$\sqrt{l}$

l	m	$\delta n(1,l,m)$	γ
0	0	$\left(1-\frac{5r^2}{3R^2}\right)\frac{1}{\sqrt{4\pi}}$	$\sqrt{5}$
1	0	$\left(r-\frac{7r^3}{5R^2}\right)\sqrt{\frac{3}{4\pi}}\cos\theta$	$\sqrt{8}$
1	±1	$\left(r-\frac{7r^3}{5R^2}\right)\sqrt{\frac{3}{8\pi}}\sin\theta\,e^{\pm i\phi}$	$\sqrt{8}$
l	m	$\left(r^l-\frac{2l+5}{2l+3}\,\frac{r^{l+2}}{R^2}\right)Y_{lm}(\theta,\phi)$	$\sqrt{3l+5}$

Table 3.1: Both Tables show special solutions of (3.56) and the corresponding eigenvalue γ. The left-hand Table is for $n_r=0$. These are the quadrupole surface modes, they have no nodes. In the right-hand Table is $n_r=1$. Here, the $l=0$ is the breathing mode.

$r_{\rm cm}$ is that of a free particle of mass $N_{\mathbf{0}}M$ moving in a potential $N_{\mathbf{0}}M\omega_0^2 r_{\rm cm}^2/2$ with the same frequency ω_0^2 that a single particle would have. The center of mass and the relative motions are separable for interactions that depend only on the relative coordinates of the particles.
For $n_r=1$ only the $l=0$ mode has a special name. It is spherical symmetric and, as one can see from equation (3.48) with the Thomas-Fermi approximation (3.45), the radial velocity field has the same sign everywhere. That is, the cloud looks like a breathing balloon. Therefor it is referred to as the breathing mode. A survey of these special modes is given in Table 3.1.

3.6 Harmonic Trap with Cylindrical Symmetry

We discuss some solutions for a cylindrical symmetric harmonic trap potential. This special trap symmetry is realized in many experiments and has been solved completely by M. Fliesser [57] in 1997. We write the potential in the form

$$V(\mathbf{x})=\frac{M}{2}\omega_z^2(\lambda^2 r_\perp^2+z^2)\,, \tag{3.67}$$

where $r_\perp=\sqrt{x^2+y^2}$ is the radius in the xy-plane and $\lambda=\omega_\perp/\omega_z$ is the anisotropy parameter. For such a trap the equilibrium density in the Thomas-Fermi approximation (3.45) is given by

$$n=\frac{\mu}{g}\left(1-\frac{\lambda^2 r_\perp^2}{R^2}-\frac{z^2}{R^2}\right)\,. \tag{3.68}$$

The condensate is an ellipsoid with a semi-axes in z-direction according to $\mu-V(0,0,R)$ of the length

$$R^2=\frac{2\mu}{M\omega_z^2}\,. \tag{3.69}$$

In cylindrical coordinates the the gradient and the Laplace operator read

$$\boldsymbol{\nabla} = \mathbf{u}_r\frac{\partial}{\partial r_\perp}+\mathbf{u}_\theta\frac{1}{r_\perp}\frac{\partial}{\partial\phi}+\mathbf{u}_z\frac{\partial}{\partial z}\,, \tag{3.70}$$

$$\boldsymbol{\nabla}^2 = \frac{1}{r_\perp}\frac{\partial}{\partial r_\perp}r_\perp\frac{\partial}{\partial r_\perp}+\frac{1}{r_\perp^2}\frac{\partial^2}{\partial\phi^2}+\frac{\partial^2}{\partial z^2}\,. \tag{3.71}$$

Thus, equation (3.50) reads

$$\hat{G}_c\,\delta n = \gamma^2\,\delta n\,, \tag{3.72}$$

with the differential operator for the cylindrical trap

$$\hat{G}_c = \lambda^2 r_\perp \frac{\partial}{\partial r_\perp} + z\frac{\partial}{\partial z} - \frac{1}{2}\left(R^2 - \lambda^2 r_\perp^2 - z^2\right)\boldsymbol{\nabla}^2\,. \tag{3.73}$$

and the eigenvalue $\gamma = \omega/\omega_z$ similar to (3.56). Because of the axial symmetry there are solutions proportional to $e^{im\phi}$, where m is an integer. One simple class of solutions is of the form

$$\delta n \propto r_\perp^l e^{\pm il\phi} = (r\sin\theta)^l e^{\pm il\phi} \propto r^l Y_{l,\pm l}(\theta,\phi)\,. \tag{3.74}$$

The first proportionality in the above relation is given in cylinder coordinates, while in the second relation we have used spherical coordinates. Furthermore, we take into account the relation $Y_{l,\pm l}(\theta,\phi) \propto \sin\theta^l$, since the spherical harmonics are defined by

$$Y_{l,m}(\theta,\phi) = N_l^m P_l^m(\cos\theta)e^{im\phi}\,, \tag{3.75}$$

where the associated Legendre polynomials P_l^m are given by

$$P_l^m(x) \;=\; \frac{(-1)^m}{2^l l!}\left(1-x^2\right)^{m/2}\frac{\mathrm{d}^{l+m}\left(x^2-1\right)^l}{\mathrm{d}x^{l+m}} \tag{3.76}$$

and the normalization coefficient N_l^m reads

$$N_l^m \;=\; \sqrt{\frac{2l+1}{4\pi}\frac{(l-m)!}{(l+m)!}}\,. \tag{3.77}$$

We transform Eq. (3.72) for the eigenfrequencies into spherical coordinates with $r_\perp = r\sin\theta$ and use (3.53) to obtain

$$\hat{G}_s(\lambda^2)\,\delta n = \gamma^2\,\delta n\,, \tag{3.78}$$

with differential operator

$$\hat{G}_s(\lambda^2) = \left(\lambda^2\sin^2\theta + \cos^2\theta\right) r\frac{\partial}{\partial r} + \sin\theta\cos\theta(\lambda^2-1)\frac{\partial}{\partial\theta} - \frac{1}{2}Q(\mu)\boldsymbol{\nabla}^2\,. \tag{3.79}$$

As a abbreviation we have introduced

$$Q(\mu) = R^2 - (\lambda^2\sin^2\theta + \cos^2\theta)r^2. \tag{3.80}$$

In the limit $\lambda = 1$, Eq. (3.79) reproduces the spherical differential operator (3.56).
In the special case $m = \pm l$, we have $\boldsymbol{\nabla}^2\delta n = 0$ for the deviation δn of the ansatz (3.75). Thus, we obtain with (C.5) from (3.78) the eigenfrequencies γ

$$\omega = \sqrt{l}\,\lambda\omega_z\,. \tag{3.81}$$

Another simple solution is obtained by the ansatz

$$\delta n = C r^l Y_{l,\pm(l-1)}(\theta,\phi)\,, \tag{3.82}$$

for which we find with (3.75) and (C.5) as well as (C.6)

$$r\frac{\partial}{\partial r}\delta n \;=\; l\delta n\,, \tag{3.83}$$

$$\frac{\partial}{\partial\theta}\delta n \;=\; \left[\frac{\cos\theta}{\sin\theta}(l-1) - \frac{\sin\theta}{\cos\theta}\right]\delta n\,. \tag{3.84}$$

Inserting (3.83) and (3.84) into (3.79) gives

$$\omega = \sqrt{(l-1)\lambda^2 + 1}\,\omega_z\,. \tag{3.85}$$

More generally, we insert the solution of the isotropic trap

$$\delta n(0,l,m) = N_l^m r^l Y_{l,m}(\theta,\phi) \tag{3.86}$$

into the differential equation for the eigenmodes (3.78). With help of (C.5) and (C.6) we eliminate the $\cos\theta$ terms in (3.79) and we find for $l-2 \geq m$:

$$\begin{aligned} G_s(\lambda^2)\,\delta n(0,l,m) &= \left(\frac{l^2-l+m^2}{2l-1}\lambda^2 + \frac{l^2-m^2}{2l-1}\right)\delta n(0,l,m) \\ &\quad + \frac{(1-\lambda^2)(l+m)(l+m-1)}{2l-1}\, r^2\, \frac{N_l^m}{N_{l-2}^m}\,\delta n(0,l-2,m)\,, \end{aligned} \tag{3.87}$$

Note that the above discussed special cases $m = \pm l$, $\pm(l-1)$ are such solutions for which the term proportional to D in (3.87) vanishes. Furthermore, we note that we obtain for spherical symmetry $\lambda^2 = 1$ the same eigenfrequencies (3.65) with $n_r = 0$ for the cloud as before .
Regarding the case $l = 2$, $m = 0$, the deviation from the equilibrium density is $\delta n = ar_\perp + bz$ with the decomposition of the radius r in spherical coordinates into cylinder components $r^2 = r_\perp^2 + z^2$ and some constants a, b. From (3.87) we obtain with $\delta n = ar_\perp + bz$

$$\hat{G}_s(\lambda^2)\left(ar_\perp^2 + bz^2\right) = cr_\perp^2 + dz^2\,, \tag{3.88}$$

with some constants a, b, c, d. Since this is nearly a solution of the eigenvalue problem we reenter (3.79) with the ansatz

$$\delta n = a + br_\perp^2 + cz^2\,. \tag{3.89}$$

Insertion of (3.89) into (3.79) yields three algebraic equations for a, b, and c which have non trivial solutions if, in matrix notation, the determinant of the matrix vanishes. We find, in matrix notation, the following set of equations

$$\begin{pmatrix} \omega & 2R^2\omega_z^2 & R^2\omega_z^2 \\ 0 & \omega^2 - 4\lambda^2\omega_z^2 & \lambda^2\omega_z^2 \\ 0 & 2\omega_z^2 & \omega^2 - 3\omega_z^2 \end{pmatrix} \begin{pmatrix} a \\ b \\ c \end{pmatrix} = \begin{pmatrix} 0 \\ 0 \\ 0 \end{pmatrix}. \tag{3.90}$$

The determinant of the matrix in (3.90) vanishes for $\omega = 0$, which is the trivial mode, or for

$$\omega^2 = \omega_\pm^2 = 2\omega_z^2\left(\frac{3}{4} + \lambda^2 \pm \sqrt{\lambda^4 - \lambda^2 + \frac{9}{16}}\right). \tag{3.91}$$

In the isotropic limit $\lambda^2 = 1$ these two eigenfrequencies are

$$\omega_- = \sqrt{2}\,\omega_z \qquad \omega_+ = \sqrt{5}\,\omega_z\,, \tag{3.92}$$

which makes it reasonable to interpret these two frequencies $\omega_\pm^2$ as a coupling of the two modes $(0,2,0)$ and $(1,0,0)$ in the isotropic trap. The solutions we have found are compared with the spherical modes in Table 3.2.

n_r	l	m	isotrop	anisotrop
0	2	± 2	$\omega = \sqrt{2}\,\omega_0$	$\omega = \sqrt{2}\,\lambda\omega_z$
0	2	± 1	$\omega = \sqrt{2}\,\omega_0$	$\omega = \sqrt{1+\lambda^2}\,\omega_z$
0	2	0	$\omega = \sqrt{2}\,\omega_0$	$\omega = \omega_-$
1	0	0	$\omega = \sqrt{5}\,\omega_0$	$\omega = \omega_+$
0	l	$\pm l$	$\omega = \sqrt{l}\,\omega_0$	$\omega = \sqrt{l}\,\lambda\omega_z$
0	l	$\pm(l-1)$	$\omega = \sqrt{l}\,\omega_0$	$\sqrt{1+(l-1)\lambda^2}\,\omega_z$

Table 3.2: Hydrodynamic collective modes in cylindrical harmonic trap. We face the lowest lying modes of the cylindrical harmonic trap with corresponding modes of a trap with spherical symmetry. The modes $\omega_\pm$ are given by (3.91).

3.7 Anharmonic Trap with Cylindrical Symmetry

Now we add to the anisotropic harmonic trapping potential an additional anharmonic term and treat the latter as a small perturbation. The trap of the Paris experiment [1] is of that form (1.17). Without rotation, the anharmonicity of this trap is small, about 1% of the harmonic part. But with increasing rotation speed Ω the situation changes and the anharmonicity becomes very large compared to harmonic potential. Therefore, in the fast rotation regime perturbation theory is not applicable. However, we have the golden tool of variational perturbation theory [58] to treat even strong couplings perturbatively and to overcome these problems. This systematic extension of a variational approximation has been proposed for path integrals by R.P. Feynman and H. Kleinert [59]. Thus, we can investigate two regimes, the first is the slow rotation and the second is the fast rotation regime.
We write in spherical coordinates the cylindrical symmetric anharmonic trapping potential as

$$V(\mathbf{x}) = \frac{M\omega_z^2}{2}\left(\lambda^2\eta\, r^2\sin^2\theta + r^2\cos^2\theta + \frac{k}{2}\, r^4\sin^4\theta\right), \tag{3.93}$$

where $k = \epsilon_z\kappa/a_z^4$ is the anharmonicity, $\lambda = \omega_\perp/\omega_z$ the anisotropy and $\eta = 1 - \Omega^2/\omega_\perp^2$ the rotation parameter similar to (1.18). Then, the differential equation (3.50) reads

$$\hat{G}_a\,\delta n = \gamma^2\,\delta n\,, \tag{3.94}$$

with $\gamma = \omega/\omega_z$ as before. The differential operator $\hat{G}_a$ decomposes as

$$\hat{G}_a = \hat{G}_s(\lambda^2\eta) + k\,\hat{G}_p\,, \tag{3.95}$$

into the unperturbed cylindrical differential operator $\hat{G}_s$ from (3.79) and the perturbative contribution

$$\hat{G}_p = r^2\sin^2\theta\left[\sin^2\theta r\frac{\partial}{\partial r} + \sin\theta\cos\theta\frac{\partial}{\partial\theta}\right] - \frac{1}{2}\left(a_z^2R^2 - \frac{1}{2}r^4\sin^4\theta\right)\boldsymbol{\nabla}^2 \tag{3.96}$$

The Thomas-Fermi radius R is determined by the normalization condition (3.2) within the Thomas-Fermi approximation (3.45). The Thomas-Fermi radius R in (3.96) can be obtained

according to A.L. Fetter [60] in the following way. The normalization condition (3.2) takes in the Thomas-Fermi approximation (3.45) the form

$$N_{\mathbf{0}} = \frac{\mu}{g}\int \mathrm{d}^3x \,\left[1 - \frac{V(\mathbf{x})}{\mu}\right]\Theta\left[\,\mu - V(\mathbf{x})\right]\,, \tag{3.97}$$

where $\Theta(x)$ denotes the Heaviside function, i.e. the integral is to be taken over the volume of the cloud. The normalization condition (3.97) in cylinder coordinates yields

$$N_{\mathbf{0}} = \frac{\mu}{g}\int_0^{r_0}\mathrm{d}r_\perp\, r_\perp \int_0^{2\pi}\mathrm{d}\phi\int_{-z_0}^{z_0}\mathrm{d}z\,\left[1 - \frac{\lambda^2\eta\, r_\perp^2}{l_{\omega_z}^2} - \frac{z^2}{l_{\omega_z}^2} - \frac{k\, r_\perp^4}{2\, l_{\omega_z}^2}\right]\,, \tag{3.98}$$

where we have introduced

$$l_{\omega_z} = \sqrt{\frac{2\mu}{M\omega_z^2}} \tag{3.99}$$

and the radius of the cloud along the z-axis z_0, which is given by

$$z_0 = \left(l_{\omega_z}^2 - \lambda^2\eta\, r_\perp^2 - \frac{k}{2}r_\perp^4\right)^{1/2}\,. \tag{3.100}$$

Integrating out the ϕ and the z dependence yields

$$N_{\mathbf{0}} = \frac{4\pi\mu}{g}\int_0^{r_0}\mathrm{d}r_\perp\, r_\perp\left[\left(1 - \frac{\lambda^2\eta\, r_\perp^2}{l_{\omega_z}^2} - \frac{k\, r_\perp^4}{2l_{\omega_z}^2}\right)z - \frac{z^3}{3l_{\omega_z}^2}\right]_0^{z_0}\,. \tag{3.101}$$

Inserting (3.100) into (3.101 we get to

$$N_{\mathbf{0}} = \frac{8\pi\mu\, l_{\omega_z}}{3g}\int_0^{r_0}\mathrm{d}r_\perp\, r_\perp\left(1 - \frac{\lambda^2\eta\, r_\perp^2}{l_{\omega_z}^2} - \frac{k\, r_\perp^4}{2\, l_{\omega_z}^2}\right)^{3/2}\,. \tag{3.102}$$

With the substitution $u = (k/2l_{\omega_z}^2)^{1/2}r_\perp^2$ we can re-write (3.102) as

$$N_{\mathbf{0}} = \frac{8\pi\mu\, l_{\omega_z}^2}{3g}\sqrt{\frac{2}{k}}\, f(\xi)\,, \tag{3.103}$$

where we have written the remaining integral in (3.102) as

$$f(\xi) = \int_0^{u_0}\mathrm{d}u\,\left(1 - 2\xi u - u^2\right)^{3/2} \tag{3.104}$$

and the radius at which the integrand vanishes as $u_0 = -\xi + (1+\xi^2)^{1/2}$. Furthermore, we have introduced a geometric parameter

$$\xi = \frac{\lambda^2\eta}{l_{\omega_z}\sqrt{2k}}\,. \tag{3.105}$$

It is very similar to the geometric parameter x (2.97) from Section 2.5, which has been the second argument of the generalized ζ-function (B.3). This integral (3.104) is easily solved or can be found i.e. in [61, (246)] and yields

$$f(\xi) = \frac{3\pi}{16}\left(1+\xi^2\right)^2\left[1 - \frac{2}{\pi}\arcsin\frac{\xi}{\sqrt{1+\xi^2}}\right] - \frac{5\xi}{8} - \frac{3\xi^3}{8}\,. \tag{3.106}$$

For small or for large η compared to $\lambda^2/(l_{\omega_z}^2\sqrt{2\kappa})$, also the parameter ξ becomes small or large and we can expand $f(\xi)$ according to

$$f(\xi) \approx \begin{cases} \dfrac{1}{5\,\xi} - \dfrac{1}{35\,\xi^3} & \text{for} \quad \xi \gg 1 \\ \dfrac{3\pi}{16}\left(\xi^2+1\right)^2 - \xi - \xi^3 & \text{for} \quad |\xi| \ll 1 \\ \dfrac{3\pi}{8}\left(\xi^2+1\right)^2 - \dfrac{1}{5\,\xi} & \text{for} \quad \xi \ll -1 \end{cases} . \tag{3.107}$$

Inserting the interaction strength g (2.159), the length l_{ω_z} (3.99), and the approximation (3.107) into the normalization condition (3.103) yields in lowest order

$$N_{\mathbf{0}} = \begin{cases} \dfrac{2\,a_z}{15\lambda^2\eta\,a}\left(\dfrac{2\mu}{\hbar\omega_z}\right)^{5/2}\left[1 - \dfrac{2\kappa}{7\,\lambda^4\eta^2}\left(\dfrac{2\mu}{\hbar\omega_z}\right)\right] & \text{for} \quad \eta \gg 1 \\ \dfrac{\pi a_z}{8\sqrt{2\kappa}\,a}\left(\dfrac{2\mu}{\hbar\omega_z}\right)^{2}\left[1 - \dfrac{16\lambda^2\eta}{3\pi\sqrt{2\kappa}}\sqrt{\dfrac{\hbar\omega_z}{2\mu}}\right] & \text{for} \quad |\eta| \ll 1 \\ \dfrac{\pi a_z}{40\lambda^2\eta a}\left(\dfrac{2\mu}{\hbar\omega_z}\right)^{5/2}\left[\dfrac{\lambda^2\eta}{\sqrt{2\kappa}}\sqrt{\dfrac{\hbar\omega_z}{2\mu}} + \dfrac{\lambda^4\eta^2}{\sqrt{2\kappa}}\left(\dfrac{\hbar\omega_z}{2\mu}\right) - \dfrac{16}{3\pi}\right] & \text{for} \quad \eta \ll -1 \end{cases} , \tag{3.108}$$

where we have, similar to (1.16) and (1.18), introduced the quantities

$$a_z = \sqrt{\frac{\hbar}{M\omega_z}}, \qquad \kappa = \frac{k}{a_z^2}\,. \tag{3.109}$$

To find μ we have to invert equation (3.108). For $\xi \gg 1$ we have to treat $\kappa\mu$ as a small quantity and perform a Taylor expansion, which yields in first order

$$\frac{\mu}{\hbar\omega_z} = \left(\frac{15\lambda^2\eta\,aN_{\mathbf{0}}}{8\sqrt{2}\,a_z}\right)^{2/5} + \frac{3\kappa a}{7\sqrt{2}\,\lambda^2\eta\,a_z}\left(\frac{15\lambda^2\eta\,aN_{\mathbf{0}}}{8\sqrt{2}\,a_z}\right)^{2/5} \tag{3.110}$$

In analogy to (3.55) Eq. (3.110) defines with (3.109) a radius of the cloud according to

$$R^2 \equiv R_0^2 + \kappa R_1^2 = 2\left[\left(\frac{15\lambda^2\eta\,aN_{\mathbf{0}}}{8\sqrt{2}\,a_z}\right)^{2/5} + \frac{3\kappa a}{7\sqrt{2}\,\lambda^2\eta\,a_z}\left(\frac{15\lambda^2\eta\,aN_{\mathbf{0}}}{8\sqrt{2}\,a_z}\right)^{2/5}\right] a_z^2 \tag{3.111}$$

with an obvious identification of R_0^2 with the first term on the right-hand side and so on. In the beginning we wanted to determine the eigenmodes of the condensate in an anharmonic trap. Unfortunately, we could not find the solution for this problem.

3.8 Low Energy Excitation

We present a variational approach to determine the collective oscillations which is based on Ritz's method. This method has been applied for a harmonic trap in 1996 [62]. We apply this method to the anharmonic trap (1.17) and recover the results for the harmonic trap in the limit of a vanishing anharmonicity.

It is convenient to use dimensionless harmonic-oscillator units (1.16) for the Gross-Pitaevskii action with ω_z setting the scale for frequency and energy and $a_z = \sqrt{\hbar/M\omega_z}$ setting the scale for the length. The condensate wave function can be chosen as $\Psi = \sqrt{N_{\mathbf{0}}/a_z^3}\,\psi$ and the normalization condition (3.2) becomes

$$a_z^3 \int \mathrm{d}^3x\,|\psi|^2 = 1\,. \tag{3.112}$$

We perform a change of variables $t' = \omega_z t$ and $\mathbf{x}' = \mathbf{x}/a_z$ in the Gross-Pitaevskii action (3.4). To this end we have to obey

$$\begin{aligned} \mathrm{d}t &= \frac{1}{\omega_z}\,\mathrm{d}t', \qquad \mathrm{d}^3x &= a_z^3\,\mathrm{d}^3x', \\ \frac{\partial}{\partial t} &= \omega_z\frac{\partial}{\partial t'}, \qquad \boldsymbol{\nabla} &= \frac{1}{a_z}\boldsymbol{\nabla}'. \end{aligned} \tag{3.113}$$

Inserting this into (3.4), we have obtain the dimensionless Gross-Pitaevskii action

$$\mathcal{A}[\Psi^*,\Psi] = \hbar\int_{t_1}^{t_2}\mathrm{d}t'\int\mathrm{d}^3x'\,\mathcal{L}'[\psi^*,\psi]\,, \tag{3.114}$$

where the dimensionless Lagrangian reads with (1.17)

$$\mathcal{L}' = i\psi^*\frac{\partial}{\partial t}\psi + \frac{1}{2}\boldsymbol{\nabla}'\psi^*\boldsymbol{\nabla}'\psi - \frac{1}{2}\left[\lambda^2\eta r'^2 + z'^2 + \frac{\kappa}{2}r'^4\right]|\psi|^2 - \frac{g'}{2}|\psi|^4\,. \tag{3.115}$$

Note, that the prime denotes a dimensionless quantity so that $z' = z/a_z$ and so on. The dimensionless interaction strength is given by $g' = 4\pi N_{\mathbf{0}} a/a_z$. In the following we omit the primes.

To obtain the evolution of the condensate wave function, we extremize $\mathcal{A}$ within a set of trial functions. The basic idea is to take a fixed shape trial function with some free time-dependent parameters. This is a variational method analogous to Ritz's optimization procedure. Hence, a proper choice of ψ is crucial to obtain good approximations. A natural choice is a Gaussian, since in the non interacting case, it is precisely the ground state of the Schrödinger equation:

$$\psi(\mathbf{x},t) = \frac{1}{\sqrt{\pi^{3/2}W_1(t)W_2(t)W_3(t)}}\exp\left\{-\sum_{k=1}^{3}\left[\frac{1}{2W_k^2(t)} + iS_k(t)\right]x_k^2\right\}. \tag{3.116}$$

At a given time t this ansatz defines a Gaussian distribution centered at the position (x_{01}, x_{02}, x_{03}). It is clear that in (3.115) the coordinates are denoted by $r = \sqrt{x_1^2 + x_2^2}$ and $z = x_3$. The time dependent dimensionless variation parameters are the widths W_k and the slopes S_k of the condensate wave function.

Performing the spatial integral in the Gross-Pitaevskii action $\mathcal{A}$ (3.114) with the Lagrangian (3.115) using the trial functions (3.116), we obtain an effective Lagrangian $L = \int_{-\infty}^{\infty}\mathrm{d}^3x\,\mathcal{L}$ with four terms $L = L_{\mathrm{time}} + L_{\mathrm{kin}} + L_{\mathrm{pot}} + L_{\mathrm{int}}$. We have a term stemming from the time derivative

$$L_{\mathrm{time}} = i\int_{-\infty}^{\infty}\mathrm{d}^3x\,\psi^*\frac{\partial}{\partial t}\psi = \frac{1}{2}\sum_{k=1}^{3}W_k^2\,\dot{S}_k\,, \tag{3.117}$$

a term corresponding to the kinetic energy

$$L_{\mathrm{kin}} = -\frac{1}{2}\int_{-\infty}^{\infty}\mathrm{d}^3x\,\boldsymbol{\nabla}\psi^*\boldsymbol{\nabla}\psi = -\frac{1}{2}\sum_{k=1}^{3}\left\{\frac{1}{2W_k^2} + 2\,S_k^2\,W_k^2\right\}, \tag{3.118}$$

a term for the trapping potential (1.17) in the dimensionless form

$$L_{\mathrm{pot}} = -\int_{-\infty}^{\infty}\mathrm{d}^3x\,V(\mathbf{x})|\psi|^2 = -\frac{1}{2}\left\{\sum_{k=1}^{2}\frac{\lambda^2\eta}{2}W_k^2 + \frac{1}{2}W_3^2 + \frac{3\kappa}{4}\left[W_1^4 + \frac{2}{3}W_1^2W_2^2 + W_2^4\right]\right\}, \tag{3.119}$$

and, last but not least, an interaction term

$$L_{\mathrm{int}} = -\frac{g}{2}\int_{-\infty}^{\infty}\mathrm{d}^3x\,|\psi|^4 = -\frac{g}{4\pi\sqrt{2\pi}\,W_1(t)W_2(t)W_3(t)}\,. \tag{3.120}$$

The integrals are all simple Gauss integrals, which we have calculated with the help of

$$\int_{-\infty}^{\infty} \mathrm{d}x\, x^{2n} \exp\left(-\xi \frac{x^2}{a^2}\right) = (-1)^n \left[\frac{\partial^n}{\partial \xi^n} \xi^{-1/2}\right]_{\xi=1} a^{2n+1}\sqrt{\pi}. \tag{3.121}$$

The action (3.4) is extremized according to the variation parameters W_k and S_k of the trial function (3.116) by the respective Euler-Lagrange equations

$$\frac{\partial L}{\partial W_i} - \frac{\mathrm{d}}{\mathrm{d}t}\frac{\partial L}{\partial \dot{W}_k} = 0\,, \qquad \frac{\partial L}{\partial S_k} - \frac{\mathrm{d}}{\mathrm{d}t}\frac{\partial L}{\partial \dot{S}_k} = 0\,. \tag{3.122}$$

Thus, we get the equations of motion for the parameters

$$-W_1\dot{S}_1 + 2W_1 S_1^2 = -\frac{\lambda^2\eta}{2}W_1 + \frac{1}{2W_1^3} + \frac{P}{W_1^2 W_2 W_3} - \frac{\kappa}{2}\left[3W_1^3 + W_1 W_2^2\right], \tag{3.123}$$

$$S_1 = -\frac{\dot{W}_1}{2W_1}, \tag{3.124}$$

where we have introduced the dimensionless interaction parameter $P = \sqrt{2/\pi}N_{\mathbf{0}}a/a_0$, who indicates the strength of the interaction. It can be positive or negative depending on the sign of the s-wave scattering length a. There are similar equations for $W_{2,3}$ and $S_{2,3}$. Finally, by eliminating the S_k with (3.124) we receive the equations of motion for the widths W_k of the condensate

$$\frac{\mathrm{d}^2}{\mathrm{d}t^2}W_1 = -\lambda^2\eta W_1 + \frac{1}{W_1^3} + \frac{P}{W_1^2 W_2 W_3} - \kappa\left(3W_1^3 + W_1 W_2^2\right), \tag{3.125}$$

$$\frac{\mathrm{d}^2}{\mathrm{d}t^2}W_2 = -\lambda^2\eta W_2 + \frac{1}{W_2^3} + \frac{P}{W_1 W_2^2 W_3} - \kappa(3W_2^3 + W_1^2 W_2)\,, \tag{3.126}$$

$$\frac{\mathrm{d}^2}{\mathrm{d}t^2}W_3 = -W_3 + \frac{1}{W_3^3} + \frac{P}{W_1 W_2 W_3^2}\,, \tag{3.127}$$

which are decoupled from the other variational parameters S_k, but are unfortunately coupled non-linearly among each other. We remark that the $1/W_k^3$-terms correspond to the kinetic energy which is important to know for the Thomas-Fermi approximation.
The Euler-Lagrange equations are of the form

$$\ddot{W}_k(t) = -\frac{\partial V_{\mathrm{eff}}\left[W_1(t), W_2(t), W_3(t)\right]}{\partial\, W_k(t)}. \tag{3.128}$$

They can be regarded as the motion of a classical point particle moving in the effective potential

$$V_{\mathrm{eff}}\big(W_1,\, W_2,\, W_3\,\big) = \frac{\lambda^2\eta}{2}W_1^2 + \frac{\lambda^2\eta}{2}W_2^2 + \frac{1}{2W_1^2} + \frac{1}{2W_2^2} + \frac{\kappa}{4}(3W_1^4 + 2W_1^2W_2^2 + 3W_2^4) + \frac{1}{2}W_3^2 + \frac{1}{2W_3^2} + \frac{P}{W_1 W_2 W_3}. \tag{3.129}$$

Thus, we can look now at low energy excitations of the stationary points. They are found either by searching for the minima of the potential (3.129) or from the equilibrium points W_{0k} of the equations of motion (3.125)–(3.127) which are constant in time.
Eqs. (3.125) and (3.126) are identical under exchange of W_{01} and W_{02}. Thus, Eq. (3.126) just tells us that both width are equal, i.e. $W_{01} = W_{02}$, wherefore we can neglect it. Then the equations of motion (3.125)–(3.127) reduce to

$$\lambda^2\eta W_{01} = \frac{1}{W_{01}^3} + \frac{P}{W_{01}^3 W_{03}} - 4\kappa W_{01}^3\,, \tag{3.130}$$

$$W_{03} = \frac{1}{W_{03}^3} + \frac{P}{W_{01}^2 W_{03}^2}\,. \tag{3.131}$$

The solutions of (3.130) and (3.131) depend on $\lambda^2\eta$, κ and P. For η and $P > 0$ there is only one stable stationary point W_{0k}, since the width W_k are all positive. For $\eta < 0$ and $P > 0$, there is a ring of stable points. In this case, the Gaussian ansatz (3.116) must be modified according to the ring shape.
Now we are able to expand the effective potential (3.129) via $W_k = W_{0k} + \delta W_k$ and get

$$V_{\text{eff}}\left(\boldsymbol{W}\right) = V_{\text{eff}}\left(\boldsymbol{W}_0\right) + \frac{1}{2}\,\delta\boldsymbol{W}\,H\,\delta\boldsymbol{W}^T + \dots\,, \tag{3.132}$$

where we have shorten the notation with $\boldsymbol{W} = (W_1, W_2, W_3)$ and analogous $\boldsymbol{W}_0$ and $\delta\boldsymbol{W}$. The Hesse matrix in the expansion (3.132) reads

$$H = \begin{pmatrix} \lambda^2\eta + \dfrac{3}{W_{01}^4} + 10\kappa W_{01}^2 + \dfrac{2P}{W_{01}^4 W_{03}} & 2\kappa W_{01}^2 + \dfrac{P}{W_{01}^4 W_{03}} & \dfrac{P}{W_{01}^3 W_{03}^2} \\ 2\kappa W_{01}^2 + \dfrac{P}{W_{01}^4 W_{03}} & \lambda^2\eta + \dfrac{3}{W_{01}^4} + 10\kappa W_{01}^2 + \dfrac{2P}{W_{01}^4 W_{03}} & \dfrac{P}{W_{01}^3 W_{03}^2} \\ \dfrac{P}{W_{01}^3 W_{03}^2} & \dfrac{P}{W_{01}^3 W_{03}^2} & 1 + \dfrac{3}{W_{03}^4} + \dfrac{2P}{W_{01}^2 W_{03}^3} \end{pmatrix}.$$

The square-root of the eigenvalues of H are the low excitation frequencies. For Hesse matrix H (3.133), we find the three eigenfrequencies

$$\omega_a = \sqrt{2}\sqrt{\lambda^2\eta + 5\kappa W_{01}^2 - 2P_{4,1}}, \tag{3.133}$$

$$\omega_{b,c} = \sqrt{2}\sqrt{1 + \lambda^2\eta + 6\kappa W_{01}^2 - P_{2,3} \pm \sqrt{\left[1 - \lambda^2\eta - 6\kappa W_{01}^2 + P_{2,3}\right]^2 + 8P_{3,2}^2 - 4P_{2,3}}}\,, \tag{3.134}$$

where the upper (plus) sign stands for the frequency ω_b and the lower (minus) sign stands for the frequency ω_c. To shorten notation, we have introduced the new symbol

$$P_{i,j} = \frac{P}{4W_{01}^i W_{03}^j}\,. \tag{3.135}$$

Similar equations were found by T.K. Gosh in 2004 [**?**]. For a large number of atoms we perform the Thomas-Fermi approximation by neglecting the $1/W_k^3$-term in (3.130) and (3.131), which then reduce to

$$P = W_{01}^2 W_{03}^3\,, \qquad W_{03}^2 = W_{01}^2\left(\lambda^2\eta + 4\kappa W_{01}^2\right). \tag{3.136}$$

With help of the Thomas-Fermi approximation (3.136), the oscillation frequencies (3.133) and (3.134) specialize to

$$\omega_a^{(\text{TF})} = \sqrt{2}\,\sqrt{\lambda^2\eta + 6\kappa W_{01}^2}\,, \tag{3.137}$$

$$\omega_{b,c}^{(\text{TF})} = \sqrt{2}\sqrt{\frac{3}{4} + \lambda^2\eta + 6\kappa W_{01}^2 \pm \sqrt{\left(\frac{3}{4} + \lambda^2\eta + 6\kappa W_{01}^2\right)^2 - \frac{1}{2}\left(32\kappa x^2 + 5\lambda^2\eta\right)}}\,. \tag{3.138}$$

A numeric evaluation of (3.133) and (3.134) and the Thomas-Fermi approximation of them (3.137) and (3.138) are shown in Figure 3.1. The stationary width W_{0k} are found numerically from the effective potential (3.129) by finding the minimum value of it. We show the dependence of the eigenfrequencies on the parameters κ and P in a cylindrical trap with an anisotropy $\lambda^2\eta = 36$. We have chosen (a) the harmonic limit $\kappa = 0$ and (b) a ten times larger anharmonicity than that of the Paris experiment, $\kappa = 4$. We note a characteristic change in the behavior of the

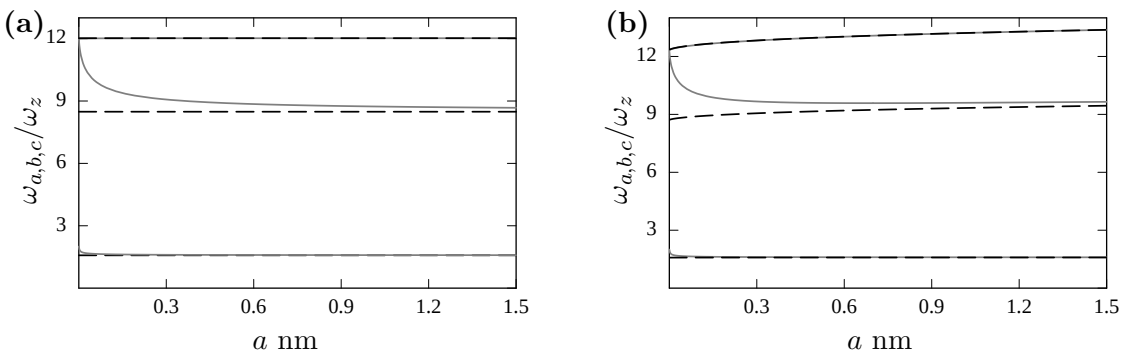

FIG. 3.1: Eigenfrequencies versus s-wave scattering length. In part (a) we show the harmonic limit $\kappa = 0$ for the frequencies (3.133) and (3.134) (grey solid) and the Thomas-Fermi approximation (3.137) and (3.138), (dashed lines). In part (b) we show a plot for the anharmonicity $\kappa = 4$. The influence of the anharmonicity is small but significant. It increases the eigenfrequencies and leads to a divergency in the Thomas-Fermi limit. In both figures, from top to bottom, the frequencies are: ω_b, ω_a, and ω_c. The stationary widths W_{0k} are determined numerically from finding the minimum of the effective potential (3.129).

eigenfrequencies. They increase with increasing interaction strength and diverge in the Thomas-Fermi limit while in the harmonic trap they tend to a constant.
To further analyze the eigenfrequencies, we expand formulas (3.137) and (3.138) for small $\kappa \ll 1$ and small $0 < \lambda^2\eta \ll 1$

$$\omega_a^{(\mathrm{TF})} = \begin{cases} \sqrt{2\lambda^2\eta} + \dfrac{3\sqrt{2}W_{01}^2}{\lambda\sqrt{\eta}}\kappa + \mathcal{O}(\kappa^2) & \text{for} \quad \kappa W_{01}^2 \ll \lambda^2\eta \\ 2\sqrt{3\kappa W_{01}^2} + \dfrac{\lambda^2\eta}{2\sqrt{3\kappa W_{01}^2}} + \mathcal{O}(\lambda^3\eta^{3/2}) & \text{for} \quad \lambda^2\eta \ll \kappa W_{01}^2 \end{cases} \tag{3.139}$$

$$\omega_{b,c}^{(\mathrm{TF})} = \begin{cases} \sqrt{2}\sqrt{\dfrac{3}{4} + \lambda^2\eta \pm \sqrt{\dfrac{9}{16} - \lambda^2\eta + \lambda^4\eta^2}} + \mathcal{O}(\kappa) & \text{for} \quad \kappa W_{01}^2 \ll \lambda^2\eta \\ \sqrt{2}\sqrt{\dfrac{3}{4} + 6\kappa W_{01}^2 \pm \sqrt{\dfrac{9}{16} - 7\kappa W_{01}^2 + 36\kappa^2 W_{01}^4}} + \mathcal{O}(\lambda^2\eta) & \text{for} \quad \lambda^2\eta \ll \kappa W_{01}^2 \,. \end{cases} \tag{3.140}$$

We note that for small κ we obtain in zeroth order the equations of [62] for the frequencies. In the isotropic case $\lambda^2\eta = 1$ they reduces to

$$\Omega_a = \sqrt{2}, \qquad \Omega_b = \sqrt{5} \qquad \Omega_c = \sqrt{2}\,, \tag{3.141}$$

which was derived by S. Stringari in [63].
For the trap (1.14) of the Paris experiment [1], the condensate, at rest $\Omega = 0$, in the harmonic confinement has been cigar shaped, and the strength of the quartic admixture was $\kappa \approx 0.4$. The interaction parameter P is proportional to the s-wave scattering length a. For ^{87}Rb which has been condensed in the Paris experiment, the scattering length is about $a = 5.2$ nm. The anisotropy of the xy-plane to the z-direction has been around $\lambda \approx 6$ with a residual anisotropy in the xy-plane <1%. For rotation speeds close to the critical rotation $\Omega \sim \omega_\perp$, the condensate was nearly spherical, and it remained stable for $\Omega \lesssim 1.05\,\omega$. However, theoretical, both numerical and analytical [**?**], there is no reason for a limited angular velocity Ω. Furthermore, for large Ω the condensate is expected to become annular with a giant vortex in the center.

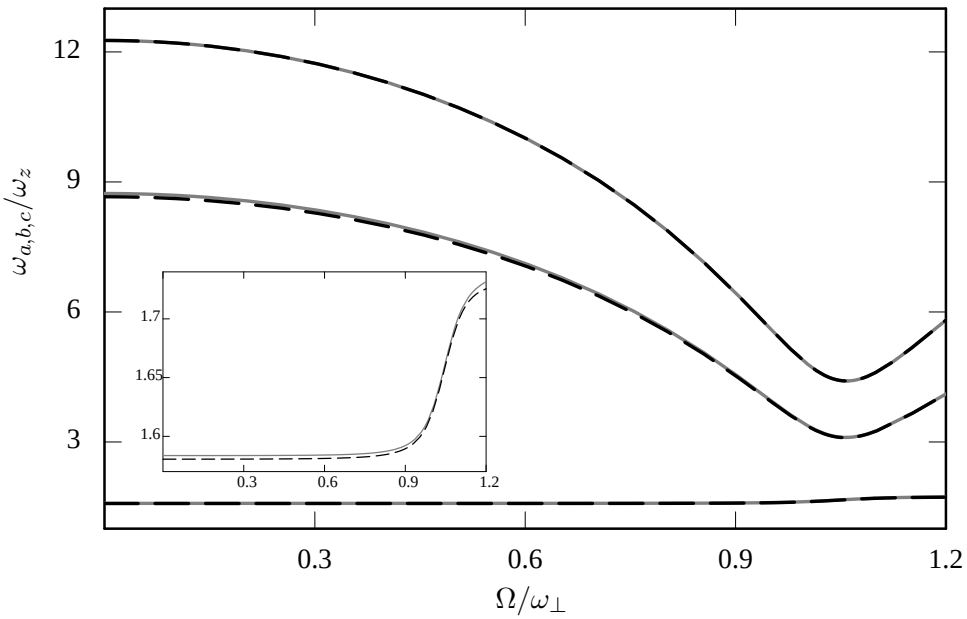

FIG. 3.2: Eigenfrequencies versus rotation speed. For the values of the Paris experiment, i.e. the anharmonicity $\kappa = 0.4$, the anisotropy $\lambda^2 = 36$, and the s-wave scattering length $a = 5.2$ nm. The small Figure is a zoom to the lowest lying frequency. The axes labeling is the same as for the big frame. From top to bottom, the frequencies are: ω_b, ω_a, and ω_c.

In Figure 3.2 we see the dependence of the frequencies on the rotation speed Ω. Although the Gaussian trial function (3.116) is only reasonable up to the critical rotation speed, we have plotted a larger range of the rotation speed. We note that the frequencies in this regime $\Omega \gg \omega_\perp$ diverges in the limit of an infinite fast rotation speed Ω, which disagrees with our experience so far with the thermodynamic quantities. They all tend to a constant value in the limit of infinite fasts rotation. This shows that the Gaussian trial function (3.116) is not a proper choice in that fast rotation regime. A natural extension to this discussion is to modify the Gaussian trial function (3.116) accounting for the ring shape of the condensate. In the overcritical rotation regime $\Omega > \omega_\perp$, this corresponds to a Gaussian centered on a circle around the origin with a radius r_0 as a variational parameter. However, this has to be left for future research.

3.9 Free Expansion

Since the gas can not be trapped forever, it is interesting to investigate the dynamics of the expansion of the gas, following the switching off the trap. This is an important issue because many informations on these Bose condensed gases are gained experimentally by taking images of the expanded atomic cloud after a time of flight. In particular, one can determine the s-wave scattering length, the release energy and the aspect ratio of the velocity distribution. For a harmonic trap, this problem has been analyzed by Y. Castin and R. Dum [26] in 1996. This work has been the basis for the evaluation of the data of the Paris experiments, although this trap is anharmonic. They have assumed the effect of the anharmonicity to be small for all rotation speeds. However, in the fast rotation regime $\Omega \sim \omega_\perp$, the influence of the anharmonicity gets more important and it is questionable if could still be neglected. Hence, for an improved quantitative evaluation it is necessary to study the expansion of the condensate from an anharmonic

trap.
In the previous Section 3.8 we have derived the equations of motion (3.125)–(3.127) for the width of a Gaussian trial function (3.116) to minimize the Gross-Pitaevskii action (3.4). We have considered oscillations around the stationary solution of these equations of motion. Now, we consider the dynamic of the width of the condensate when the trap is switched off at the time $t = 0$. The switching off mechanism is described by

$$\omega_\perp(t) = \omega_\perp \Theta(-t)\,, \qquad \omega_z(t) = \omega_z \Theta(-t)\,, \qquad \kappa(t) = \kappa\Theta(-t)\,, \tag{3.142}$$

where Θ denotes the Heaviside function. We re-write the equations of motion (3.125)–(3.127) in the following way:

$$\ddot{b}_\perp = \frac{1}{W_\perp^4 b_\perp^3} - \left(\frac{\omega_\perp^2(t)}{\omega_\perp} - \frac{\Omega^2}{\omega_\perp^2}\right) b_\perp - 4\kappa(t) W_\perp^2 b_\perp^3 + \frac{P}{W_\perp^3 W_z\, b_\perp^3 b_z}\,, \tag{3.143}$$

$$\ddot{b}_z = \frac{1}{W_z^4 b_z^3} - \frac{\omega_z(t)}{\omega_z} b_z(t) + \frac{P}{W_\perp^2 W_z^3 b_\perp^2 b_z^2}\,, \tag{3.144}$$

where we have set $W_\perp = W_{01} = W_{02}$ and $W_z = W_{03}$, and introduced the scaling

$$b_\perp(t) = \frac{W_\perp(t)}{W_\perp}\,, \qquad b_z(t) = \frac{W_z(t)}{W_z}\,. \tag{3.145}$$

The initial conditions for the scaling parameters $b_\perp$ and b_z are given by

$$b_\perp(0) = b_z(0) = 1\,, \qquad \dot{b}_\perp(0) = \dot{b}_z(0) = 0\,. \tag{3.146}$$

The initial velocities $\dot{b}_\perp$ and $\dot{b}_z$ vanish at $t = 0$ due to the equilibrium condition. We perform the Thomas-Fermi approximation for the equations of motion (3.143) and (3.144) in the following way. We expect the terms corresponding to the kinetic energy $1/W_\perp^3$ and $1/W_z^3$ to be initially small. With the expansion the scaling parameters increase, i.e. $b_\perp(t) \geq b_\perp$ and $b_z(t) \geq b_z$. Therefore, we neglect the kinetic energy terms. In the Thomas-Fermi approximation the equations of motion (3.143) and (3.144) reduces with (3.136) to

$$\ddot{b}_\perp = \tilde{\Omega}^2 b_\perp + \frac{\lambda^2\eta + 4\kappa W_\perp^2}{b_\perp^3 b_z} \tag{3.147}$$

$$\ddot{b}_z = \frac{1}{b_\perp^2 b_z^2}\,, \tag{3.148}$$

where $\tilde{\Omega} = \Omega/\omega_\perp$ denotes the reduced rotation frequency. We can approximate the width in the radial direction $W_\perp$ by the Thomas-Fermi radius (3.111). For slow rotation $\tilde{\Omega} \ll 1$ and the parameters of the Paris experiment, the term proportional to κ in Eq. (3.147) is of the order ~ 0.3 and the anisotropy is $\lambda^2 \approx 36 \gg 1$. Therefore, we assume that the expansion of the cloud in z-direction is much slower than in the radial direction. We approximate the scaling parameter in z-direction according to $b_z = 1 + \epsilon$ with a small time depending ϵ.
Then, the differential equations for the scaling parameters in the Thomas-Fermi approximation (3.147) and (3.148) reduces in zeroth order to

$$\ddot{b}_\perp = \tilde{\Omega}^2 b_\perp + \frac{\lambda^2\eta + 4\kappa W_\perp^2}{b_\perp^3}\,, \tag{3.149}$$

$$\ddot{\epsilon} = \frac{1}{b_\perp^2} \tag{3.150}$$

The initial conditions for the deviation ϵ are due to (3.146) given by

$$\epsilon(0) = 0\,, \qquad \dot{\epsilon}(0) = 0\,. \tag{3.151}$$

We obtain the solution of (3.149) in zeroth order of ϵ by multiplying it with $\dot{b}_\perp$ and using relations like

$$\dot{b}_\perp \ddot{b}_\perp = \frac{1}{2}\frac{\mathrm{d}}{\mathrm{d}t}\,\dot{b}_\perp^2\,. \tag{3.152}$$

Then, (3.149) reduces to

$$\frac{1}{2}\frac{\mathrm{d}}{\mathrm{d}t}\,\dot{b}_\perp^2 = \tilde{\Omega}^2\frac{1}{2}\frac{\mathrm{d}}{\mathrm{d}t}\,b_\perp^2 + \left(\lambda^2\eta + 4\kappa W_\perp^2\right)\frac{1}{2}\frac{\mathrm{d}}{\mathrm{d}t}\,\left(-\frac{1}{b_\perp^2}\right)\,. \tag{3.153}$$

Integration over the time t yields

$$\dot{b}_\perp^2 = \tilde{\Omega}^2\,b_\perp^2 - \left(\lambda^2\eta + 4\kappa W_\perp^2\right)\frac{1}{b_\perp^2} + C_1\,, \tag{3.154}$$

where $C_1 = \lambda^2\eta + 4\kappa W_\perp^2 - \tilde{\Omega}^2$ is the integration constant obtained from the initial conditions (3.146). Taking the square root of (3.154) and separating the variables leads with the initial conditions (3.146) to the remaining integral

$$\int_1^{b_\perp(t)} \mathrm{d}b_\perp\,\frac{b_\perp}{\sqrt{\tilde{\Omega}^2\,b_\perp^4 + \left(\lambda^2\eta + 4\kappa W_\perp^2 - \tilde{\Omega^2}\right)b_\perp^2 - \lambda^2\eta - 4\kappa W_\perp^2}} = t\,. \tag{3.155}$$

Integrating [61, (241)] and inverting (3.155) results in

$$b_\perp = \frac{1}{\sqrt{2}\,\tilde{\Omega}}\sqrt{\tilde{\Omega}^2 - \lambda^2\eta - 4\kappa W_\perp^2 + \left(\tilde{\Omega}^2 + \lambda^2\eta + 4\kappa W_\perp^2\right)\cosh\left(2\tilde{\Omega}t\right)} \tag{3.156}$$

Next, we insert (3.156) into (3.150) to obtain the time evolution of the deviation ϵ of the scaling parameter b_z

$$\epsilon = \int_0^t \mathrm{d}t' \int_0^{t'} \mathrm{d}t''\frac{2\,\tilde{\Omega}^2}{\tilde{\Omega}^2 - \lambda^2\eta - 4\kappa W_\perp^2 + \left(\tilde{\Omega}^2 + \lambda^2\eta + 4\kappa W_\perp^2\right)\cosh\left(2\tilde{\Omega}t\right)} \tag{3.157}$$

The first integration in (3.157) over t'' [35, (2.443.3)] yields

$$\epsilon = \frac{1}{\sqrt{\lambda^2\eta + 4\kappa W_\perp^2}}\int_0^t \mathrm{d}t' \arctan\left[\sqrt{\lambda^2\eta + 4\kappa W_\perp^2}\,\frac{\tanh\left(\tilde{\Omega}t'\right)}{\tilde{\Omega}}\right]. \tag{3.158}$$

The remaining integral (3.158) is not so easy to solve analytically. Therefore, we perform a Taylor expansion of the integrand for small $\Omega \ll \omega_\perp$ and for small $\Omega \approx \omega_z$. Then, the integration in (3.158) in zeroth order results in

$$\epsilon \approx \begin{cases} \dfrac{t\arctan\left(\sqrt{\lambda^2\eta + 4\kappa W_\perp^2}\,t\right)}{\sqrt{\lambda^2\eta + 4\kappa W_\perp^2}} - \dfrac{\ln\left[1 + \left(\lambda^2\eta + 4\kappa W_\perp^2\right)t^2\right]}{2\lambda^2\eta + 4\kappa W_\perp^2} & \text{for} \quad \tilde{\Omega} \ll 1\,, \\ \ln\left(\cosh\tilde{\Omega}t\right) & \text{for} \quad \tilde{\Omega} \approx 1\,. \end{cases} \tag{3.159}$$

The scaling parameters (3.145) of the width of the Gaussian trial function (3.116) simplifies for slow rotation speeds $\Omega \ll \omega_\perp$ to

$$b_\perp = \sqrt{1 + \left(\lambda^2\eta + 4\kappa W_\perp^2\right)t^2}\,, \tag{3.160}$$

$$b_z = 1 + \frac{t\arctan\left(\sqrt{\lambda^2\eta + 4\kappa W_\perp^2}\,t\right)}{\sqrt{\lambda^2\eta + 4\kappa W_\perp^2}} - \frac{\ln\left[1 + \left(\lambda^2\eta + 4\kappa W_\perp^2\right)t^2\right]}{2\lambda^2\eta + 4\kappa W_\perp^2}\,, \tag{3.161}$$

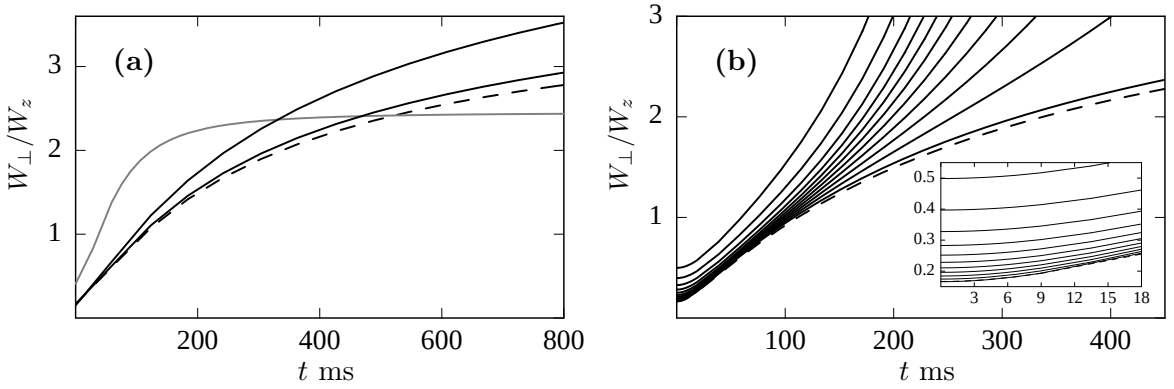

FIG. 3.3: Aspect ratio of the condensate versus reduced time for the values of the Paris experiment. In part (a) we show for a non rotating condensate $\Omega = 0$ the effect of the anharmonicity for varying κ. The dashed line corresponds to the harmonic trap $\kappa = 0$ [26]. The lines above the dashed from bottom to top correspond to $\kappa = 0.4$ and $\kappa = 4$. The gray solid line corresponds to the interaction free Bose gas in the non rotating Paris trap with $\kappa = 0.4$. In part (b) we show the influence of the rotation speed Ω for fixed anisotropy and anharmonicity corresponding to the Paris experiment. The Dashed line is the same as in part a). For the lines above the dashed one we vary the rotation parameter $\eta = 1...0$ in steps of 0.1. The inlet in part (b) is a zoom to the first 18 ms. The axes labels are the same as for the bigger plot.

which reproduces the results of Castin and Dum [26] for a vanishing anharmonicity $\kappa = 0$. In the fast rotating regime $\Omega \approx \omega_\perp$, we obtain for the scaling parameters in zeroth order

$$b_\perp = \frac{2}{1+\cosh 2\tilde{\Omega}t}\,, \tag{3.162}$$

$$b_z = \frac{\ln\left(\cosh\tilde{\Omega}t\right)}{\tilde{\Omega}^2}\,. \tag{3.163}$$

For the general solution of the integral (3.158) we will perform a numerical integration. The aspect ratio of the cloud is given by

$$\frac{W_\perp(t)}{W_z(t)} = \frac{b_\perp(t)W_\perp}{b_z(t)W_z}\,, \tag{3.164}$$

where the width $W_\perp$ and W_z are determined through the stationary Eqs. (3.130) and (3.131) for the trap of the Paris experiment [1] and for the s-wave scattering length of ^{87}Rb, see Table 1.2. An interesting special situation is the interaction free Bose gas. In this case the Gross-Pitaevskii equation (3.1) reduces to a linear Schrödinger equation and the equations of motion (3.143) and (3.144) for the width decouples since the interaction parameter $P = 0$ vanishes. Then, the equations of motion are very similar to the Thomas-Fermi approximated ones (3.149) and (3.150):

$$\ddot{b}_\perp = \frac{1}{W_\perp^4\, b_\perp^3} + \tilde{\Omega} b_\perp\,, \tag{3.165}$$

$$\ddot{b}_z = \frac{1}{W_z^4\, b_z^3}\,. \tag{3.166}$$

Similarly to the above calculation, we obtain for the width the exact solution

$$b_\perp = \frac{1}{\sqrt{2}\tilde{\Omega}W_\perp^2}\sqrt{\tilde{\Omega}^2W_\perp^4 - 1 + \left(1+\tilde{\Omega}^2W_\perp^4\right)\cosh\left(2\tilde{\Omega}t\right)}\,, \tag{3.167}$$

$$b_z = \frac{\sqrt{W_z^4+t^2}}{W_z^2}\,. \tag{3.168}$$

We show a plot of the aspect ratio in Figure 3.3. In part (a) of the Figure we show the effect of varying anharmonicities. The anharmonicity influences the aspect ratio just a little. It increases the expansion in the xy-plane compared to the harmonic trap. Also in part (a) we show the aspect ratio for an interaction free Bose gas in the anharmonic trap of the Paris experiment [1]. Its character differs significantly from the Thomas-Fermi approximated aspect ratio. This characteristic difference can be utilized to determine the s-wave scattering length by a fit to the experimental data. In part (b) we show for the trap of the Paris experiment the effect of increasing rotation speeds. In the first 100 ms of the expansion, the change of the aspect ratio is only little. From there on the change is drastically. The rotation increases the velocity of the expansion in the xy-plane very much. Hence, this effect can also be utilized to determine the speed of rotation.
In the Paris experiment [1], the condensate has been probed by switching off the confining potential, letting the cloud expand during 18 ms and performing absorption imaging. For a quantitative analysis of the pictures, they have assumed that the expansion of the cloud out of an anharmonic trap is approximately the same as the expansion out of a harmonic trap. However, the time evolution of the cloud does depend strongly on the speed of rotation, even in the first few $\sim$20 ms, as shown in the inlet of Figure 3.3b. Hence, the evaluation of the experimental data could be improved with our calculations.
For instance, one problem has been to determine the effective rotation speed Ω. One method has been to measure the density of the cloud in the xy-plane and to compare it with the initial atomic distribution. The initial Thomas-Fermi approximated density (3.45) varying in the xy-plane like the integrand in (3.104). This initial distribution is scaled with the scaling parameter (3.160) and $\kappa = 0$. Then, the scaled Thomas-Fermi approximated density is fitted to the measured atomic distribution choosing the chemical potential μ and the rotation speed Ω as adjustable parameters. Unfortunately, the agreement of this fit has not been as well as for a condensate confined in a purely harmonic trap and has led to some speculations.
Although, our calculation is only valid up to the critical rotation speed $\Omega = \omega_\perp$, we could expect it to be a good approximation even slightly above the critical rotation speed, since then most atoms are still close to the center of the trap.

Chapter 4

Conclusions and Outlook

In the following we recapitulate the results of our thesis and the questions arising from them. In Chapter 2 we have examined the critical temperature T_c at which the condensation of an ideal bosonic gas occurs in the anharmonic trap. Surprisingly, our established critical temperature $T_c \approx 64$ nK for the critical rotation speed $\Omega = \omega_\perp$ is about three times smaller than measured in the Paris experiment. Actually we have expected the semiclassical approximation to give very good results like it does for a pure harmonic trap [55,51]. Sabine Stock, a PhD student of the Jean Dalibard, agreed with us that the transition temperature should indeed be lower than stated in Ref. [1].
In particular, we have compared the thermodynamic properties of an ideal Bose gas in an anharmonic with a harmonic trap. For instance, we have observed the critical temperature T_c in the anharmonic trap to be larger than it would be in the harmonic trap. This is initially clear because the ground-state energy is larger. The difference between both temperatures amounts to only 3% for slow rotation speeds Ω, because the anharmonicity is small, however for fast rotation $\Omega \sim \omega_\perp$ they are totally different, see Figure 2.4. The critical temperature T_c in the anharmonic trap tends to a finite constant value for $\Omega \to \infty$, while for the harmonic trap the regime $\Omega \geq \omega_\perp$ certainly does not exist. In the limit of an infinite fast rotation speed, this constant corresponds to the transition temperature of a Bose-Einstein condensate living on a cylindrical ring. In order to improve the semiclassical approximation of the critical temperature T_c, we have determined perturbatively two corrections, which are due to the finite size of the system and due to the two-body δ-interaction. Both effects lower the transition temperature T_c in the order of about 2.5% to 3.3% and depend strongly on the rotation speed Ω. It would be challenging to observe both effects in experimental measurements.
Furthermore, we have determined the heat capacity of the ideal, i.e. non-interacting, bosonic gas. In the high temperature regime $T > T_c$ we obtain the Dulong-Petit law of the heat capacity per particle which is 0.5 smaller in the anharmonic trap than in a harmonic one. The rotation effect in that regime is rather small, since the high energy levels of the trap well above the ground state do not "feel" the bottom of the trap and its effective harmonic contribution, which depends on the rotation speed Ω. But we have found a characteristical change in the approach of the Dulong-Petit law. In the undercritical rotation regime $\Omega < \omega_\perp$, the heat capcity is always larger than the Dulong-Petit law, while in the overcritical regime $\Omega > \omega_\perp$ it crosses the Dulong-Petit limit. At zero temperature, the heat capacity tends to zero for all rotation speeds, so that we are not in conflict with the third law of thermodynamics. However, the approach to zero is different in the case of undercritical rotation speeds $\Omega < \omega_\perp$ compared to overcritical speeds of rotation $\Omega > \omega_\perp$. In both cases the approach is a power-law behavior in T, but the power changes from three in the under-critical regime to 5/2 in the over-critical regime.
Another quantity of interest, which one likes to examine in this context, is the compressibility of the system. It corresponds to density fluctuations and is like the heat capacity a good test

for the stability of the regarded system. However, the determination of this quantity is left for future investigations.

Summarizing we can state that the thermodynamic properties investigated in this work are rather influenced by the rotation speed Ω than by the anharmonicity κ, although the anharmonicity made both the analytical and the numerical calculation a lot more complicated.

In Chapter 3 we have elaborated some dynamical aspects of the condensate in the anharmonic Paris trap. First we examined the influence of the rotation to the Hamiltonian of the system by transforming the Gross-Pitaevskii equation, which describes the ground-state wave function of the system, into the corotating reference frame. In this way we obtained an effective additional centrifugal term, which is quadratic, perpendicular to the rotation axis, and oppositely orientated to the trapping potential.

Then we have investigated the collective modes of the Bose condensed gas at zero temperature $T = 0$ within the hydrodynamical limit, which consist of availing the fact that the Gross-Pitaevskii equation fulfil the continuity equation and a modified Euler equation. This can be used to analyze density oscillations within the Thomas-Fermi approximation, where the quantum pressure and the kinetic energy are neglected. However, the solution for the anharmonic trap is still an open question.

We have also analyzed the density oscillations directly within a variational approach, which is due to Ritz's method. We have chosen a Gaussian trial function with parameters for the shape and the momentum of the ground-state wave function and have minimized the energy according to these parameters. We have found three eigenmodes which strongly depend on both the anharmonicity κ and the rotation speed Ω. Compared to the same modes in the harmonic trap they are very different. In the harmonic trap the eigenfrequencies tend to a finite value in the limit of infinite strong interaction $a \to \infty$, where a denotes the s-wave scattering length. In the anharmonic trap the frequencies tend to infinity for strong interaction $a \to \infty$. Because of the chosen shape of the Gaussian trial function our results are only valid in the undercritical regime $\Omega < \omega_\perp$, which could be improved by a new trial function which accounts for the ring shape of the condensate in the overcritical regime $\Omega > \omega_\perp$.

Finally, we have examined the free expansion of the condensate after switching off the trap. This expansion is essential for evaluating time of flight pictures and could improve the experimental analysis.

At this stage it is necessary to mention that we have neglected during the whole work the nucleation of vortices. The Paris experiment showed that there are quite a lot of quantized vortices visible, especially in the fast rotation regime, see Figure 1.4. The vortices are arranged in an Abrikosov lattice which is slightly disturbed and seems to melt in the middle, when the rotation speed Ω approaches the trap frequency $\omega_\perp$. The nucleation of vortices should influence both the thermodynamic and the dynamic properties of the system. However, the task to incorporate vortices into the calculations must be delayed to future investigations.

Appendix A

Euler-MacLaurin Formula

The general Euler-MacLaurin formula is (for simplicity a and b shall be integers)

$$\sum_{n=a}^{b} f(n) = \int_a^b f(x)\mathrm{d}x + \frac{1}{2}\Big(f(a)+f(b)\Big) + \sum_{k=1}^{m} \frac{B_{2k}}{(2k)!}\Big(f^{(2k-1)}(b) - f^{(2k-1)}(a)\Big) - \int_a^b \frac{B_{2m+1}([1-t])}{(2m+1)!} f^{(2m+1)}(t)\mathrm{d}t\,, \tag{A.1}$$

which is sometimes called the *Euler-MacLaurin formula with remainder*. To derive this formula we will follow [65]. The prove is presented in the non-standard calculus method, which works with small quantities that are smaller than any number but greater than zero. Simply put, it is ordinary calculus without taking limits.

Definition. *Consider an arbitrary function $f(x)$. Its h-differential is*

$$\mathrm{d}_h f(x) = f(x+h) - f(x)\,, \tag{A.2}$$

and a h-derivative of f is denoted by

$$D_h f(x) = \frac{\mathrm{d}_h f(x)}{\mathrm{d}_h x} = \frac{f(x+h)-f(x)}{h}\,. \tag{A.3}$$

Note that

$$D_0 \equiv \lim_{h\to 0} D_h f(x) = \frac{\mathrm{d}f(x)}{\mathrm{d}x}\,, \tag{A.4}$$

if $f(x)$ is differentiable.

The advantage of the nonstandard formulation is to avoid infinitesimals, which can be rather confusing and need an elaborate explanation. Without going to much into details, the function $F(x)$ is called an antiderivative of $f(x)$, if $D_h F(x) = f(x)$.

Definition. *If $b-a \in h\mathbb{N}$, we define the definite h-integral to be*

$$\int_a^b f(x)\mathrm{d}_h x = h\Big(f(a) + f(a+h) + \ldots + f(b-h)\Big)\,. \tag{A.5}$$

The fundamental theorem of ordinary calculus applies also here. Suppose $D_h F(x) = f(x)$. Using the ordinary Taylor formula, we have

$$F(x+h) = \sum_{n=0}^{\infty} \frac{F^{(n)}(x)h^n}{n!} = \left(\sum_{n=0}^{\infty} \frac{h^n D_0^n}{n!}\right) F(x)\,, \tag{A.6}$$

so that formally,

$$F(x+h) = e^{hD_0} F(x)\,, \tag{A.7}$$

hence, we have

$$f(x) = \frac{F(x+h)-F(x)}{h} = \frac{e^{hD_0}-1}{h} F(x)\,,$$

or

$$F(x) = \frac{hD_0}{e^{hD_0}-1} \int f(x)\mathrm{d}x\,. \tag{A.8}$$

Definition *The Bernoulli polynomials appear as coefficients in the Taylor expansion*

$$\frac{ze^{zx}}{e^z-1} = \sum_{n=0}^{\infty} \frac{B_n(x)}{n!} z^n\,, \tag{A.9}$$

which give the Bernoulli numbers $B_n = B_n(0)$ *for* $n \geq 0$.

Using Bernoulli numbers, (A.8) gets

$$F(x) = \sum_{n=0}^{\infty} \frac{b_n}{n!} (hD_0)^n \int f(x)\mathrm{d}x\,. \tag{A.10}$$

As we know that $B_n = 0$ for odd integers if $n \geq 3$ and $B_1 = -1/2$, we get the Euler-MacLaurin formula (without remainder)

$$F(x) = \int f(x)\mathrm{d}x - \frac{h}{2} f(x) + \sum_{n=0}^{\infty} \frac{B_{2n} h^{2n}}{(2n)!} f^{(2n-1)}(x)\,. \tag{A.11}$$

Suppose $h = 1$ and $b-a \in \mathbb{N}$. Using the fundamental theorem of calculus $F(b)-F(a) = \int_a^b \mathrm{d}x f(x)$ and (A.5) we have

$$\sum_{n=a}^{b-1} f(n) = \int_a^b f(x)\mathrm{d}x - \frac{1}{2}\Big(f(b)-f(a)\Big) + \sum_{n=0}^{\infty} \frac{B_{2n}}{(2n)!}\Big(f^{(2n-1)}(b) - f^{(2n-1)}(a)\Big)\,, \tag{A.12}$$

which is the Euler-MacLaurin formula without remainder (A.1), if we add $f(b)$. To get the formula with the remainder (A.1), we should replace the infinite sum by a finite and find for the rest an integral representation. This can be found in e.g. [34,65] and is a more sophisticated problem. However, studying the remainder is crucial for convergence tests and the applicability of the approximation via the Euler-MacLaurin formula.

Appendix B

Generalized ζ-Functions and Relations

As an overview of the introduced ζ-functions in Chapter 2, we summarize the definitions and list useful relations for these new functions. Because of their close relation to the Bose-Einstein condensation they are sometimes called Bose-Einstein functions, however for special arguments they reproduce also the Riemann ζ-function, which plays an important role in complex analysis.

B.1 First Generalization

The Riemann ζ-function is defined for complex ν by

$$\zeta(\nu) = \sum_{j=1}^{\infty} \frac{1}{j^{\nu}}\,, \tag{B.1}$$

with $\mathrm{Re}(\nu) > 1$. The semiclassical treatment of a harmonic trap leads to the following generalization of (B.1)

$$\zeta_{\nu}(z) = \sum_{j=1}^{\infty} \frac{z^j}{j^{\sigma}}\,, \tag{B.2}$$

for $|z| \leq 1$. The variable z could be real or complex, but for the condensate it is of course real, it is the fugacity $z = \exp(\beta\mu)$. Since the chemical potential satisfies the relation $\mu < 0$, the ζ-function (B.2) has no singularities. Formula (B.2) reproduces the Riemann ζ-function for $z = 1$, which marks the transition point of the Bose gas.

B.2 Second Generalization

The next generalization of (B.1) is inspired by the treatment of the anharmonic trap (1.17) and leads to

$$\zeta_{\nu}(z, x) = \sum_{j=1}^{\infty} \frac{z^j}{j^{\nu}} \mathrm{E}_{\sigma}(xj)\,, \tag{B.3}$$

where

$$\mathrm{E}_{\sigma}(x) = \sqrt{\pi x} e^{x} \mathrm{erfc}(\sigma\sqrt{x})\,. \tag{B.4}$$

Here, σ can have the value 1 or -1, corresponding to an undercritical or overcritical rotation of the trap.

The functions E_σ in (B.3) play an important role in fractional kinetic theory [41] and are related to generalized Mittag-Leffler functions [38,39]. They can be regarded as a generalization of the exponential function, which becomes clear if we regard the Taylor expansion of (B.4)

$$\mathrm{E}_\sigma(x) = \sqrt{\pi x}\left(1 - \sigma 2\sqrt{\frac{x}{\pi}} + x - \sigma\frac{4}{3}\sqrt{\frac{x^3}{\pi}} + \frac{x^2}{2} \mp \dots\right) = \sqrt{\pi x}\sum_{j=0}^{\infty}\frac{(-\sigma\sqrt{x})^j}{\Gamma\left(1+\frac{j}{2}\right)}\,. \tag{B.5}$$

If we consider the Γ-function as the analytic continuation of the factorial function, the Taylor expansion (B.5) is closely related to the exponential function.
In particular, two limits are of special interest, namely the high and the low temperature limit. They correspond to the limits $x \to 0$ and $x \to \infty$ respectively. For the asymptotic behavior we have for $\sigma = 1$ the formula

$$\mathrm{E}_1(x) \approx 1 - \frac{1}{2x} + \frac{3}{4x^2} - \dots + \frac{(2j-1)!!}{(-2x)^j} + \dots \qquad x \to \infty\,. \tag{B.6}$$

For the other case $\sigma = -1$, however, we have due to the relation $\mathrm{erfc}(-x) = 2 - \mathrm{erfc}(x)$:

$$\mathrm{E}_{-1}(x) \approx 2\sqrt{\pi x}e^x - \left(1 - \frac{1}{2x} + \frac{3}{4x^2} - \dots + \frac{(2j-1)!!}{(-2x)^j} + \dots\right) \qquad x \to \infty\,. \tag{B.7}$$

B.3 Some Special Limits

For the Bose gas in an anharmonic trap of the form (1.14) the second variable x in (B.3) depends on the anharmonicity κ, the rotation speed Ω, and the temperature T. Physically important limits are given by

$$x \to \begin{cases} 0 \quad \text{for} \quad \begin{cases} T \to \infty & \text{high temperature limit} \\ \Omega \to \omega_\perp & \text{critical rotation} \end{cases} \\ \\ \infty \quad \text{for} \quad \begin{cases} T \to 0 & \text{low temperature limit} \\ \kappa \to 0 & \text{harmonic trap} \end{cases} \end{cases} . \tag{B.8}$$

Relevant for us are the two regimes above and below the critical temperature. Below the critical temperature we are interested in the low temperature limit. Here, we have the asymptotic expansions

$$\zeta_\nu(z_c, x) = \begin{cases} \zeta(\nu) - \dfrac{1}{2x}\zeta(\nu+1) + \dots + \dfrac{(2k-1)!!}{(-2)^k x^k}\zeta(\nu+k) + \dots & ;\, x \to \infty \quad,\quad \sigma = 1 \\ \\ 2\sqrt{\pi x}\,\zeta(\nu-1/2) - \zeta_\nu(z_c) + \dfrac{1}{2x}\zeta_{\nu+1}(z_c) \mp \dots & ;\, x \to \infty \quad,\quad \sigma = -1\,. \end{cases} \tag{B.9}$$

Above the critical temperature the expansions read

$$\zeta_\nu(z, x) = \begin{cases} \zeta_\nu(z) - \dfrac{1}{2x}\zeta_{\nu+1}(z) + \dots + \dfrac{(2k-1)!!}{(-2)^k x^k}\zeta_{\nu+k}(z) + \dots & ;\, x \to \infty \quad,\quad \sigma = 1 \\ \\ 2\sqrt{\pi x}\displaystyle\sum_{j=0}^{\infty}\frac{z^j e^{xj}}{j^{\nu-1/2}} - \zeta_\nu(z) + \dfrac{1}{2x}\zeta_{\nu+1}(z) \mp \dots & ;\, x \to \infty \quad,\quad \sigma = -1\,. \end{cases} \tag{B.10}$$

For the high temperature regime we have

$$\zeta_\nu(z, x) = \sqrt{\pi x}\left[\zeta_{\nu-1/2}(z) - 2\sigma\sqrt{\frac{x}{\pi}}\zeta_{\nu-1}(z) \pm \dots\right] \quad \text{for } x \to 0\,. \tag{B.11}$$

Below the critical temperature we have to replace z by the critical fugacity z_c in the above equation.

Appendix C

Hypergeometric Function

C.1 Comment on the hypergeometric differential equation

1. The hypergeometric differential equation (3.62) possesses two linearly independent solutions. These solutions have analytic continuations to the entire complex plane except possibly for the three points 0,1 and ∞. Generally speaking the points $u = 0, 1, \infty$ are branch points of at least one of the branches of each solution of the hypergeometric differential equation.

2. Every second-order ordinary differential equation with at most three regular singular points can be transformed into the hypergeometric differential equation.

3. If c is not an integer, the linearly independent solutions $F_1(u)$ and $F_2(u)$ of (3.62) are given by

$$F_1(u) = F(a, b; c; u) \tag{C.1}$$

$$F_2(u) = u^{1-c} F(a - c + 1, b - c + 1; 2 - c; u) \tag{C.2}$$

   For $c > 1$ the second solution $F_2(u)$ is singular at the origin.

4. The hypergeometric series is convergent for arbitrary a, b, and c within the unit circle $|u| < 1$, and for $u = \pm 1$ if $c > a + b$.

5. Goursat [66] and Erdélyi et al. [67] give many hypergeometric transformation formulas, including several cubic transformations. Many functions of mathematical physics can be expressed as special cases of the hypergeometric functions. For example, the Legendre polynomial $P_l(z)$ is recovered according to

$$F(-l, l + 1; 1; (1 - z)/2) = P_l(z)\,. \tag{C.3}$$

C.2 Legendre polynomials

We state without proof some useful relations of the associated Legendre polynomials, which are defined by

$$P_l^m(x) = \frac{(-1)^m}{2^l l!} (1 - x^2)^{m/2} \frac{\mathrm{d}^{\,l+m}}{\mathrm{d}x^{\,l+m}} (x^2 - 1)^l. \tag{C.4}$$

With $x = \cos\theta$, we have for the derivative with respect to θ

$$\frac{\partial}{\partial\theta} P_l^m(x) = \frac{1}{\sqrt{1 - x^2}} \left[l x P_l^m(x) - (l + m) P_{l-1}^m(x) \right] . \tag{C.5}$$

The associated Legendre polynoms also obey the following recurrence relations

$$(2l+1)xP_l^m(x) = (l+m)P_{l-1}^m(x) + (l-m+1)P_{l+1}^m(x) \tag{C.6}$$

and

$$P_l^{-m}(x) = (-1)^m \frac{(l-m)!}{(l+m)!} P_l^m(x)\,. \tag{C.7}$$

Acknowledgements

This thesis could not have been written without important input from many people. I would like to thank Professor Dr. Hagen Kleinert for the opportunity to prepare this thesis under his supervision. His aureate universal knowledge, his many brilliant ideas and especially his magic scientific curiosity encircling him everyday, created the ground for a fascinating and inspiring research atmosphere which affected the whole group. In particular his physical intuition clarified many problems of this thesis and reminded me that physics is great. Being part of this community is a privilege.
I'm indebted to Priv. Doz. Dr. Axel Pelster for his personal engagement in my thesis and many valuable hints. His time-intensive patient education from the very beginning has made this thesis possible. Despite his grand physical knowledge, he is an excellent teacher and I apprise his kind advice.
Special thanks apply to Professor Dr. Vyacheslav I. Yukalov for teaching me BEC and playing table tennis for hours.
I like to thank Professor Dr. Robert Graham for the hospitality at the University Duisburg-Essen and the opportunity to discuss my results with his group.
I am especially grateful to Konstantin Glaum for his friendly explanations concerning physical and mathematical questions and his valuable critics. But despite of this, he is also a good table tennis partner. All in all he is the best office-mate one could imagine.
Thank you Asier Berra and Dr. Jürgen Dietel for drinking coffee/tee and inspiring as well as amusing discussions about physics.
Finally, I thank my family and friends for their support and encouragement during all difficulties in life and other subtleties.

List of Figures

List of Tables

Bibliography

[1] V. Bretin, S. Stock, Y. Seurin, and J. Dalibard, *Fast Rotation of a Bose-Einstein Condensate*, Phys. Rev. Lett. **92**, 050403 (2004)

[2] S. Stock, V. Bretin, F. Chevy, and J. Dalibard, *Shape Oscillation of a Rotating Bose-Einstein Condensate*, Europhys. Lett. **65**, 594 (2004)

[3] A. Einstein, *Quantentheorie des einatomigen idealen Gases*, Sitzber. Kgl. Preuss. Akad. Wiss., 261 (1924)

[4] A. Einstein, *Quantentheorie des einatomigen idealen Gases. Zweite Abhandlung*, Sitzber. Kgl. Preuss. Akad. Wiss., 3 (1925)

[5] S.N. Bose, *Plancks Gesetz und Lichtquantenhypothese*, Zeitschrift für Physik **26**, 178 (1924)

[6] F. London, *On the Bose-Einstein Condensation*, Phys. Rev. **54**, 947 (1938)

[7] F. London, *The λ- Phenomenon of Liquid Helium and the Bose-Einstein Degeneracy*, Nature **141**, 913 (1938)

[8] P. Sokol, *Bose-Einstein Condensation*, p. 51 (Cambridge Univ. Press, 1995)

[9] J.P. Wolfe, J.L. Lin, and D.W. Snoke, *Bose-Einstein Condensation*, p. 281 (Cambridge Univ. Press, 1995)

[10] M.H. Anderson, J.R. Ensher, M.R. Matthews, C.E. Wiemann, and E.A. Cornell, *Observation of Bose-Einstein Condensation in a Dilute Atomic Vapor*, Science **269**, 198 (1995)

[11] K.B. Davis, M.-O. Mewes, M.R. Andrews, N.J. van Druten, D.S. Durfee, D.M. Kurn, and W. Ketterle, *Bose-Einstein Condensation in a Gas of Sodium Atoms*, Phys. Rev. Lett. **75**, 1687 (1995)

[12] *JILA BEC Homepage*, `http://jilawww.colorado.edu/bec/`

[13] Universtät Innsbruck, *Institute for Theoretical Physics*, `http://th-physik.uibk.ac.at/qo/bec.html`

[14] M.R. Andrews, C.G. Townsend, H.-J. Miesner, D.S. Durfee, D.M. Kurn, and W. Ketterle, *Observation of Interference Between Two Bose Condensates*, Science **275**, 637 (1997)

[15] Z. Hadzibabic, S. Stock, B. Battelier, V. Bretin, and J. Dalibard, *Interference of an Array of Independent Bose-Einstein Condensates*, Phys. Rev. Lett. **93**, 180403 (2004)

[16] W. Ketterle, D.S. Durfee, and D.M. Stamper-Kurn, *Making, Probing and Understanding Bose-Einstein Condensates*, cond-mat/9904034

[17] A. Griesmaier, J. Werner, S. Hensler, J. Stuhler, and T. Pfau, *Bose-Einstein Condensation of Chromium*, Phys. Rev. Lett. **94**, 160401 (2005)

[18] A.L. Leggett, *Bose-Einstein Condensation in the Alkali Gases: Some Fundamental Concepts*, Rev. Mod. Phys. **73**, 307 (2001)

[19] P.W. Courteille, V.S. Bagnato, and V.I. Yukalov, *Bose-Einstein Condensation of Trapped Atomic Gases*, Laser Phys. **11**, 659 (2001)

[20] J.V. Prodan, W.D. Phillips, and H. Metcalf, *Laser Production of a Very Slow Monoenergetic Atomic Beam*, Phys. Rev. Lett. **49**, 1149 (1982)

[21] S. Chu, L. Hollberg, J.E. Bjorkholm, A. Cable, and A. Ashkin , *Three-Dimensional Viscous Confinement and Cooling of Atoms by Resonance Radiation Pressure*, Phys. Rev. Lett. **55**, 48 (1985)

[22] S. Chu, *Laser Manipulation of Atoms and Ions*, Proceedings of the International School of Physics "Enrico Fermi", Course CXVIII, edited by E. Arimondo, W.D. Phillips, and F. Strumia, (North-Holland, Amsterdam, 1992), p. 239

[23] A. Aftalion and I. Danaila, *Giant Vortices in Combined Harmonic and Quartic Traps*, Phys. Rev. A **69**, 033608 (2004)

[24] T.P. Simula, A.A. Penckwitt, and R.J. Ballagh, *Giant Vortex Lattice Deformations in Rapidly Rotating Bose-Einstein Condensates*, Phys. Rev. Lett. **92**, 060401 (2004)

[25] A.L. Fetter, B. Jackson, and S. Stringari, *Rapid Rotation of a Bose-Einstein Condensate in a Harmonic plus Quartic Trap*, Phys. Rev. A **71**, 013605 (2005)

[26] Y. Castin and R. Dum, *Bose- Einstein Condensates in Time Dependent Traps*, Phys. Rev. Lett. **77**, 5315, (1996)

[27] M. Greiner, O. Mandel, T. Esslinger, T.W. Hänsch, and I. Bloch, *Quantum Phase Transition from a Superfluid to a Mott Insulator in a Gas of Ultra Cold Atoms*, Nature **415**, 39 (2002)

[28] S. Stock, *The LLL and the Semiclassical Approximation*, unpublished results (2005)

[29] E.P. Gross, *Structure of a Quantized Vortex in a Boson System*, Nuovo Cimento **20**, 454 (1961)

[30] L.P. Pitaevskii, *Vortex Lines in an Imperfect Bose Gas*, Sov. Phys. JETP **13**, 451 (1961)

[31] S. Grossmann and M. Holthaus, *On Bose-Einstein Condensation in Harmonic Traps*, Phys. Lett. A **208**, 188 (1995)

[32] H. Haugerud, T. Haugset, and F. Ravndal, *A More Accurate Analysis of Bose-Einstein Condensation in Harmonic Traps*, Phys. Lett. A **225**, 18 (1997)

[33] T. Haugset, H. Haugerud, and O. Andersen, *Bose-Einstein Condensation in Anisotropic Harmonic Traps*, Phys. Rev. A **55**, 2922 (1997)

[34] A. Ivic, *The Riemann Zeta-Function* (John Wiley-Interscience, New York, 1985)

[35] I.S. Gradshteyn and I.M. Ryzhik, *Tables of Integrals, Series and Products*, (Acadamic Press, New York, 1965)

[36] W. Ketterle and N.J. van Druten, *Bose-Einstein Condensation of a Finite Number of Particles Trapped in One or Three Dimensions*, Phys. Rev. A **54**, 656 (1996)

[37] J.R. Ensher, D.S. Jin, M.R. Matthews, C.E. Wieman, and E.A. Cornell, *Bose-Einstein Condensation in a Dilute Gas: Measurement of Energy and Ground-State Occupation*, Phys. Rev. Lett. **77**, 4984 (1996)

[38] G.M. Mittag-Leffler, C.R. Acad. Sci. Paris (Ser.II) **137**, 554 (1903)

[39] G.M. Mittag-Leffler, Acta. Math. **29**, 101 (1905)

[40] E.W. Weisstein, *MathWorld*, `http://mathworld.wolfram.com/`

[41] R.K. Saxena, A.M. Mathai, and H.J. Haubold, *On Generalized Fractional Kinetic Equations*, math-ph/0406046

[42] J. Spanier and K.B. Oldham, *An Atlas of Functions* (Hemisphere Publishing Corporation, USA, 1987)

[43] H. Kleinert, *Path Integrals in Quantum Mechanics, Statistics, Polymer Physics, and Financial Markets*, 4th Edition, `http://www.physik.fu-berlin.de/~kleinert/public_html/kleiner_reb5/psfiles/pthic07.pdf`

[44] V. Bagnato, D.E. Pritchard, and D. Kleppner, *Bose-Einstein Condensation in an External Potential*, Phys. Rev. A **35**, 4354 (1987)

[45] K. Glaum, A. Pelster, and T. Pfau, *Critical Temperature of Trapped Chrom Condensate* (in preparation)

[46] E. Fermi, *Notes on Quantum Mechanics*, Second Edition, p.145 (University of Chicago Press, Chicago & London, 1995)

[47] A. Pelster and K. Glaum, *Many-Body Vacuum Diagrams and their Recursive Graphical Construction*, Phys. Stat. Sol. B **237**, 72 (2003)

[48] A. Pelster, H. Kleinert, and M. Bachmann, *Functional Closure of Schwinger-Dyson Equations in Quantum Electrodynamics –Part 1: Generation of Connected and One-Particle Irreducible Feynman Diagrams*, Ann. Phys. (N.Y.) **297**, 363 (2002)

[49] A. Pelster and K. Glaum, *Recursive Graphical Solution of Closed Schwinger-Dyson Equations in ϕ^4-Theory – Part1: Generation of Connected and One-Particle Irreducible Feynman Diagrams*, Physica A **335**, 455 (2004).

[50] S. Giorgini, L.P. Pitaevskii, and S. Stringari, *Condensate Fraction and Critical Temperature of a Trapped Interacting Bose Gas*, Phys. Rev. A **54**, R4633 (1996)

[51] F. Gerbier, J.H. Thywissen, S. Richard, M. Hugbart, P. Bouyer, and A. Aspect, *Critical Temperature of a Trapped, Weakly Interacting Bose Gas*, Phys. Rev. Lett. **92**, 030405 (2004)

[52] S.J. Putterman, *Superfluid Hydrodynamics* (North-Holland Publishing Company, Amsterdam, 1974)

[53] C.J. Pethick and H. Smith, *Bose-Einstein Condensation in Dilute Gases* (Cambridge Univ. Press, 2002)

[54] L.P. Pitaevskii and S. Stringari, *Bose-Einstein Condensation*, (Science Pub., Oxford, 2003)

[55] F. Dalfovo, S. Giorgini, L.P. Pitaevskii, and S. Stringari, *Theory of Bose-Einstein Condensation in Trapped Gases*, Rev. Mod. Phys. **71**, 463 (1999)

[56] A.L. Fetter and A.A. Svidzinsky, *Vortices in a Traped Dilute Bose-Einstein Condensate*, J.Phys.: Condensed Matter **13**, R135 (2001)

[57] M. Fliesser, A. Csordás, P. Szépfalusy, and R. Graham, *Hydrodynamic Excitations of Bose Condensates in Anisotropic Traps*, Phys. Rev. A, **56**, R2533 (1997)

[58] H. Kleinert, *Path Integrals in Quantum Mechanics, Statistics, Polymer Physics, and Financial Markets*, Third Edition (World Scientific, Singapore, 2004)

[59] R.P. Feynman and H. Kleinert, *Effective Classical Partition Functions*, Phys. Rev. A **34**, 5080 (1986)

[60] A.L. Fetter, *Rotating Vortex Lattice in a Condensate Trapped in Combined Quadratic and Quartic Radial Potentials*, Phys. Rev. A **64**, 3608 (2001)

[61] I.N. Bronŝtein, K.A. Semendjajew, G. Musiol, and H. Mühlig, *Taschenbuch der Mathematik*, (Verlag Harri Deutsch, Frankfurt a.M. , 1993)

[62] V.M. Pérez-García, H. Michinel, J.I. Cirac, M. Lewenstein, and P. Zoller, *Low Energy Excitations of a Bose-Einstein Condensate: A Time-Dependent Variational Analysis*, Phys. Rev. Lett. **77**, 5320 (1996)

[63] S. Stringari, *Collective Excitations of a Trapped Bose-Condensed Gas*, Phys. Rev. Lett. **77**, 2360 (1996)

[64] T.K. Ghosh, *Vortex Formation in a Fast Rotating Bose-Einstein Condensate*, Phys. Rev. A **69**, 043606 (2004)

[65] V. Kac and P. Cheung, *Quantum Calculus* (Springer, New York, 2002)

[66] M.E. Goursat, *Sur l'équation différentielle linéaire qui admet pour intégrale la série hypergéométrique*, Ann. Sci. École Norm. Super. Sup. 10 (1881)

[67] A. Erdélyi, W. Magnus, F. Oberhettinger, and F.G. Tricomi, *Higher Transcendental Functions*, Vol. 1, (New York: Krieger, 1981)